# 25TH ANNIVERSARY

1998
2023

EUROPEAN MICROSCOPY SOCIETY

# Small details make big differences

## From the inner workings of proteins and viruses to atomic details in cutting-edge materials and technologies, Thermo Scientific™ electron microscopes can help you see—and understand—your samples like never before.

Learn how you can go from questions to usable data at **thermofisher.com/EM**

thermo scientific

Peter Hawkes
EMS President 1998-2000

José Maria Valpuesta
EMS President
2020 - 2024

José-Maria Carrascosa
EMS President
2000 - 2004

25TH ANNIVERSARY
1998 2023 EUROPEAN MICROSCOPY SOCIETY

Josef Zweck
EMS President
2016 - 2020

Ueli Aebi
EMS President
2004 - 2008

Roger Wepf
EMS President
2012 - 2016

Paul Midgley
EMS President
2008 - 2012

# 25 successful years of the **European Microscopy Society**

***Front cover credits:***

Prof. Peter Hawkes: Hawkes, Wiley / Prof. José-Maria Carrascosa: Carrascosa / Prof. Ueli Aebi: © Biozentrum, Universität Basel / Prof. Paul Midgley: Midgley / Prof. Roger Wepf: Wepf / Prof. Josef Zweck: Conventus / Prof. José Maria Valpuesta: Inés Poveda (CNB-CSIC)

# TABLE OF CONTENTS


# ANALYZERS FOR ELECTRON MICROSCOPY

## Discover the QUANTAX Family

Bruker's unique range of analytical tools for electron microscopes enables researchers to analyze the composition and structure of materials on the micro- and nanoscale. The QUANTAX measurement systems include EDS for SEM and TEM, WDS, EBSD and micro-XRF on SEM. Seamless integration of each tool within the comprehensive ESPRIT software allows easy combination of data obtained across these complementary techniques. The QUANTAX family empowers researchers to see the whole picture and get the best results.

**For more information please visit www.bruker.com/quantax**




# Elucidate Thermal Transitions

## By Heating or Cooling While You Observe Your Sample

METTLER TOLEDO hot-stage systems

- **Heating above and below the sample** – reliable results thanks to outstanding temperature homogeneity
- **Interactive control using manual keys** – gives the user manual temperature control
- **Easy and intuitive imaging software** – for visual documentation with temperature overlay

**METTLER TOLEDO GmbH, Analytical**
CH-8606 Nänikon, Switzerland

**www.mt.com/ta-hotstage**

METTLER TOLEDO

## PREFACE

# 25 years of the European Microscopy Society

The European Microscopy Society (EMS)[1] emerged from the previous CESEM[2] organisation and was founded in 1998. Since then, it has adhered to its goals, which include, in short and thus incomplete, organizing microscopy-related meetings of various kinds, such as the quadrennial European Microscopy Congress (EMC) series. Additionally, EMS supports young researchers financially to attend these meetings, promotes interaction between academia and industry, and produces a yearbook to inform our members about the society's activities.

Now, after more than 25 years, it seems appropriate to look back at the progress that has been made in microscopy and to recapitulate the major advances and achievements. This, however, is a delicate task! How does one identify the most important steps forward in microscopy, achieved by individuals or groups, without neglecting others who have also worked hard to expand our knowledge and techniques? To avoid this dilemma, we chose to rely on the expertise of numerous committees who have decided on recipients of various awards, such as the European Microscopy Award, the Ernst-Ruska-Prize, the IFSM Awards, the Kavli Prize, and the Nobel-Prize. When asked to contribute to the booklet you are holding, more than 20 awardees spontaneously agreed to contribute a manuscript about the topics for which they were awarded, often in co-authorship with fellow scientists who contributed to their work.

*Continued on next page*


[1] Below this text, the members of the current as well as of previous boards are listed, as far as they are documented.

[2] Committee of European Societies of Electron Microscopy (CESEM), dates back to 1975. For more details, see also https://www.eurmicsoc.org/en/the_ems/whoarewe/thesociety/

We are grateful to all contributors for their work and are pleased to present a collection of papers that describe some of the most significant advancements in microscopy, both scientifically and in terms of instrumentation. We sincerely hope that this collection will serve for senior scientists remember exciting discoveries and developments, while at the same time providing younger scientists at the beginning of their careers with a concise summary of what happened during the last 25 years, enriched with references to foster their own, individual studies of selected topics. The contributions are ordered by the date when the award was received, except for the introductory piece, a poem written by our valued colleague, Prof. Archie Howie.

Finally, we extend our thanks to the companies that advertised in this booklet and helped finance it, allowing us to distribute it free of charge.

**Josef Zweck**
**(Past President)**

**Virginie Serin**
**(Secretary)**

**José Maria Valpuesta**
**(President)**

*Dear reader,*

*You may have wondered what the image "The EMS word cloud" on the previous page, stands for.*

*In short, it displays a so-called "word cloud", which is a computer-generated assembly of words found in a certain text. The frequency of words within this text is reflected by the size and colouring of the single words.*

*The word cloud has been generated using a free software, which can be found at https://tagcrowd.com/.*

*The text that was used to create the cloud was the "AIMS OF THE SOCIETY" section, taken from https://www.eurmicsoc.org/en/the_ems/whoarewe/thesociety/ and reflects quite nicely the main intentions and goals of our society. "applications", "award", "ems", "european", "member", "publications", "sciences/scientific" and "support" stick out clearly, but the word cloud is dominated by "microscopy" and "society".*

*So, the cloud represents nicely what EMS stands for, what it did successfully over the past 25 years in progressing efficiency and importance and what it will pursue in the future for the benefit of our members and microscopy.*

# On occasion of the EMS 25th anniversary, a list of current and previous executive board members is given below:

## Current Executive Board

### (2020 – 2024)

- President ..... Prof. Dr. José Maria Valpuesta
- Secretary ..... Prof. Dr. Virginie Serin
- Treasurer ..... Prof. Dr. Christian Schöfer
- Past President ..... Prof. Dr. Josef Zweck
- ECMA Representative ..... Kornelia Weidemann
- EMC2024 Chair ..... Prof. MD PhD Klaus Qvortrup
- Board Members ..... Prof. Dr. Cristiano Albonetti
  Prof. Dr. Lucy Collinson
  Prof. Dr. Randi Holmestad
  Prof. Dr. Agnes Kittel
  Prof. Dr. Saso Sturm
  Prof. Dr. Servet Turan
  Prof. Dr. Igor Weber

## Previous Executive Boards

### (2016 – 2020)

- President ..... Prof. Dr. Josef Zweck
- Secretary ..... Prof. Dr. Virginie Serin
- Treasurer ..... Prof. Dr. Christian Schöfer
- Past President ..... Prof. Dr. Roger Albert Wepf
- ECMA Representative ..... Rod Shipley
- EMC2020 Chair ..... Prof. MD PhD Klaus Qvortrup
- Board Members ..... Prof. Dr. Cristiano Albonetti
  Prof. Dr. Serap Arbak
  Prof. Dr. Randi Holmestad
  Prof. Dr. Agnes Kittel
  Prof. Dr. Peter Nellist
  Prof. Dr. José Maria Valpuesta
  Prof. Dr. Igor Weber

### (2012 – 2016)

- President ..... Prof. Dr. Roger Albert Wepf
- Secretary ..... Prof. Dr. Dominique (Nick) Schryvers
- Treasurer ..... Prof. Dr. Christian Schöfer
- Past President ..... Prof. Dr. Paul Midgley
- ECMA Representative ..... Dr. Stefan Kuypers
- EMC2016 Chair ..... Prof. Dr. Thierry Epicier
- Board Members ..... Prof. Dr. Serap Arbak
  Prof. Dr. Rik Brydson
  Prof. Dr. Maria Carmo-Fonseca
  Prof. Dr. Aleksandra Czyrska-Filemonowicz
  Prof. Dr. Randi Holmestad
  Prof. Dr. Pavel Hozak
  Prof. Dr. Joachim Mayer

## (2008 – 2012)

- President ..... Prof. Dr. Paul Midgley
- Secretary ..... Prof. Dr. Dominique (Nick) Schryvers
- Treasurer ..... Prof. Dr. Christian Schöfer
- Past President ..... Prof. Dr. Ueli Aebi
- ECMA Representative ..... Dr. Bob Hertsens
- EMC2012 Chair ..... Prof. Dr. Debbie Stokes
- Board Members ..... Prof. Dr. Serap Arbak
  Prof. Dr. Rik Brydson
  Prof. Dr. Aleksandra Czyrska-Filemonowicz
  Prof. Dr. Raija Sormunen
  Prof. Dr. Pavel Hozak
  Prof. Dr. Marie Cheynet

## (2004 – 2008)

- President ..... Prof. Dr. Ueli Aebi
- Secretary ..... Prof. Dr. Dominique (Nick) Schryvers
- Treasurer ..... Prof. Dr. Leo Ginsel
- Past President ..... Prof. Dr. José-Maria Carrascosa
- ECMA Representative ..... Dr. Bob Hertsens
- EMC2012 Chair ..... Prof. Dr. Joachim Mayer
- Board Members ..... Prof. Dr. Serap Arbak
  Prof. Dr. Rik Brydson
  Prof. Dr. Aleksandra Czyrska-Filemonowicz
  Prof. Dr. Pavel Hozak
  Prof. Dr. Marco Vittori Antisari

## (2000 – 2004)

- President ..... Prof. Dr. José-Maria Carrascosa
- Secretary ..... Prof. Dr. Eddi Wisse
- Treasurer ..... Prof. Dr. Heinz Gross
- Past President ..... Prof. Dr. Peter Hawkes

## (1998 – 2000)

- President ..... Prof. Dr. Peter Hawkes
- Secretary ..... Prof. Dr. Eddi Wisse
- Treasurer ..... Prof. Dr. Heinz Gross
- Future President ..... Prof. Dr. José-Maria Carrascosa

# Previous European Congresses

More information and images here: *https://www.eurmicsoc.org/en/meeting-calendar/emc-series/*

## (pre-EMS era)

1956 ..... Stockholm (European Regional Conference on Electron Microscopy. See *https://archive.org/details/electronmicrosco00euro/mode/2up*
1960 ..... Delft
1964 ..... Prague
1968 ..... Rome
1972 ..... Manchester
1976 ..... Jerusalem
1980 ..... The Hague
1984 ..... Budapest
1988 ..... York
1992 ..... Granada
1996 ..... Dublin

## (EMS era)

2000 ..... Brno
2004 ..... Antwerp
2008 ..... Aachen
2012 ..... Manchester
2016 ..... Lyon
2024 ..... Copenhagen

More on the history of EMS can be found in the EMS2013 Yearbook *(https://www.eurmicsoc.org/medias/files/02_association/03_documentation/01_yearbook/EMS-2013-COMPLET.pdf)* on pages 11 -12.

The yearbooks also contain the details and photographs of the corresponding executive board members: *(https://www.eurmicsoc.org/en/organisation/ems-documentation/yearbook/).*

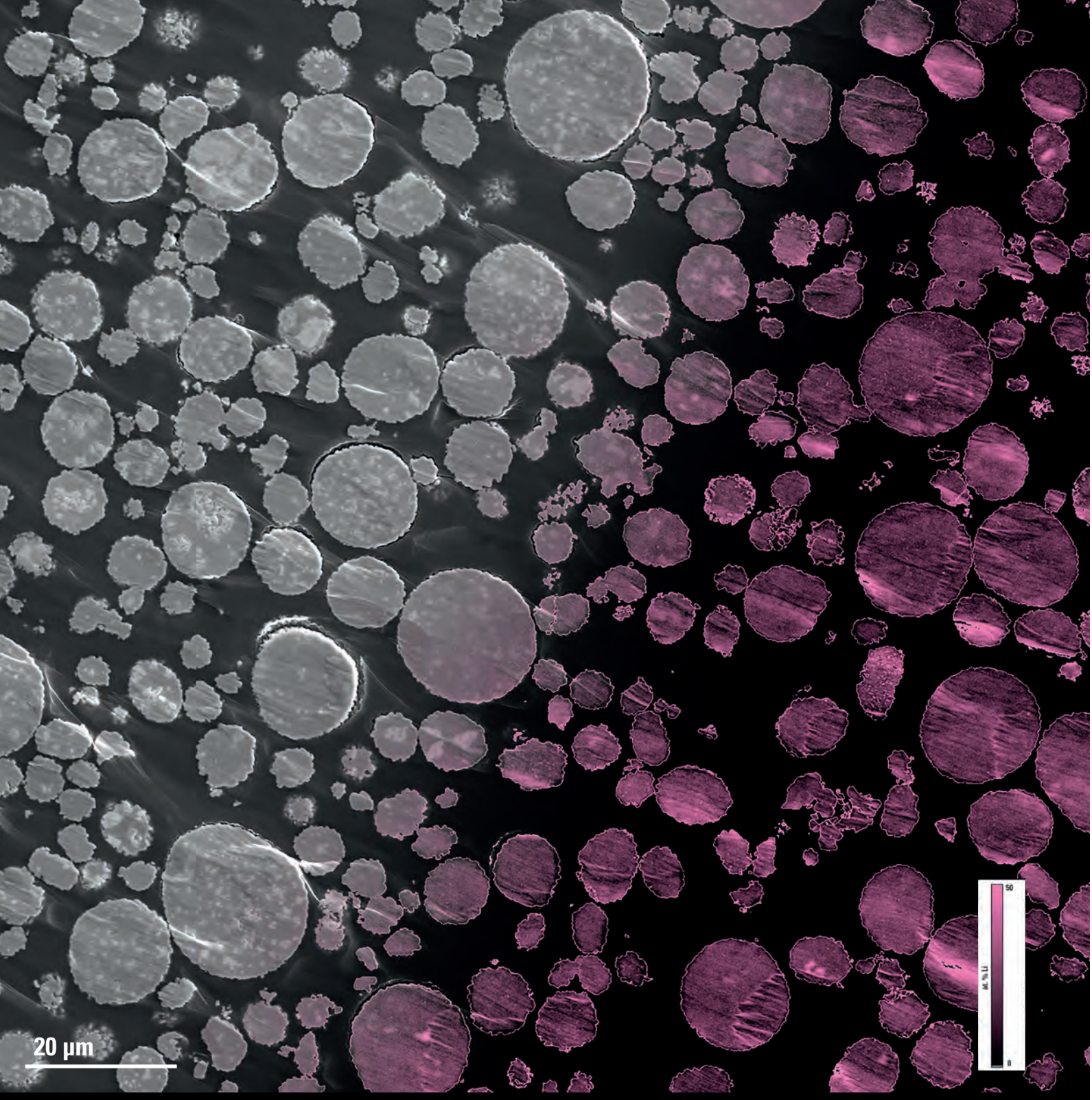


# 60 Years of Discovery

Celebrating 60 years of electron microscopy excellence, our journey has been one of relentless exploration and discovery. From unveiling intricate structures to driving technological breakthroughs, we've shaped scientific understanding. As we mark this milestone, we reaffirm our commitment to pioneering exploration, igniting curiosity, and inspiring innovation for the decades ahead.

## Enables the detection of lithium down to single-digit weight % levels

Cipher light element detection system reveals lithium distribution quantitatively in cathode material NMC 811 ($LiNi_{0.8}Mn_{0.1}Co_{0.1}O_2$); in this example, an accuracy better than 2 at. % was achieved. Cipher allows battery and alloy researchers to precisely identify lithium content and distribution by charge states and cycling conditions.

gatan.com

GATAN
AMETEK

# *Microscopy from Europe*

*When Hooke and Leeuwenhoek and Malpighi*
*Long battles with their early lenses waged*
*To bring first light to our microscopy*
*The whole of Europe found itself engaged!*
*Next Swammerdam, Linnaeus and R. Brown*
*Core truths of Nature's structure then tracked down.*

*And now three cryo-EM pioneers*
*Have added to the triumphs at Nobel,*
*That Europeans won in earlier years -*
*Zernike, Gabor, Ruska, Rohrer, Hell.*
*While lens correction and ptychography*
*Are so far sitting in the wings maybe.*

*Though National Societies have thrived*
*And grew success within their local scene,*
*Wisse and Baumeister a plan contrived*
*To launch the needed more wide-based regime.*
*Through sponsored meetings and its own Congress*
*We strengthen not supplant through EMS!*

*To teach and keep all Europe on its toes*
*For past and future, EMC be proud!*
*You spotlight where exciting action grows,*
*But please archive our abstracts in the cloud.*
*So twisted paths for history stay clear*
*Let steps to great discoveries appear!*

*Archie Howie*

**José María Valpuesta**
Centro Nacional de Biotecnología (CNB-CSIC), Madrid, Spain.

## CHAPERONINS

# More than 25 years of discoveries

Eukaryotic cells have developed numerous strategies to maintain protein homeostasis, the balance between synthesis, folding, trafficking and degradation of intracellular and extracellular proteins; imbalances of these contribute to the appearance of various pathologies including neurodegenerative disorders and cancer. Key players in this multifaceted set of processes are a large family of molecular chaperones, most of which are nanomachines that use ATP hydrolysis to induce structural changes that are subsequently used to assist in the folding, degradation or disaggregation of their client proteins.

Chaperonins (HSP60) are the only group of chaperones found in all kingdoms of life, and electron microscopy has been instrumental in the structural characterisation of this large family of macromolecular complexes. As early as 1980, electron images of the most studied chaperonin, GroEL from *E. coli*, revealed the characteristic two-ring structure, with each ring composed of seven identical subunits (Burton & Eisenberg, 1980) **(Fig. 1A)**. Different studies showed that folding takes place in the cavity and that there are two final conformations: an open one where the unfolded client protein is recognised and trapped; and the closed one where folding takes place. In the case of GroEL, closure of the cavity occurs upon binding of a small oligomer, GroES (generally termed cochaperonin; **Fig. 1A**), to the entrance of the cavity. This occurs after ATP binding and hydrolysis of the seven subunits of a ring. Cochaperonin binding blocks the entrance and forces the release of the client protein in the GroEL cavity, where folding takes place.

Not long after the discovery of GroEL, another type of chaperonin was found, leading to the creation of a general classification that categorized all chaperonins in two groups (Horwich & Willison, 1993): group I, which includes the eubacterial ones such as GroEL and those located in endosymbiotic organelles (e.g., mitochondria and chloroplasts); and group II, which includes all the chaperonins from archaea (thermosomes) and the one found in the eukaryotic cytosol.

The latter group turned out to be more complex, particularly because of the variable number of different subunits making up the ring structures (1-3 in the case of thermosomes, 8 for the eukaryotic chaperonin). The discovery of eukaryotic chaperonin in the early 1990s caused something of a stir in the field (see Ellis, 1992).

At about that time, I had returned to Spain after a postdoctoral stay at the Laboratory of Molecular Biology (Cambridge), where I had learnt the basics of cryoelectron microscopy (cryoEM) and image processing, under the supervision of Richard Henderson, one of the "fathers" of this technique and awardee of the Nobel Prize of Chemistry in 2017. On my return to Spain, I stopped working on membrane proteins and decided to work in the then-new field of chaperonins, in collaboration with José L. Carrascosa, who introduced electron microscopy image processing techniques in Spain.

From the very beginning I worked with the eukaryotic chaperonin, which has maintained two different names over the years: CCT (Chaperonin Containing TCP1 protein); or TRiC (T-complex protein-1 ring complex). My group was the first to publish a low-resolution structural characterisation of CCT using standard, negatively-stained electron microscopy images (Marco et al., 1994) **(Fig. 1B)**. At the low resolution of these early studies, CCT seemed very similar to GroEL, which by then had a solved crystallographic structure (Braig et al., 1994). Besides the number and composition of subunits, the major difference in CCT was that the closed conformation (like the rest of group II chaperonins) was generated by the presence

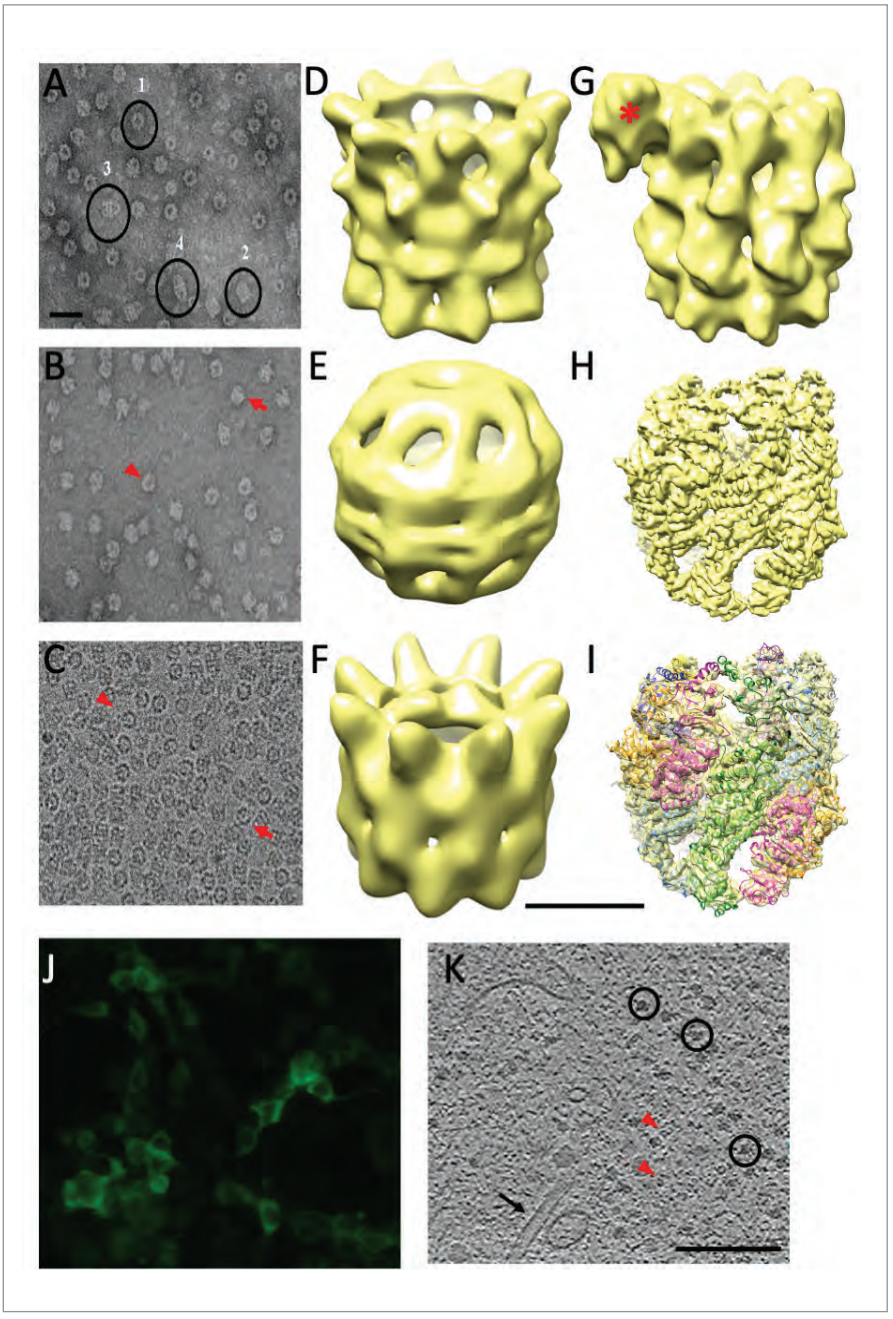


**Figure 1. (A)** A negatively-stained field of GroEL particles, with (1) showing an end-on view (revealing a cavity) and (2) a side view, while (3) shows a side view of a complex between GroEL and the cochaperonin GroES, and (4) shows a GroES molecule bound to each of the two GroEL rings. **(B)** A negatively-stained field of CCT particles, with the arrow pointing to a side view and the arrowhead to an end-on view. **(C)** A cryoelectron image of a vitrified sample of CCT. Arrow and arrowhead as in (B). **(D)** CryoEM 3D reconstruction of the CCT open conformation (Llorca et al., 1999a). **(E)** CryoEM 3D reconstruction of the CCT closed conformation (Llorca et al., 2000). **(F)** CryoEM 3D reconstruction of a complex between CCT and its client protein, actin (Llorca et al., 1999a). **(G)** CryoEM 3D reconstruction of a complex between CCT and a fragment of the chaperone Hsp70 (red asterisk) (Cuéllar et al., 2008). **(H)** CryoEM 3D reconstruction of CCT using state-of-the-art cryoEM technology. **(I)** The same view as in (H) showing the atomic model of CCT (all 16 subunits) docked into the 3D reconstruction. **(J)** Epifluorescence image of HEK293T cells expressing CCT, with one of its subunits (CCT3) labelled with the fluorescent protein GFP. **(K)** A section of a cryoET tomogram that shows, besides a microtubule (black arrow) and several ribosomes (black circles), the presence of CCT particles (red arrowheads). Scale bar in (A) represents 200 Å for A-C; Scale bar in (D-I) represents 100 Å; Scale bar in (K) represents 200 nm.

of an extra helical extension, which blocked the cavity upon ATP binding and hydrolysis in the CCT subunits.

Soon after the aforementioned publication on CCT, my group began a long and fruitful collaboration with the group of Keith Willison, then at the Institute of Cancer Research (London), which included not only electron microscopy but also biochemical and biophysical analysis of CCT. This was in the mid-1990s, and we had at that time acquired some basic equipment to carry out cryoEM experiments. Although the literal definition of cryoEM is “electron microscopy carried out at low temperatures”, it is actually more complicated than that; in its more developed form (established around the mid-1980s by the Nobel laureate Jacques Dubochet), it involves flash freezing the biological sample (e.g., a protein) so that the surrounding water molecules have no time to crystallise and remain in an amorphous (vitreous) state, which maintains the fine (atomic) structure of the target molecules **(Fig. 1C)**.

A low temperature (basically, $LN_2$ temperature) is maintained throughout the workflow, including storage (if needed) and data acquisition. For the latter, our 120 kV electron microscope (with a tungsten filament source) was equipped with a cryostage and an anti-contamination device that sought to prevent (without much success) contamination from the water molecules present in the microscope column. With this equipment, at the turn of the century we started the structural characterisation of CCT by cryoEM, which allowed us to determine, always at low resolution (20-25 Å), the general structure of the two main CCT conformations (open and closed) **(Fig. 1D and E)** (Llorca et al., 1999a; 2000).

We also showed that actin and tubulin, the major CCT clients, bind to the chaperonin in a very specific configuration

(Llorca et al., 1999b; 2000), unlike what happens with the much better characterised GroEL **(Fig. 1F)**.

This finding caused quite a stir, because it went against the "official line" dictated by some prominent scientists who proclaimed that CCT was no more than the eukaryotic equivalent of GroEL. Since then, it has been found that CCT not only guides protein folding, but also is active in quaternary interaction and regulation, serving as an important hub in the execution of various cellular processes. Another differential feature of CCT is its interaction with a plethora of cochaperones (PFD, PhLPs, TBCs) that direct the chaperonin towards specific client proteins and modulate its activity. Our group, again using cryoEM, was the first to structurally characterise the interaction of CCT with cochaperones like PFD and PhLP1 (Martín-Benito et al., 2002; 2004).

The subsequent cryoEM work benefited from the acquisition of a 200 kV electron microscope equipped with a field emission gun and a better vacuum system, which made water contamination less problematic (although always present). With this new equipment, the quality of our work improved enough to allow a more detailed determination of CCT interaction with different chaperones **(Fig. 1G)**, cochaperones and substrates (Cuéllar et al., 2008; Plimpton et al., 2015), but always at low-medium resolution (>10 Å), which was not enough to resolve the protein secondary structure. In truth, the promise of revolution in the field of structural biology that cryoEM seemed to offer in the early 1990s were not fulfilled: only a handful of structures of either large complexes (ribosomes) or of particles with a high symmetry order (icosahedral viruses) were determined at really high resolution.

This changed in the early 2010s when two technical advancements, one in hardware (direct electron detectors, with a much higher electron recording efficiency) and the other in software (better image classification methods based on maximum likelihood techniques), caused a commotion in the structural biology field that has rightly been termed "the resolution revolution". Although the new software was freely available (most of it had been developed by Academia), the new hardware was very expensive and only available to wealthy groups and national or international cryoEM facilities. Thanks to the latter, we were able to determine the high-resolution structure (4.0 Å) of CCT in the presence of a client protein, mLST8, the result of a fruitful and long-standing collaboration with the group of Barry Willardson (Brigham Young University, Provo, USA) (Cuéllar et al., 2019) **(Fig. 1H)**.

This level of resolution (which continues to improve in subsequent, unpublished works) allows the building of atomic models **(Fig. 1I)** that help to analyse interactions in fine detail, in this case between CCT and clients, or the chaperones and cochaperones that modulate its action. We have recently acquired state-of-the-art infrastructure that allow us not only to acquire high-resolution data from *in vitro*, purified samples such as CCT, but to study these complexes *in vivo*, in their cellular environment, using a set of techniques collectively termed cryocorrelative microscopy.

We believe these techniques are going to have an impact on structural cell biology as they allow the study of the dynamics of a given biological problem (e.g., the cellular arrangement of CCT complexes) using light microscopy and fluorescently tagged proteins, and structural analysis of the very same sample (a given cell or subcellular structure) at high (even atomic) resolution using cryoelectron tomography (cryoET) of that particular area. We are currently working in that direction by labelling CCT, finding suitable areas using cryoconfocal microscopy **(Fig. 1J)**, and using cryoscanning electron microscopy coupled to focused ion beam (cryoFIB-SEM), thinning this particular area to carry out cryoET **(Fig. 1K)**.

Though light and electron microscopy technologies have undergone a revolution in many ways, the study of biological problems such as chaperonin function does not come to an end, rather it gets more exciting. ■

## References


1. Braig K, Otwinowski Z, Hegde R, Boisvert DC, Joachimiak A, Horwich AL, Sigler PB (1994) Nature 371 (6498): 578–86.
2. Burton ZF, Eisenberg D (1980) **Arch Biochem Biophys** 205:478-88.
3. Cuéllar J, Martín-Benito J, Scheres SWH, Sousa R, Moro F, López-Viñas E, Gómez-Puertas P, Muga. A, Carrascosa JL, Valpuesta JM (2008) **Nat. Struct Mol Biol** 15, 858-864.
4. Cuéllar J, Ludlam WG, Tensmeyer NG, Aoba T, Dhavale M, Bueno T, Santiago C, Plimpton RL, Makaju A, Franklin S, Willardson BM, Valpuesta JM (2019) **Nat. Commun.** 10:2865
5. Ellis J (1992) Nature 358:191.
6. Horwich AL, Willison KR (1993) Philos Trans R Soc Lond B Biol Sci. 339:313-25.
7. Llorca O, Smyth MG, Carrascosa JL, Willison KR, Radermacher M, Steinbacher S, Valpuesta JM (1999a) **Nat Struct Biol** 6. 639-642.
8. Llorca O, McCormack E, Hynes G, Grantham J, Cordell J, Carrascosa JL, Willison KR, Fernández JJ, Valpuesta JM (1999b) **Nature** 402, 693-696.
9. Llorca O, Martín-Benito J, Ritco-Vonsovici M, Grantham J, Willison KR, Carrascosa JL, Valpuesta JM (2000) **EMBO J** 19, 5971-5979.
10. Llorca O, Martín-Benito J, Grantham J, Ritco-Vonsovici M, Willison KR, Carrascosa JL, Valpuesta, JM (2001) **EMBO J** *20*, 4065-4075.
11. Marco S, Carrascosa JL, Valpuesta JM (1994) **Biophys J**, 67, 364-368,
12. Martín-Benito J, Boskovic J, Gómez-Puertas P, Carrascosa JL, Simons C, Lewis SA, Bartolini F, Cowan NC, Valpuesta JM (2002) **EMBO J** 21, 6377-6386.
13. Martín-Benito J, Bertrand S, Hu T, Ludtke PJ, McLaughlin JN,Willardson BM, Carrascosa JL,Valpuesta JM (2004) **PNAS USA** 101, 17410-17415.
14. Plimpton RL, Cuéllar J, Lai CWJ, Aoba T, Makaju A, Franklin S, Mathis AD, Prince JT, Carrascosa JL, Valpuesta JM, Willardson BM (2015) "Structures of the Gβ-CCT and PhLP1–Gβ-CCT complexes reveal a mechanism for G-protein β-subunit folding and Gβγ dimer assembly" **PNAS USA** 112, 2413-2418.

JEOL

**Scientific/Metrology Instruments**

FIB-SEM System

# JIB-PS500i

*High Performance FIB-SEM from JEOL technologies*

- Automatic TEM sample preparation
- 3D acquisition (imaging, EDS, EBSD)
- New EOS design with dual mode operation
- Check & Go directly from FIB to TEM
- Omniprobe integrated inside GUI

**STEMPLING 2**

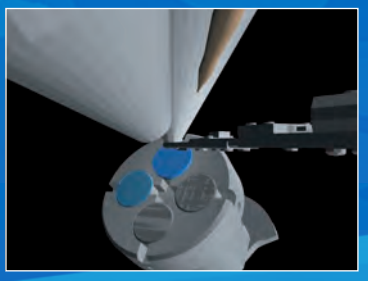

**New stage design**

**Check & Go directly from FIB to TEM**

**Large specimen chamber**

**www.jeol.com**

# ADVANCING

## SAMPLE PREP BY

# INNOVATING

## TECHNOLOGY

**X-Prep®**
High Precision
Mechanical Thinning

Precision interposer(IO)
targeting through
FR4 6x6 & 2x2, 1.8 mm deep

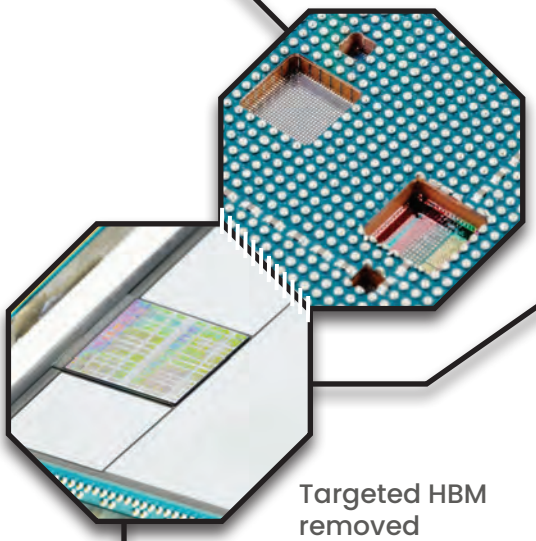

Targeted HBM
removed

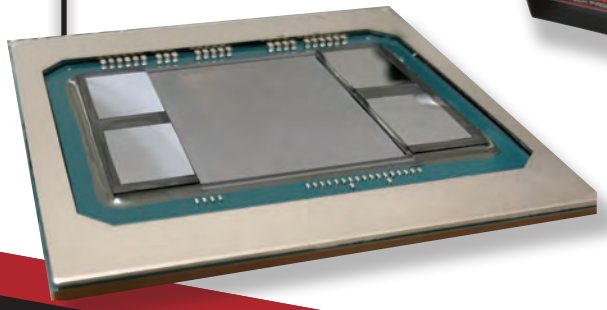

Large, targeted die
thinning - 5 µm RST


ALLIED
HIGH TECH PRODUCTS, INC.

Find your Sample Prep Solutions at: www.alliedhightech.com | info@alliedhightech.com
800.675.1118 US/Canada | 310.635.2466 Worldwide

**Paul Midgley**
Department of Materials Science and Metallurgy,
University of Cambridge, 27 Charles Babbage RoadCambridge, CB3 0FS, United Kingdom

# Happy **Silver Jubilee**!

Around about the time, 25 years ago, when the EMS was being founded, thoughts in my group were turning towards how best to image materials at the nanoscale in three dimensions. The idea of using tomography (3D imaging) in the TEM was of course not new, it had been a key method in structural biology for some years – either using a tilt series or through single particle analysis - and had also begun to be applied to some soft (generally non-crystalline) materials, especially polymers. The electron tomography technique ca. 25 years ago was based very much on using bright-field conventional TEM imaging and on the assumption that the signal in the image was a monotonic (close to linear) function of projected thickness. Such an assumption lies at the heart of many tomographic reconstruction processes. By acquiring images at different specimen tilts across a 'tilt series' the ensemble of projections (Radon transforms) and their inverse can then be used to recover the 3D structure (tomogram).

However to be used more universally in materials science there was a problem to overcome. Most of the specimens analysed by materials scientists are crystalline in nature, often composed of strongly scattering atoms and, as such, highly non-linear 'diffraction contrast' may dominate BF (and DF) TEM images; such non-linear contrast makes using such images difficult, if not impossible, for tomographic reconstruction. To overcome this, a new technique emerged [1] based on STEM tomography (initially using HAADF images). With a sufficiently large inner angle (ca. 50mrad or more) STEM HAADF images contain very little (of the unwanted) diffraction contrast and the HAADF signal varies, to a good approximation, monotonically with thickness, up to typically a few hundred nm.

In addition, STEM HAADF images encode information about the sample composition (the intensity is approximately proportional to the square of the atomic number) and so provides a (semi-quantitative) means to map changes in composition in 3D as well as a detailed investigation of the sample morphology. (It should be mentioned that an equivalent imaging mode in TEM exists, ADF-TEM [2], but over the years the STEM technique has proven considerably more popular.)

The success of 3D imaging using HAADF STEM tomography for materials science applications quickly led to other tomography techniques being developed, which combined STEM imaging with other, analytical techniques, adding further 'dimensions' to the data – what is now sometimes called 'multi-dimensional electron microscopy'. These included:

(i) STEM tomography plus analytical techniques such as EDX and core-loss EELS so that at each pixel in the 2D real space scan, a full EDX or EELS spectrum is acquired. Through a tilt series of such 'spectrum-images' it is possible to reconstruct a 3D elemental or phase map [3].

(ii) STEM tomography with electron diffraction whereby a 2D diffraction pattern is acquired at every real space pixel revealing how the local crystallography varies in 3D – and in one example led to a novel 3D orientation relationship found in a Ni base superalloy [4].

(iii) STEM tomography with low loss EELS. Low-loss EELS can provide information that is complementary to optical spectroscopy and as an example enabled the localized surface plasmon resonances of a silver nanocube to be reconstructed, for the first time seeing these near-field excitations in three dimensions [5]. Similar work has now been achieved with ultra-high energy resolution and visualizing phonon excitations in 3D [6].

Although STEM imaging proved highly applicable across many crystalline materials, with careful acquisition, conventional imaging, and in particular weak-beam DF imaging, could reveal the 3D distribution of dislocations. To do this successfully, a tilt series of weak beam images of dislocations has to be acquired with (near-) constant deviation parameter (excitation error) for whichever Bragg reflection is used [7]. Whilst it proved successful, keeping the acquisition conditions constant is experimentally very demanding. Later work returned to use STEM and 'medium-angle' annular dark-field imaging in which the contrast in the image is composed, in effect, of a summation of multiple DF images (recorded at different deviation parameters). The net effect of those superimposed DF images was to enhance the dislocation contrast, and minimize other unwanted diffraction contrast, such as thickness fringes or bend contours [8], to provide clear 3D images of dislocation networks and circumventing the difficulties of the weak-beam technique.

Electron holography allows imaging of electrostatic and magnetic fields using the TEM. Combining with tomography enabled the 3D visualization of, for example, p-n junctions in semiconductor devices [9] and, recently using a newly developed wavelet-based algorithm, an improved reconstruction of 3D magnetic fields [10].

STEM-based tomography in materials science is now a routine technique. Other groups have pushed the resolution – and atomic electron tomography is now possible [11], complementing the remarkable power of the atom probe microscope. Others still have developed ever-more powerful algorithms to both cope efficiently with large data sets and to minimize artefacts from the somewhat limited tilt series (typically 50-100 images over, say, +/- 70°).

Looking back at the ca. 25 years of electron tomography in my group, it has struck me how I have benefitted enormously from the hard work of many students and postdocs from around the world coming to Cambridge to work with me, but especially those from other European countries. The relative ease with which researchers could move to/from the UK to/from the rest of Europe and the opportunities offered by European-based funding were important factors that helped in the development of electron tomography. We still await the full impact of Brexit but what remains crucial going forward is that scientific and cultural links across Europe should remain strong, and 'building bridges' wherever we can should remain paramount. Organizations such as the EMS are crucially important in bringing people together, fostering scientific debate and discussion and highlighting common European goals.

I had the very great pleasure and honour of being President of the EMS from 2008-2012 (and then Past-President until 2016). In that time the Society grew in number as the EM community as a whole grew, both in

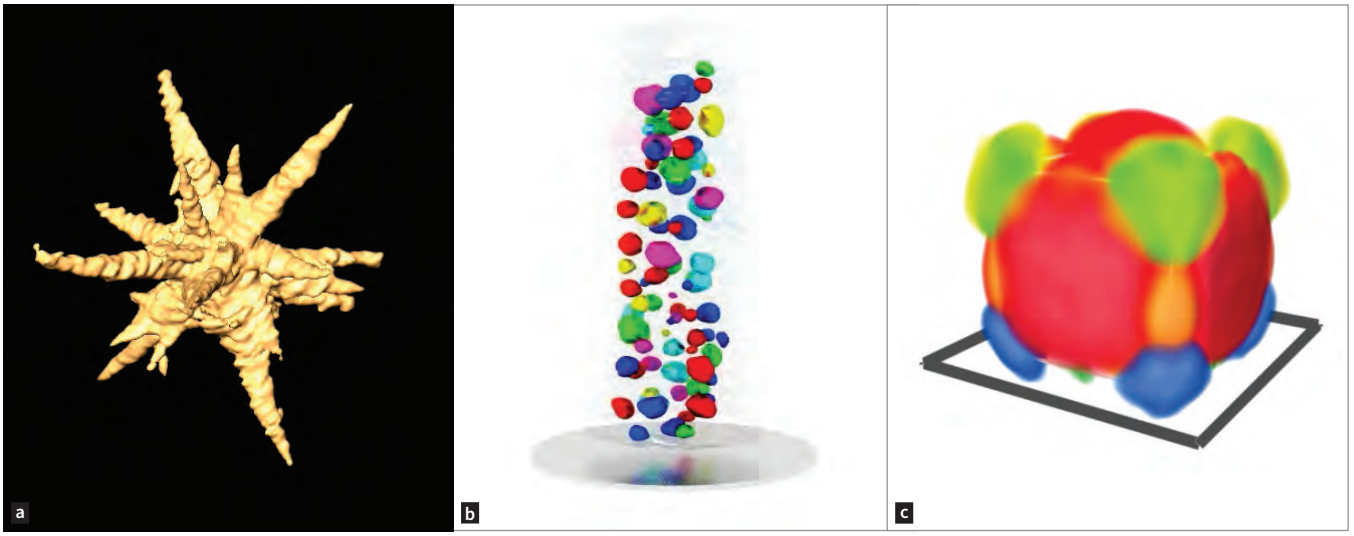


**Figure 1.** 3D tomographic reconstructions of (a) a CdTe 'multipod' using HAADF-STEM imaging; (b) precipitates in a Ni base superalloy using STEM-EDX tomography [3]; (c) localized surface plasmons on the surface of a Ni nanocube using low loss EELS tomography [5].

the life sciences and in materials science. It was a joy to be invited to different European countries to see the strength of European microscopy, the development and application of new techniques and the real sense of community. The Manchester-based EMC in 2012, at the end of my tenure as President, is one I'll always remember with great fondness, and particularly the Congress Dinner at the home of Manchester United, Old Trafford! It is very exciting that the European community of microscopists get a chance to meet once again in person in Copenhagen at EMC2024, as always an opportunity to meet old friends, make new contacts and hear and see great science.

Many congratulations to the EMS on its silver jubilee, I look forward to the next 25 years of European microscopy and in celebrating the EMS golden jubilee in 2048! ■

## References


1. Midgley, PA et al, Chem. Commun. (2001) 907-908
2. Bals S et al, Adv. Mater. (2006) 18, 892–895
3. Rossouw D et al Acta Mat (2016) 107, 229-238
4. Eggeman A et al Nat Commun (2015) 6 7267
5. Nicoletti O, et al, Nature (2013) 502 80-84.
6. Li X et al, Science (2021) 371 1364-1367.
7. Barnard JS et al Science (2006) 313(5785) 319.
8. Sharp JH et al J Phys: Conf Ser (2008) 126 012013
9. Twitchett-Harrison AC Nano Lett. (2007) 7 2020
10. Lewis GR et al Ultramicroscopy (2023) 253 113804.
11. Van Aert S et al Nature (2011) 470 374-377


**Koji Yonekura [1, 2], Saori Maki-Yonekura [1, 2]**

[1] Biostructural Mechanism Laboratory, RIKEN SPring-8 Center, 1-1-1 Kouto, Sayo, Hyogo 679-5148, Japan
[2] Institute of Multidisciplinary Research for Advanced Materials,
Tohoku University, 2-1-1 Katahira, Aoba-ku, Sendai 980-8577, Japan

## 2009 ERNST-RUSKA-PRIZE

# Elucidating the Mechanisms of Biological Macromolecular Machines by Cryo-Electron Microscopy

Single particle cryo-EM has made significant advancements in the last decade. It has now achieved what is known as atomic resolution, where individual atoms are visualized as isolated spherical entities [1-2-3]. Furthermore, it has enabled the measurement of charges in acidic amino acids and chemical bonding between hydrogen and bonded non-hydrogen atoms [3]. These remarkable achievements have been made possible by the introduction of direct electron detectors to the field. These detectors provide high-quality real images of protein molecules embedded in a thin layer of vitreous ice.

In 2003, approximately a decade before the development of the direct electron detector, we reported the structure of the bacterial flagellar filament using cryo-EM **(Figure)**. The bacterial flagellar filament serves as a helical propeller for bacterial locomotion and is composed of a single protein, flagellin. At that time, images of frozen-hydrated

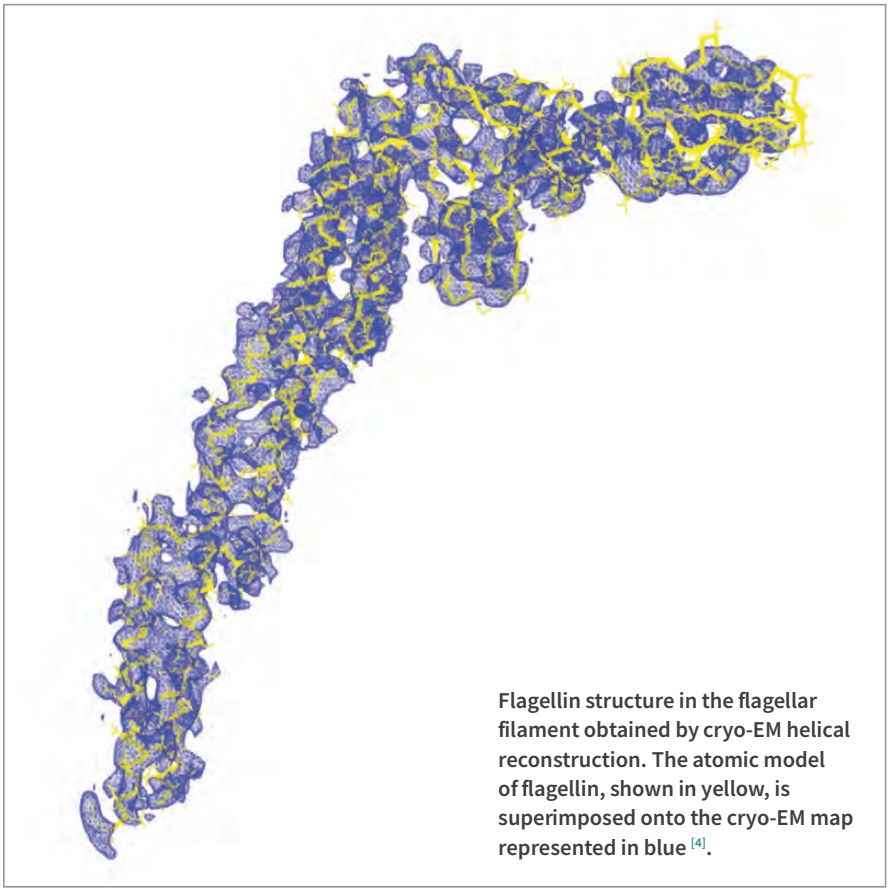

**Flagellin structure in the flagellar filament obtained by cryo-EM helical reconstruction. The atomic model of flagellin, shown in yellow, is superimposed onto the cryo-EM map represented in blue [4].**

proteins were recorded on photographic film. We utilized the helical symmetry of the flagellar filament to reconstruct its three-dimensional structure and also developed various software programs to achieve higher-resolution helical reconstruction [4-5-6-7-8]. The resulting cryo-EM map, reconstructed at a resolution of 4 Å from approximately 40,000 molecular images, revealed the twists of α-helices and bulky side chains **(Figure)**. We then constructed an atomic model based on this first high-resolution cryo-EM structure obtained through bright-field electron imaging **(Figure)**. The study revealed intricate molecular packing and a mechanism for the stabilization of the filament. More importantly, it demonstrated that cryo-EM image analysis can yield a three-dimensional density map that is adequate for constructing an atomic model.

We also analyzed the tip of the flagellar filament using single-particle cryo-EM. The growth of the flagellar filament occurs at its distal end by the self-assembly of flagellin transported from the cytoplasm through the narrow central channel. The cap at the growing end is essential for the filament growth, remaining stably attached while permitting the flagellin insertion. The obtained cryo-EM structure provided insights into the dynamical mechanism of filament growth facilitated by the cap proteins [9, 10]. ■

## References


1. K. M. Yip, N. Fischer, E. Paknia, A. Chari, H. Stark, Atomic-resolution protein structure determination by cryo-EM. *Nature* **587**, 157–161 (2020).
2. T. Nakane et al., Single-particle cryo-EM at atomic resolution. *Nature* **587**, 152–156 (2020).
3. S. Maki-Yonekura, K. Kawakami, K. Takaba, T. Hamaguchi, K. Yonekura, Measurement of charges and chemical bonding in a cryo-EM structure. *Commun. Chem.* **6**, 98 (2023).
4. K. Yonekura, S. Maki-Yonekura, K. Namba, Complete atomic model of the bacterial flagellar filament by electron cryomicroscopy. *Nature* **424**, 623 - 650 (2003).
5. K. Yonekura, C. Toyoshima, Structure determination of tubular crystals of membrane proteins. III. Solvent flattening. *Ultramicroscopy* **84**, 29 – 45 (2000).
6. K. Yonekura, C. Toyoshima, S. Maki-Yonekura, K. Namba, GUI programs for processing individual images in early stages of helical image reconstruction. --- for high-resolution structure analysis. *J. Struct. Biol.* **141**, 184 – 194 (2003).
7. K. Yonekura, S. Maki-Yonekura, K. Namba, Building the atomic model for the bacterial flagellar filament by electron cryomicroscopy and image analysis. *Structure* **13**, 407 – 412 (2005).
8. K. Yonekura, C. Toyoshima, Structure determination of tubular crystals of membrane proteins. IV. Distortion correction and its combined application with real-space averaging and solvent flattening. *Ultramicroscopy* **107**, 1141 – 1158 (2007).
9. K. Yonekura, S. Maki et al., The bacterial flagellar cap as the rotary promoter of fagellin self-assembly. *Science* **290**, 2148 – 2152 (2000).
10. S. Maki-Yonekura, K. Yonekura, K. Namba, Domain movements of HAP2 in the cap-filament complex formation and growth process of the bacterial flagellum. *Proc. Natl. Acad. Sci. USA* **100**, 15528 – 15533 (2003).

**Wolfgang Baumeister**
Max-Planck-Institute of Biochemistry, Am Klopferspitz 18, 82152 Martinsried, Germany

# **Studying macromolecules** in their natural habitats by cryo-electron tomography

Traditionally, structural biologists approach the complexity of cellular proteomes in a reductionist manner [1]. Cells are taken apart and their molecular components are purified and studied one-by-one using the experimental tools structural biologists have at their disposal, such as X-ray crystallography or cryo EM single particle analysis. Powerful as these methods are, all information about context and interaction networks is irrecoverably lost when macromolecules are released from their functional cellular environments. Hence, there is a compelling need for methods that allow the visualization of macromolecular and supramolecular structures *in situ*, i. e. in unperturbed cellular environments. Cryo-electron tomography allows to do that: It combines the power of high-resolution three-dimensional imaging with the best structural preservation that is physically possible to achieve.

Although the physical principles underlying electron tomography are relatively simple, putting them into practice has been challenging. One has to reconcile the radiation sensitivity of biological material embedded in vitreous ice with the need to expose the sample multiple times to the electron beam in recording a tilt series needed for three-dimensional reconstructions. This can be achieved by taking advantage of the principle of dose fractionation, i. e. distributing the allowable cumulative dose over as many projection images as possible and by automating the process of image acquisition. We began to develop such procedures in the late nineteeneighties [2,3] and, in the face of strong skepticism, we could demonstrate in 1995 the feasibility of doing cryo-ET [4]. Initially, cryo ET could only be used to visualize molecular landscapes in small objects (< 1 µm), such as prokaryotic cells or viruses [5, 6]. Eukaryotic cells are much larger and not sufficiently electron transparent for imaging them in their entity. Only thin peripheral regions or appendages were accessible to cryo ET [7, 8].

This changed with the advent of Cryo-Focused Ion-Beam milling (cryo-FIB milling) [9] cutting thin slices through cells that cryo-ET can peer into. This has opened up new perspectives for studying the molecular sociology of cells [10, 11]. Essentially it has created a new field, structural biology *in situ*, which meanwhile has provided unprecedented glimpses of the nanoscale architecture of cells [12].

It is now possible to visualize macromolecules such as ribosomes or proteasomes in their functional cellular context [13, 14] and in favorable cases, i. e. when sufficiently large and abundant, subvolume averaging allows to bring resolution well into subnanometer range [15]. Alternatively, high-resolution experimental structures, where they exist, can be docked computationally into medium resolution (1 to 2 nm) tomograms. Also predictive models as generated by AI methods such as Alpha-Fold can be used in integrative approaches for 'upgrading' the tomograms.

For realizing the full potential of cryo ET and for fulfilling the promises of visual proteomics, i. e. the comprehensive description of cellular proteomes, populated by myriads of molecular

species further advances on several frontiers are needed [16]. New optical devices such as contrast enhancing phase plates will improve the quality of the primary data and thereby facilitate their interpretation. The biggest challenge is the identification and annotation of all the densities, large and small in the tomograms. The physical integration of instruments for Correlative Light-Electron Microscopy (CLEM) and cryo-FIB milling along with automation will accelerate the workflow and improve throughput. Machine learning tools are beginning to revolutionize image processing and help to extract a maximum of information from tomograms even when data quality is compromised [17]. ■

## References


1. *Asano S., Engel B.D., Baumeister W.: In Situ Cryo-Electron Tomography:* A Post-Reductionist Approach to Structural Biology, J Mol Biol., **428**(2 Pt A):332-343 (2016)
2. *Dierksen, K., D. Typke, R. Hegerl, A.J. Koster, Baumeister, W.:* Towards automatic electron tomography. Ultramicroscopy **40**, 71-87 (1992)
3. *Dierksen, K., D. Typke, R. Hegerl, Baumeister, W.:* Towards automatic electron tomography. II. Implementation of autofocus and low-dose procedures. Ultramicroscopy **49**, 109-120 (1993)
4. *Dierksen, K., D. Typke, R. Hegerl, J. Walz, E. Sackmann, Baumeister, W.:* Three-dimensional structure of lipid vesicles embedded in vitreous ice and investigated by automated electron tomography. Biophys. J. **68**, 1416-1422 (1995)
5. *Grünewald, K., P. Desai, D.C. Winkler, J.B. Heymann, D.M. Belnap, W. Baumeister, Steven, A.C.:* Three-dimensional structure of Herpes Simplex virus from cryo-electron tomography. Science **302**, 1396-1398 (2003)
6. *Kürner, J., A.S. Frangakis, Baumeister, W.:* Cryo-electron tomography reveals the cytoskeletal structure of spiroplasma mellifierum. Science **307**, 436-438 (2005)
7. *Medalia, O., I. Weber, A.S. Frangakis, D. Nicastro, G. Gerisch, Baumeister, W.:* Macromolecular architecture in eukaryotic cells visualized by cryoelectron tomography. Science **298**, 1209-1213 (2002)
8. *Medalia, O., M. Beck, M. Ecke, I. Weber, R. Neujahr, W. Baumeister, Gerisch, G.:* Organization of actin networks in intact filopodia. Curr. Biol. **17**, 79-84 (2007)
9. *Villa, E., Schaffer, M., Plitzko, J.M., Baumeister, W.:* Opening Windows into the Cell: Focused-Ion-Beam Milling for Cryo-Electron Tomography, Current Opinion in Structural Biology **23**:1-7 (2013)
10. *Robinson, C.V., A. Sali, Baumeister, W.:* The molecular sociology of the cell. Nature **450**, 973-982 (2007)
11. *Mahamid J., Pfeffer S., Schaffer M., Villa E., Danev R., Cuellar L.K., Förster F., Hyman A.A., Plitzko J.M., Baumeister, W.:* Visualizing the molecular sociology at the HeLa cell nuclear periphery, Science, **351**(6276):969-72 (2016)
12. *Baumeister W.: Cryo-electron tomography:* A long journey to the inner space of cells, Cell, **185**(15):2649-2652 (2022)
13. *Brandt, F., L.-A. Carlson, F.U. Hartl, W. Baumeister, Grünewald, K.*: The three-dimensional organization of polyribosomes in intact human cells. Mol. Cell **39**, 560-569 (2010)
14. *Asano S., Fukuda Y., Beck F., Aufderheide A., Förster F., Danev R., Baumeister, W.:* Proteasomes. A molecular census of 26S proteasomes in intact neurons, Science, **347**(6220):439-42 (2015)
15. *Tegunov, D., Xue, L., Dienemann, C., Cramer, P., Mahamid, J.:* Multi-particle cryo-EM refinement with M visualizes ribosome-antibiotic complex at 3.5 Å in cells, Nature meth. **18**:186-193 (2021)
16. *Bäuerlein F., Baumeister W.:* Towards Visual Proteomics at High Resolution, J. Mol. Biol., **433**(20):167187 (2021)
17. *Moebel E., Martinez-Sanchez A., Lamm L., Righetto R.D., Wietrzynski W., Albert S., Laviriere D., Fourmentin E., Pfeffer S., Ortiz J., Baumeister W., Peng T., Engel B.D., Kervrann C.:* Deep learning improves macromolecule identification in 3D cellular cryo-electron tomograms, Nat. Methods, **19**(1):129 (2021)



**Francisco Vega Ibáñez [1,2], Armand Béché [1,2,3], Jo Verbeeck [1,2,*]**

[1]University of Antwerp, EMAT, Groenenborgerlaan 171, 2020, Antwerp, Belgium.
[2]NANOlab Center of Excellence, University of Antwerp, Groenenborgerlaan 171, 2020 Antwerp, Belgium.
[3]Adaptem BV, Interleuvenlaan 63, 3001 Heverlee, Belgium
[*]jo.verbeeck@uantwerpen.be

# **Wavefront** Shaping the Future of Electron Microscopy

**ABSTRACT**

**This report presents the progress in bringing electrostatic phase plates for electrons to reality in the transmission electron microscope (TEM). We survey potential applications of these devices and demonstrate the capabilities of our current state-of-the-art 48-element programmable phase plate for coherent electron waves consisting of chip-based microscopic electrostatic elements. This brings the highly successful concept of wavefront shaping from light optics into the realm of electron optics and provides an essential new degree of freedom to tailor the quantum state of electron waves.**

## Introduction: Bringing adaptive optics to the electron world

If a wave is the carrier of information, controlling the waveform is the key to communication. People talk by creating and shaping sound waves in forms that can be mutually understood. Mobile phones encode data in electromagnetic waves by carefully constructing their spectral content.

In 1924, de Broglie introduced the idea that accelerated particles could also show wave properties. This discovery is at the heart of electron microscopes that can reveal the detailed atomic structure of materials by encoding this information in electron waves while flying through very thin slabs of materials before being recorded on some detector. However, trying to reveal more information from ever smaller volumes of the sample has limits, as the amount of energy exchanged in the interaction will start to degrade the material we would like to observe.

Just as in telecommunication, it becomes essential to think about the most efficient or robust way to transmit the desired information contained in the sample to the receiver/detector.

The trend in microscopy has been up till now to maximize the attainable spatial resolution up to the point where we can routinely reach spatial resolution below the fundamental Bohr radius. This makes it unlikely that further improvements will reveal a fundamentally new level of detail (at least in 2D projection).

However, having the ability to control the wavefront or phase of the electron beam freely, creating electron probe shapes that are unattainable with conventional round apertures could offer alternative ways to "interrogate" a sample and make it reveal the information we are seeking for.

This idea is commonly applied in, e.g., the telecommunications and light optics field. Indeed, the spatial and time-dependent control over the phase of coherent waves has created a breakthrough in many research fields ranging from acoustics and telecommunications [1-3], radar [4], radio and light astronomy [5,6], and many more [7].

Tunable electron optics, in the form of electron lenses, have been part of electron microscopy from the first instrument by Ernst Ruska and collaborators in the early 1930s [8]. Indeed, the ability to tune the strength of a

lens or stigmator by simply changing the current is one of the very convenient features of an electron microscope and forms the basis of all modern instruments.

Expanding on this idea, a series of multi-pole lenses have allowed for the correction of the inevitable lens aberrations occurring in round magnetic lenses under the form of aberration correctors [9-11], which is undoubtedly the most significant breakthrough in modern electron microscopy. However, these tunable electromagnetic elements cannot reproduce entirely what a spatial light modulator [12] can do for light optics regarding arbitrary wavefront shapes, speed, drift, versatility, and automatisation.

Aiming to bridge this gap between light and electron optics, we have put much effort into bringing the fast and versatile wavefront shaping capabilities of a spatial light modulator into the field of electron beams, arriving at a first proof of concept in 2018, where we showed the viability of the implementation on a 2x2 array of individual electrostatic phase shifters (pixels) [13]. This concept has been recently expanded into the current state-of-the-art design with 48 individually programmable pixels, shown in **Figure 1** along the 2x2 version [14].

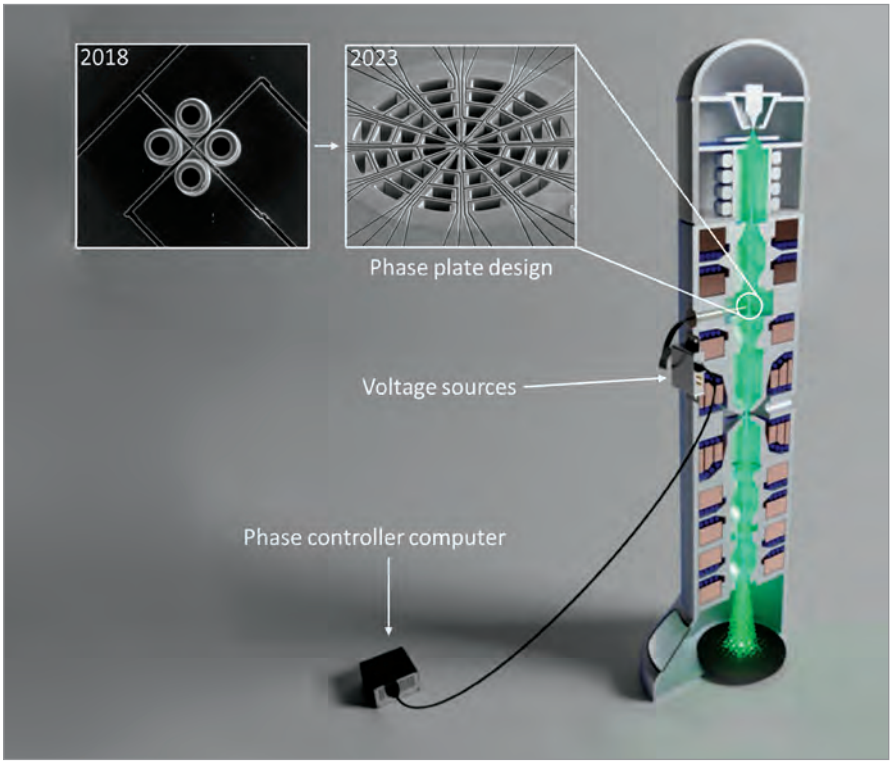


**Figure 1. Implementation of the electrostatic phase plate in the electron microscope. Our 2018 design has been improved to the current state-of-the-art phase plate (2023), controlled by a phase controller computer that sends commands to the voltage sources for each pixel.**

## Electron beam shaping: Wavefront designer

This device allows us to shift focus from making the smallest possible probe to making a series of well-constructed, non-trivial probe shapes to interrogate the sample with the newly gained degrees of freedom. **Figure 2** shows an experimental demonstration of this concept where the phase plate was inserted into the sample plane of a TEM at 200kV, and the far-field diffraction patterns of various phase-modulated electron waves were recorded. These patterns form rather complex phase configurations that can be used as a basis set to optimize the information transfer between the sample and the electron beam intensity at a specific detector plane. Some potential applications of exotic beams or structured illumination have already been proposed in electron microscopy, expanding on standard methods such as electron energy loss spectroscopy (EELS) [15], ptychography [16], and ghost imaging [17].

## Adaptive Probe Correction: User-free optimisation

The fast and hysteresis-free response of the electrostatic phase plate lends itself ideally to automating the tedious tuning process that is still common in even the most advanced instruments. One example could be the automatic improvement of image contrast (or alternative figure of merit describing specific features in an image).

The 48 individual phase elements, in combination with a synchronised control loop, can be left to solve a particular “question” we want to get from our sample, i.e., maximise contrast, or enhance a specific edge in a spectrum. A proof of concept of this optimisation scheme is shown in **Figure 3**, where we set the phase plate inserted in the C2 aperture plane of a ThermoFisher Scientific Titan microscope, to automatically sharpen the image of a probe **(Figure 3a)** or correct a deliberately defocused high-angle annular dark field (HAADF) image **(Figure 3b)**. The basic optimisation workflow is shown in **Figure 3c**.

The applications mentioned above serve as early proof of concept examples and are just some of the many possible measurement schemes we are currently exploring. Taking inspiration from its light optics counterpart, we envision many more opportunities for programmable phase plates in electron microscopy (and other fields which take advantage of coherent electron beams).

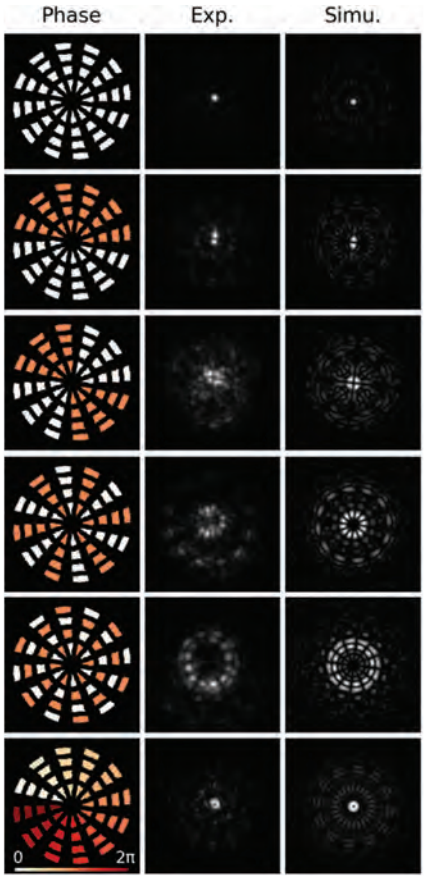


**Figure 2.** **Experimental realisation of exotic beams. The left column shows the phase configuration sent to the device, while the middle and left columns show the experimental and simulated image of the probe, respectively.**

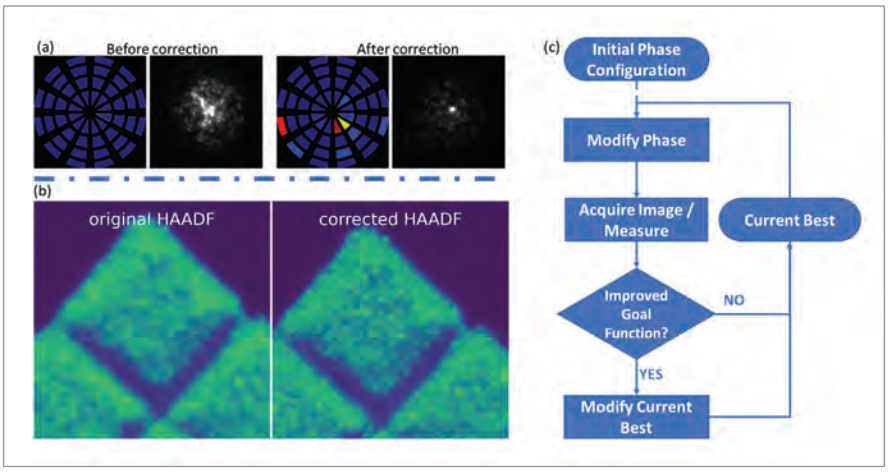


**Figure 3.** **Demonstration of the automated correction using an electrostatic phase plate on the image of the probe (a) and a HAADF image (b). The automated workflow is shown in (c).**

## Conclusion: Present and Future of electron wave shaping

We reported the implementation of an electrostatic phase plate for electrons in the electron microscope. This opens up a new "language" to interrogate our samples, potentially yielding an optimal information transfer.

Furthermore, we show the capability of the setup to reach fully automated schemes that can further improve the experimental versatility, ease of use, and time to result of the instrument, possibly increasing its adoption outside focused research centers. Furthermore, the device poses a compact, low-power, stable, and rapidly switching solution for electron wavefront shaping.

Future development includes improvements of hardware and software, as well as exploration of novel applications that might emerge.

The experimental work presented in this text can be traced back to a plenary lecture delivered by JV back in 2011 at the EMC in Lyon. What once could have been seen as a conceptual "day-dreaming" exercise or food for thought is now starting to become an experimental reality. Seeing the amount of effort and time needed to reach this point is humbling. Nonetheless, there is still a fascinating journey ahead of us with many potential applications to be developed. ■

## ACKNOWLEDGEMENTS

*JV and AB acknowledge funding from an ERC proof of concept project DLV-789598 ADAPTEM, as well as a University IOF proof of concept project towards launching the AdaptEM spin-off and the eBEAM project, supported by the European Union's Horizon 2020 research and innovation program FETPROACT-EIC-07-2020: emerging paradigms and communities. This project has received funding from the European Union's Horizon 2020 research and innovation program under grant agreement No 823717 – ESTEEM3 and via The IMPRESS project from the HORIZON EUROPE framework program for research and innovation under grant agreement n.101094299. FV and JV acknowledge funding from G042820N 'Exploring adaptive optics in transmission electron microscopy.'*

## References

1. Michel, U. (2006). In 1st. Berlin Beamforming Conference.
2. Davids, N., Thurston, E. G., & Mueser, R. E. (1952). The Journal of the Acoustical Society of America, 24(1), 50-56.
3. Billingsley, J., & Kinns, R. (1976). Journal of Sound and Vibration, 48(4), 485-510.
4. Brennan, L. E., & Reed, L. S. (1973). IEEE transactions on Aerospace and Electronic Systems, (2), 237-252.
5. Roddier, F. (Ed.). (1999). Adaptive optics in astronomy.
6. Barnbaum, C., & Bradley, R. F. (1998). The astronomical journal, 116(5), 2598.
7. Bliokh, K. Y., et al., (2023). arXiv preprint arXiv:2301.05349.
8. Ruska, E. (1987). Reviews of modern physics, 59(3), 627.
9. Haider, M., Braunshausen, G., & Schwan, E. (1995). Optik (Stuttgart), 99(4), 167-179.
10. Haider, M., et al., (1998). Nature, 392(6678), 768-769.
11. Rose, H. (1990). Optik, 85, 19-24.
12. Maurer, C., et al., (2011). *Laser & Photonics Reviews*, *5*(1), 81-101.
13. Verbeeck, J., et al., (2018). Ultramicroscopy, 190, 58-65.
14. Yu C.P. et al., (under review), PRX
15. Guzzinati, G., et al., (2017). Nature Communications, 8(1), 14999.
16. Stockmar, M., et al., (2013). Scientific reports, 3(1), 1927.
17. Kallepalli, A., et al., (2022). arXiv preprint arXiv:2204.09997.

**David N. Mastronarde**
Dept. of MCD Biology, University of Colorado, Boulder, Co 80309

# The **IMOD Software Package** for Tomographic Reconstruction

IMOD is a package of programs for creating, visualizing, and analyzing three-dimensional reconstructions from microscope images (Kremer et al., 1996). Its primary focus is on reconstructions for electron tomography, in which a specimen is tilted to a series of angles (typically between +/-60-70° at 1-3° intervals) and a projection image is acquired at each angle. Initially, the main uses of tomography were for studying cellular structures in thick sections (200-400 nm) of fixed, embedded, stained specimens at a range of scales, from whole cells through complex systems of membrane-bounded compartments, down to large macromolecular complexes. The method was also applied in materials science. More recently, the dominant use has been with frozen-hydrated samples, where the excellent structural preservation gives the opportunity to align and average multiple copies of a structure in subtomograms, to obtain high-resolution molecular structures, down to resolutions of ~3 Å (Briggs, 2013).

For tomographic reconstruction, images are aligned and transformed so that, ideally, they represent projections of a rigid structure tilting around a single axis. This alignment is done using either features in the images themselves, or the positions of gold beads placed on or contained within the specimen. Although alignment and tomogram computation are the main steps, there are several other processing steps involved in getting a useful single-axis reconstruction.

Moreover, it is common to acquire two series by tilting around orthogonal axes in the specimen, accomplished by rotating the specimen by 90° between the series. When the data are merged in some fashion to produce a single dual-axis tomogram, information missing in a single-axis tomogram is filled in by the second axis (Mastronarde, 1997; Penczek et al., 1995). Specifically, features oriented nearly parallel to the tilt axis are poorly resolved in a single axis tomogram, whereas features at all orientations show up well in the dual-axis tomogram.

IMOD provides a comprehensive set of tools for all these steps. The goal has been to make the steps run as automatically as possible, while still providing the flexibility for manual intervention when automation fails. Thus, a suite of image processing programs provides many options for handling a variety of difficulties that can arise with a particular tilt series. The running of these programs is managed by the program Etomo, which presents a user interface organized to guide users through the sequence of steps. Etomo opens in a Basic mode with only the most important, commonly used options shown, but it can be switched to an Advanced mode that presents additional parameters and problem-solving features.

One theme in IMOD development has been the pursuit of large reconstructions, containing substantial volumes within a cell with good resolution of fine details. From the early days, there was a strong motivation to go beyond what could be obtained from single images, especially when tilt series started to be taken automatically with CCD cameras, which had a limited field of view. One method of extending the volume is to acquire a montage of overlapping frames at each tilt angle. One of the major programs in IMOD can process such montages to produce a single, seamless image at

each tilt. The interface in Etomo allows users to process montaged tilt series just as easily as single-frame ones.

Such tilt series can be obtained automatically with the data acquisition program SerialEM, also developed by me (Mastronarde, 2005). With the widespread adoption of SerialEM for tilt series acquisition, processing of montages became routine. The tomographic volume can also be extended in the other direction, by obtaining tomograms from serial thick sections and stacking them together. Alignment programs were adapted, scripts were developed, and an interface was added in Etomo to allow straightforward alignment and stacking of tomograms.

Embedded specimens are progressively damaged by the electron beam, with an initial rapid collapse followed primarily by more gradual shrinkage in all three dimensions (Luther et al., 1988). Even after pre-exposing the specimen to stabilize it, there will be changes during the tilt series that need to be accounted for when aligning for reconstruction. Moreover, the changes are usually not uniform over the whole area. These non-uniformities limit how well a single alignment model fits the image positions, and the fit becomes progressively poorer for larger areas (consider that a model fitting well to the center of an area will fit worse the farther it is extrapolated to peripheral regions that changed differently.) The program in IMOD that computes the alignment solves this problem with "local alignments", in which the alignment model is fit to a subset of positions in each local area, and separate solutions are obtained over a grid of overlapping areas (Mastronarde, 2007).

The reconstruction program uses the local alignment information to compute an accurate position within each tilt series image corresponding to a particular pixel in the tomogram. The problems caused by changes in the specimen between the two axes of a dual-axis series are handled in a completely different way. In IMOD, a separate tomogram is computed for each axis, using the local alignments to correct for distortions within each series. Then after getting the two tomograms approximately into register, 3-D correlations between the two volumes are done in small patches throughout the volume. This collection of displacements is used to derive a warping transformation that can be applied to one of the volumes to bring it into subpixel registration with the other. Information from the two volumes can then be combined to obtain the final tomogram, without having misalignments that would blur out the features.

The pursuit of even larger reconstructions, containing a substantial fraction of a mammalian cell, led to further major developments in IMOD. This work was done in collaboration with Brad Marsh's group at the University of Queensland. For various reasons, it becomes impractical to acquire montaged tilt series of areas bigger than ~8 µm with a pixel size around 1 nm. To reconstruct larger areas, "supermontaging" was developed, in which an array of overlapping tomograms (each from a montaged tilt series) is acquired, computed, and stitched together (Mastronarde et al., 2008). Developments in SerialEM were needed to facilitate acquiring the multiple dual-axis tilt series with appropriate overlap. The additional beam exposure in multiple areas produces even more nonlinear distortions that need to be accommodated. Aligning these tomograms involves first determining linear transformations for each volume that will bring them all into alignment at the centers of the zones where they overlap. Then, local correlations in the overlap zones are used to derive transformations for warping the volumes so that their overlap zones are in good registration throughout, after which it becomes straightforward to stitch them into a single volume (O'Toole et al., 2018).

Although supermontaging is not often undertaken, two problems in stacking serial sections became acute with super-montages and led to solutions that are more widely used. First, distortions under the beam often make the section curve or form a dome, requiring extra slices to hold the entire curved volume and leaving large gaps in material when sections are stacked. Thus, a method was developed to flatten the section within the tomogram by deriving a 3-D warping transformation either from lines drawn along the section surfaces or from the positions of gold beads on the surfaces, if they are sufficiently numerous. For many specimens, the lines can be generated automatically by a program that detects the surfaces of the stained material.

The second problem is that lateral distortions make it impossible to align features well between successive sections. Thus, a general 2-D warping capability was developed. For aligning serial tomograms, images at the surfaces of adjacent sections are presented in a visual alignment program where the images can be shifted into local alignment at a series of selected points and the shift recorded at each. A warping transformation is derived from these shifts using geometric methods and is applied right in the alignment program. This 2-D warping has also proven quite useful for aligning serial images from either TEM of thin sections or scanning EM of a block face after sections are cut away or milled away with a focused ion beam. In this case, automated alignment is often possible by doing local correlations over a complete grid of positions and using the shifts in the warping transformation. (Information for aligning serial tomograms is often too patchy for automated alignment because material is lost between sections (Ladinsky et al., 1999).) Interfaces in Etomo for stacking tomograms and aligning serial sections both make it easy to apply these methods.

As the focus in tomography has shifted from stained material to frozen hydrated samples, IMOD has also incorporated features needed in cryo-tomography, where much lower electron dose must be used to avoid destroying the structures of interest. The largest component is a program for measuring the parameters needed to correct the effects of the microscope contrast transfer function (CTF). In cryoEM, images are taken with a defocus that results in zero signal transfer at a series of spatial frequencies, and a reversal in the sign of the signal at each zero point. We developed a program to detect defocus with methods to handle the problems unique to cryo-tilt series: the small amount of signal reflecting the CTF in each image, and the tilt of the specimen, which makes the defocus vary continuously across the image (Xiong et al., 2009). The defocus gradient is compensated by measuring signal at each frequency in strips parallel to the tilt axis, so that each strip has a common defocus. The frequencies of the signals are scaled to align zeros between the strips before summing, so that the oscillations are reinforced rather than blurred out. The weak information is enhanced when necessary by summing over multiple tilt images.

With the development of cameras that can record electrons directly in the chip and detect single electron events, defocus can now usually be determined reliably from single tilt images. More recently, this CTF program can determine other parameters needed for accurate correction of the sign of the signals, primarily astigmatism, the variation in defocus with angle. Astigmatism is measured with a novel method of summing signals as a function of angle, estimating the defocus at each angle, and fitting to these estimates to find the angle and magnitude of the astigmatism. Other developments have enhanced the ability of the program to be run automatically and give accurate results with many kinds of data.

Other notable developments to support cryo-tomography include:

- A program for aligning the multiple frames that can be obtained when acquiring a single image with direct detectors and some other cameras. Alignment of frames eliminates the loss of image detail from drift (Brilot et al., 2012). This program is designed to handle input from all the images in a tilt series, align and sum the frames from each, and produce a file directly usable for tilt series processing. The basic alignment module is shared with SerialEM, where it can be used to align frames from 5 different kinds of cameras.

- Adaptation of the program that automatically finds the gold markers for aligning tilt series to work well with tilt series for high-resolution subtomogram averaging. Such tilt series have very small pixel sizes relative to the gold beads and often have a larger tilt increment than is used for reconstructing cellular structures, leading to larger jumps in bead positions between adjacent angles.

- Addition of “dose weighting”, in which progressively more high frequency information is removed from images with higher electron dose, to filter out signal from structures that have been damaged by the beam (Grant and Grigorieff, 2015).

- Reconstruction with “super-sampling”, in which a slice of the tomogram is computed with sub-pixel resolution and then reduced to the original pixel size. This procedure removes some characteristic artifacts that appear in the Fourier transform of the slice, which otherwise produce extra noise in the tomogram.

IMOD also has a program for fully automated reconstruction of multiple tilt series, including all the ancillary steps required for a high-quality tomogram (Mastronarde and Held, 2017). This capability has become increasingly important as microscope hardware and acquisition software have improved to the point where many tilt series can be collected efficiently in one session. The implementation is highly flexible, allowing different alignment and reconstruction methods to be used and ~250 different parameters to be set.

To handle this complexity, the user interface in Etomo provides a Basic mode with just the essential parameters collected onto a single window. A separate advanced window gives access to all the available options, organized by step in the process, and with the ability to see parameters for one step or a few steps at a time. This batch processing is completely compatible with processing through the regular reconstruction interface. One way of using it is to process all sets completely and check them after the fact, handling failures that occurred. However, it is also possible to run all sets just to a known trouble spot, open them in the regular interface to check them or perform a step manually, and resume the automatic processing. Thus, the batch processing provided in IMOD can be beneficial even for difficult data where not all steps can be done automatically. ■

**ACKNOWLEDGEMENTS**

*I thank the other developers who have contributed to IMOD, primarily Rick Gaudette, Sue Held, John Heumann, Suraj Khochare, James Kremer, and Quanren Xiong. IMOD development was supported by grants from the National Institutes of Health (NCRR, NIBIB, and NIGMS).*

## References


1. Briggs, J.A. 2013. Structural biology in situ--the potential of subtomogram averaging. *Curr Opin Struct Biol*. 23:261-267.
2. Brilot, A.F., J.Z. Chen, A. Cheng, J. Pan, S.C. Harrison, C.S. Potter, B. Carragher, R. Henderson, and N. Grigorieff. 2012. Beam-induced motion of vitrified specimen on holey carbon film. *J. Struct. Biol.* 177:630-637.
3. Grant, T., and N. Grigorieff. 2015. Measuring the optimal exposure for single particle cryo-EM using a 2.6 A reconstruction of rotavirus VP6. *Elife*. 4:e06980.
4. Kremer, J.R., D.N. Mastronarde, and J.R. McIntosh. 1996. Computer visualization of three-dimensional image data using IMOD. *J. Struct. Biol.* 116:71-76.
5. Ladinsky, M.S., D.N. Mastronarde, J.R. McIntosh, K.E. Howell, and L.A. Staehelin. 1999. Golgi structure in three dimensions: functional insights from the normal rat kidney cell. *J. Cell Biol.* 144:1135-1149.
6. Luther, P.K., M.C. Lawrence, and R.A. Crowther. 1988. A method for monitoring the collapse of plastic sections as a function of electron dose. *Ultramicroscopy*. 24:7-18.
7. Mastronarde, D.N. 1997. Dual-axis tomography: an approach with alignment methods that preserve resolution. *J. Struct. Biol.* 120:343-352.
8. Mastronarde, D.N. 2005. Automated electron microscope tomography using robust prediction of specimen movements. *J. Struct. Biol.* 152:36-51.
9. Mastronarde, D.N. 2007. Fiducial marker and hybrid alignment methods for single- and double-axis tomography. *In* Electron Tomography. J. Frank, editor. Springer, New York. 163-185.
10. Mastronarde, D.N., and S.R. Held. 2017. Automated tilt series alignment and tomographic reconstruction in IMOD. *Journal of structural biology*. 197:102-113.
11. Mastronarde, D.N., P.A. van der Heide, G.P. Morgan, and B.J. Marsh. 2008. Supermontaging: Reconstructing large cellular volumes by stitching together laterally adjacent tomograms. *Microsc. Microanal.* 14(Suppl 2):106-107.
12. O'Toole, E., P. van der Heide, J.R. McIntosh, and D. Mastronarde. 2018. Large-Scale Electron Tomography of Cells Using SerialEM and IMOD. *In* Cellular Imaging. E. Hanssen, editor. Springer, New York. 95-116.
13. Penczek, P., M. Marko, K. Buttle, and J. Frank. 1995. Double-tilt electron tomography. *Ultramicroscopy*. 60:393-410.
14. Xiong, Q., M.K. Morphew, C.L. Schwartz, A.H. Hoenger, and D.N. Mastronarde. 2009. CTF determination and correction for low dose tomographic tilt series. *J. Struct. Biol.* 168:378-387.


**Mathieu Kociak and Odile Stéphan**
Université Paris-Saclay, CNRS, Laboratoire de Physique des Solides, 91405, Orsay, France

# Enlightning **electrons**

**In 2012, one of the authors received the EMS-FEI prize for the work we were pursuing for a decade in the STEM group in Orsay. This old prize was a good alibi for the EMS to ask for a short paper on the subject to appear in the booklet "25 years of microscopy progress" on the occasion of EMS 25th anniversary. We have happily agreed on writing an ultra-short review trying to highlight the works of few generations of electron microscopists and spectroscopists to build a field we had the chance to contribute to.**

In the 90's, a new field at the crossroad of the emerging nanotechnologies and nanophysics, and the well-established optical sciences emerged. The science of nanooptics was concerned by the physics of optical phenomena that arise at scales which are much smaller than the equivalent wavelength of light in vacuum - say, 600 nm for a yellow light. Such phenomena typically arose for systems where some sort of confinement takes place, should it be classical (surface plasmons, photonic modes ...) or quantum (quantum confined nanostructures ...). The optics community struggled with the schizophrenic injunction to look at phenomena which are much lower than the diffraction limit of light. But they found incredibly smart solutions to break this limit, using near-field techniques (SNOM ...) [1] or even far-field ones (STED ...) [2], the later leading to the Nobel prize for their inventors. Along these exciting adventures that we won't discuss further, they also invented new physical concepts, such as the electromagnetic local density of states (EMLDOS), which have proven to be particularly useful in the field of electron spectroscopy.

Interestingly enough, physicists have been using electrons for a long time to study optical phenomena at the incredible spatial resolution offered by fast electrons. For example, cathodoluminescence (CL), a technique that uses the light emitted by a sample upon electron irradiation was already a well-established technique in the 80s and before. It is still used in e. g. geology for the identification of materials and trace elements [3]. Also, the rise of III-V materials in the 80s-90s pushed CL to high spatial resolution [4]. EELS, on the other hand, has been genuinely tight to the physics of plasmons - the first EELS experiments having been performed on bulk plasmons [5], and EELS having been used early on to study surface plasmons. Also, EELS has long been used to and extract optical quantities such as the dielectric constant.

Finally, before nano-optics was even a thing, the advent of cluster physics and nanophysics in the 80s-90s provided occasions for researchers to perform measurements of plasmons in metallic nanoparticles (notably [6]) or nano-objects like carbon nanotubes [7]. However, to sketch it grossly, electron spectroscopists were having a condensed matter view on phenomena while optician were having an optical physics view on them; concepts to bridge both worlds were missing, and EELS and CL techniques were hardly

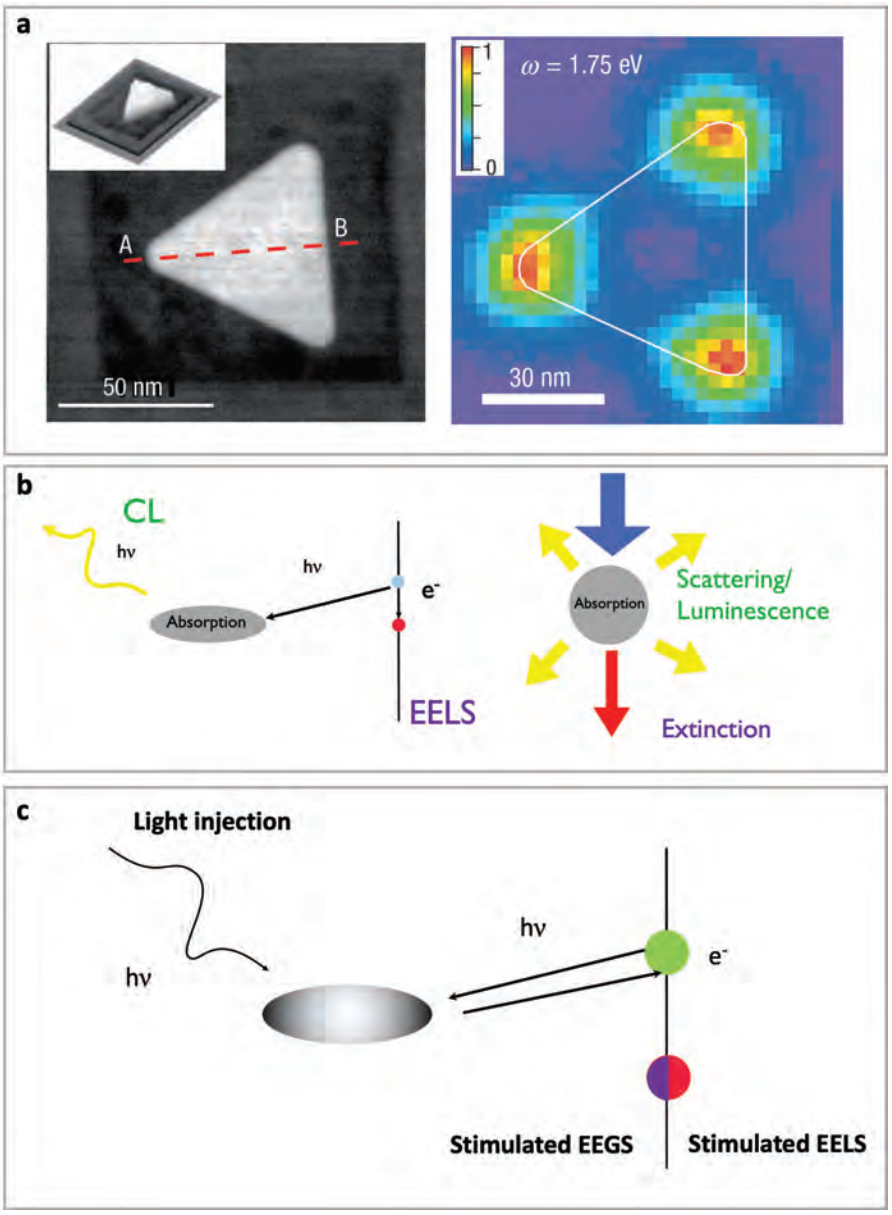


**Fig. 1 a. Spectral-imaging of surface plasmons within a silver particle. Left: High Angle Annular dark field of the particle and Right: energy filtered map of the dipolar surface plasmon mode of the particle. From [9]. b. Principle of the EELS and CL phenomena, and comparison with the classical linear extinction and scattering/luminescence spectroscopies. c. Principle of stimulated EELS and EEGS.**

optimized to meet the promises to benefit from the spatial resolution of electrons in studying optical phenomena.

Building on continuous technical and conceptual advances since the 70s, the situation changed radically in the first half of the 2000s. Certainly, a milestone was buried by Yamamoto, Araya and de Abajo [8], when they demonstrated the possibility to map the near-field of a plasmon dipolar mode of a 140 nm diameter metallic sphere using polarized CL. It took our team 6 more years to demonstrate the spectral-mapping of surface plasmons modes within a nanoparticle by EELS **(see Figure 1)** [9] - in parallel to the team of M. Bosman [10] also in EELS, and that of A. Polman by CL [11]. In addition, we showed, under our co-author Javier Garcia de Abajo's lead, that EELS is theoretically extremely close to the EMLDOS [12], eventually showing without dispute that EELS was a technique of choice for nanooptics. This series of works awarded the EMS-FEI 2012 prize.

But of course, the story was just beginning. Indeed, CL was rapidly shown to also be related to the EMLDOS [13]. More generally, it was shown that EELS can be seen as the nanometer counterpart of extinction spectroscopy, while CL is the nanometer counterpart of scattering spectroscopy (for plasmonic and photonic objects) or luminescence spectroscopy (for luminescent objects), as schematized in the **Figure 1**. EELS and CL (the last one either in SEM or STEM) are now strongly established tools for the nanooptics community, fuelled by the advent of high efficiency CL system in SEM and STEMs, and electron beam monochromation. The former are now so efficient that they permit to detect single photon emission, an hallmark of quantum optics, and the latter allow to probe nanooptics in the far-infra-red. The amount of applications is exploding. Also, with the advent of new generation of detectors with high efficiency and little to no readout time, exciting new spectroscopies correlating energy-loss, emitted photons or other physical quantities will without doubt open new frontiers.

In parallel to the above-mentioned development, another related field of electron spectroscopy was nascent in the late 2000s, and is now a major field of research. Indeed, after the initial idea of A. Howie that light injection and electron microscopy could be married to lead to new forms of electron spectroscopies, the electron energy gain spectroscopy was proposed [14]. In this new form of spectroscopy, a laser is pumping a nanostructure of interest so that its scattered field can be used to accelerate an electron **(see Figure 1)**. The promise of the technique, which was only realized 13 years later [15] was to ally the spatial resolution of electrons to the spectral resolution of lasers. Rapidly, the team of late H. Zewail presented the first acceleration of electrons in a TEM by a laser [16]. One

of the reasons for the success of the experiment was the use of fs lasers to create ultra-short electron and light pulses. This produced, in addition to stimulated gain events, stimulated loss events. This strong, stimulated interaction of the laser with the sample and electrons is at the basis of the highlighting, in 2015, by the team of C. Ropers of the possibility to create quantum coherent states of the electron beam. Since then, studying the quantum properties of photonic samples, intense light fields and pulsed electron beams has become a field by itself.

To conclude, we feel we have been lucky to have seen fields almost orthogonal for tens of years (optics and electron spectroscopy) to start merging in the 2000s, and now being totally interleaved. The applications are already numerous for the study of the optical properties of plasmonic nanoparticles, quantum confined heterostructures or photonic materials, to name a few. The future is bright, with the Graal of mixing quantum coherence of the electron beam and the sample ahead. ■

**ACKNOWLEDGEMENTS**

*In the last twenty years, we have been lucky to collaborate with key colleagues and students in the STEM group at Orsay or outside. Among them, we want to point out and warmly thank Marcel Tencé, Christian Colliex, Luiz Tizei, Javier Garcia de Abajo, Jaysen Nelayah, Luc Henrard, Luiz Zagonel, Jean-Denis Blazit, Sophie Meuret, Hugo Lourenço-Martins, Arthur Losquin, Yves Auad, Guillaume Boudarham, Alfredo Campos, Ulrich Hohenester, Zackaria Mahfoud, Malo Bézard, Laura Bocher, Noémie Bonnet, Romain Bourrellier, Pabitra Das, Alexandre Gloter, Xiaoyan Li, Anna Tararan, Steffi Woo and Alberto Zobelli.*

## References

1. L. Novotny and B. Hecht, Principles of Nano-Optics (Cambridge University Press, Cambridge,2012).
2. E. Rittweger, K. Y. Han, S. E. Irvine, C. Eggeling, and S. W. Hell, STED microscopy reveals crystal colour centres with nanometric resolution, Nature Photonics 3, 144 (2009).
3. B. G. Yacobi and D. B. Holt, Cathodoluminescence Microscopy of Inorganic Solids (Springer US, Boston, MA, 1990).
4. M. A. Herman, D. Bimberg, and J. Christen, Heterointerfaces in quantum wells and epitaxial growth processes: Evaluation by luminescence techniques, Journal of Applied Physics 70, 10.1063/1.349613 (1991).
5. R. F. Egerton, Electron Energy-Loss Spectroscopy in the Electron Microscope (1996).
6. P. E. Batson, Surface plasmon coupling in clusters of small spheres, Phys. Rev. Lett. 49, 936 (1982).
7. O. Stephan, D. Taverna, M. Kociak, K. Suenaga, L. Henrard, and C. Colliex, Dielectric response of isolated carbon nanotubes investigated by spatially resolved electron energy-loss spectroscopy: From multiwalled to single-walled nanotubes, PHYSICAL REVIEW B 66, 10.1103/PhysRevB.66.155422 (2002).
8. N. Yamamoto, K. Araya, and F. J. García de Abajo, Photon emission from silver particles induced by a high-energy electron beam, Physical Review B - Condensed Matter and Materials Physics 64, 2054191 (2001).
9. J. Nelayah, M. Kociak, O. Stéphan, F. J. G. de Abajo, M. Tence, L. Henrard, D. Taverna, I. Pastoriza-Santos, L. M. Liz-Marzan, and C. Colliex, Mapping surface plasmons on a single metallic nanoparticle, NATURE PHYSICS 3, 348 (2007).
10. M. Bosman, V. J. Keast, M. Watanabe, A. I. Maaroof, and M. B. Cortie, Mapping surface plasmons at the nanometre scale with an electron beam, Nanotechnology 18, 10.1088/0957-4484/18/16/165505 (2007).
11. E. J. R. Vesseur, R. De Waele, M. Kuttge, and A. Polman, Direct observation of plasmonic modes in Au nanowires using high-resolution cathodoluminescence spectroscopy, Nano Letters 7, 2843 (2007).
12. F. J. G. de Abajo and M. Kociak, Probing the photonic local density of states with electron energy loss spectroscopy, Physical Review Letters 100, 106804 (2008).
13. A. Losquin, L. F. Zagonel, V. Myroshnychenko, B. Rodriguez-Gonzalez, M. Tence, L. Scarabelli, J. Forstner, L. M. Liz-Marzan, F. J. G. de Abajo, O. Stephan, and M. Kociak, Unveiling Nanometer Scale Extinction and Scattering Phenomena through Combined Electron Energy Loss Spectroscopy and Cathodoluminescence Measurements, NANO LETTERS 15, 1229 (2015).
14. F. J. García de Abajo and M. Kociak, Electron energy-gain spectroscopy, New Journal of Physics 10, 073035 (2008).
15. J.-W. Henke, A. S. Raja, A. Feist, G. Huang, G. Arend, Y. Yang, F. J. Kappert, R. N. Wang, M. Möller, J. Pan, J. Liu, O. Kfir, C. Ropers, and T. J. Kippenberg, Integrated photonics enables continuous-beam electron phase modulation, Nature 600, 653 (2021), arXiv:2105.03729.
16. B. Barwick, D. J. Flannigan, and A. H. Zewail, Photon-induced near-field electron microscopy, Nature 462, 902 (2009).

**P. Schattschneider**
Univ. Service Centre for Transmission Electron Microscopy
TU Wien, A-1040 Wien, Austria

# **A brief history** of Energy-loss Magnetic Chiral Dichroism (EMCD)

X-ray magnetic circular dichroism (XMCD) is a well-established method to study magnetic materials. It is related to magnetically active electronic transitions. They cause a preferred absorption of either left- or right-handed circularly polarized X-rays in the material. It is analogous to optical activity in left- or right-handed organic molecules in a non-racemic mixture. Detailed information on the atom-specific magnetic moments, even distinguishing spin and orbital contributions, can be derived from XMCD spectra.

Before 2000, such magnetic transitions were considered to be undetectable with electron probes because there is no counterpart of photon helicity in EELS.

In other words, EELS seemed to be unable to measure a left-/right-handed symmetry breaking (as Friedel's law for diffraction in crystals shows, by the way). This was a pity because an XMCD-equivalent performed in the electron microscope could offer a much better spatial resolution, perhaps down to the atomic level.

In about 2000, I attended a talk on the occasion of an EELS conference. When the speaker presented an energy filtered diffraction pattern of some non-centrosymmetric crystal in which a usually present mirror symmetry was broken, I realized that Friedel's law does not apply to inelastic scattering, and I began to wonder if we didn't overlook an important aspect in the theory of EELS.

With my post-doc Cécile Hébert, we delved into the details of XMCD in an effort to find a way for measuring XMCD with electrons instead of photons. We first focussed on the spin of the electron beam but this turned out to be a dead-end. A meeting with an expert from the European Synchrotron Facility in Grenoble showed us the correct approach [1]: There is a formal equivalence of the EELS cross section to the X-ray absorption cross section. The scattering vector in an EELS experiment plays the same role as the polarization vector in X-ray absorption. (This explains the equivalence of X-ray linear dichroism with direction-dependent EELS cross sections, better known as EELS anisotropy). The counterpart of a circular polarization vector for photons $\varepsilon_x \pm i\varepsilon_y$ is a scattering vector $q_x \pm iq_y$ in EELS. But what is a complex scattering vector? Sticking to the formal equivalence, it is a coherent superposition of two inelastic processes with scattering vectors $q_x$ and $q_y$ and a relative phase shift of $\pm\pi/2$ between them, symbolized by the imaginary unit $i$.

The mechanism can easily be visualized. From **Fig. 1a**, it is intuitively clear that the electric field F that acts on the atom during the close encounter between atom and probe is parallel to the scattering vector $q$. This electric field oscillates with a frequency $\nu$ given by the energy loss $E=h\nu$. Two mutually perpendicular scattering vectors $q_x, q_y$ phase shifted by a quarter of an oscillation period which is of the order of attoseconds create a rotating electric field at the position of the atom **(Fig. 1b)**, exactly as a circularly polarized photon does.

One could use a biprism and a phase shifter to set the experiment up. But nature provides us with a more convenient beam splitter, the very crystal to be studied. Bragg diffraction, in the two-beam case, creates two coherent incident beams (the 0 and the G spot,

say). Cleverly tuning the excitation error, the two beams can be phase shifted by + or - $\pi/2$. An additional bonus is the lattice periodicity that locks the phase shift at each equivalent lattice site to the same value.

This is the basic idea. It took us some years to cope with all the problems that come with a presumably simple experiment, such as the thickness dependence, the low signal, the coherence etc. In 2006, we published the first "XMCD" electron energy loss spectrum within the European CHIRALTEM collaboration [2]. We decided to name the method Energy Loss Magnetic Chiral Dichroism (EMCD). The acronym should stress the similarity with XMCD by the fortunate choice of *Chiral* because it is the chirality of a transition that is measured rather than a circular polarisation that does not exist in EELS. Interestingly, users tended to retranslate the acronym as "Electron Circular Magnetic Dichroism".

The following years saw progress in spectral quality and in spatial resolution, reaching 2 nm in 2008 [3], EMCD of single atomic rows in an antiferromagnet in 2012 [4] and of individual atomic layers in a perovskite oxide in 2018 [5].

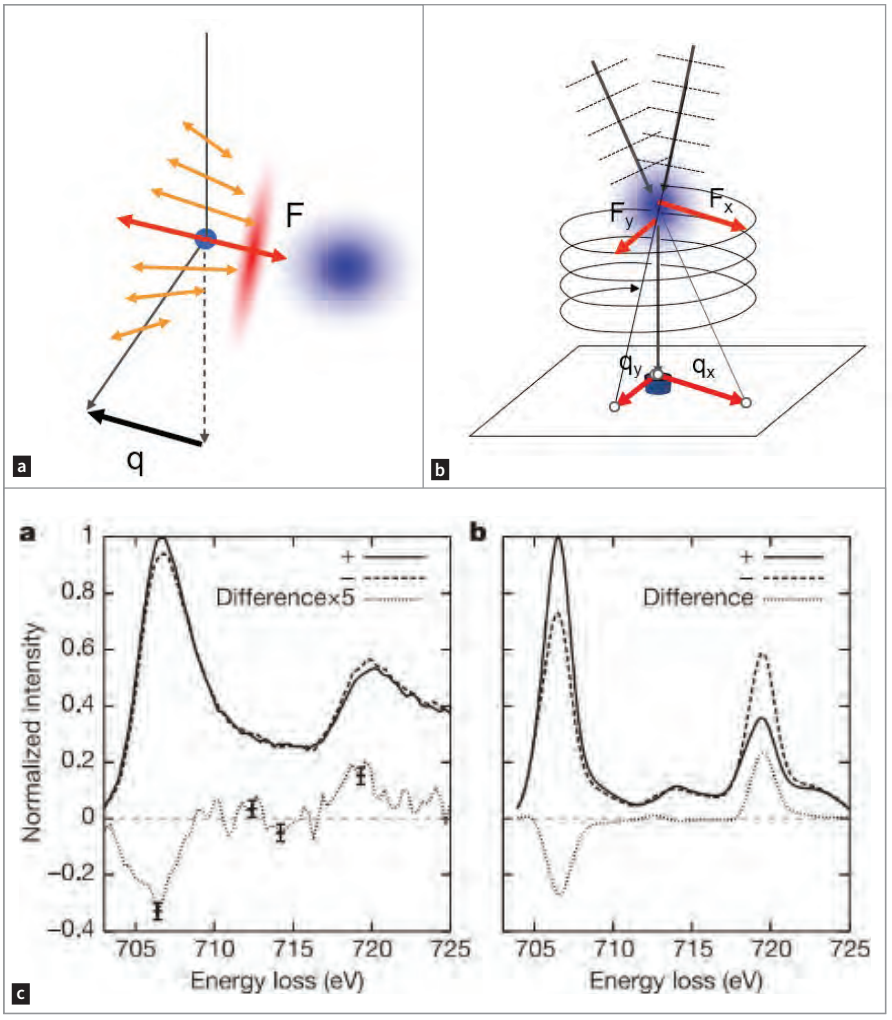


**Fig.1. a)** The electric field F of a rapid probe electron on an atom (blue cloud) at closest approach is parallel to the scattering vector q. The field components perpendicular to F before and after the closest approach cancel. **b)** two coherent plane waves interact with the atom. They are oriented such that the detector defines perpendicular scattering vectors $q_x$ and $q_y$. When the incident waves are phase shifted by $\pi/2$, the superposition of the corresponding electric fields $F_x$ and $F_y$ rotates clockwise. c) First EMCD spectrum on a 10 nm thick Fe sample. a) experiment, b) simulation [2].

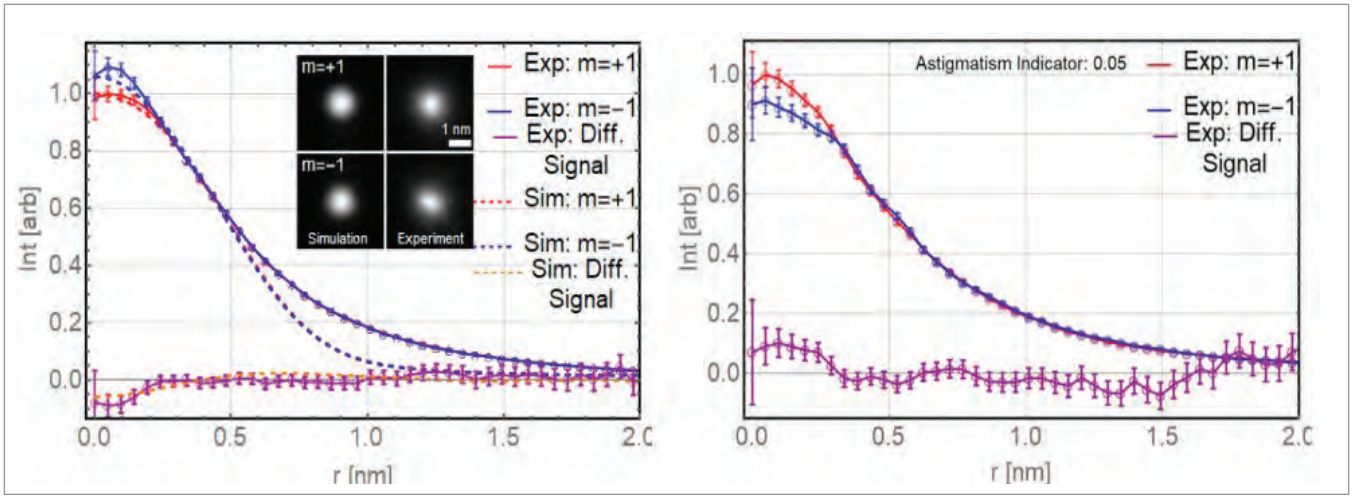


**Fig.2:** EMCD with a vortex filter on a 70 nm thick Fe sample. Radial profiles of the $m$=±1 vortices (shown in the insert) compared with simulations. Left: Fe $L_3$-edge using a slit of 10 eV. Right: Same for the $L_2$ edge [8].

For a good EMCD signal, it is important to optimize the collection angle and the specimen thickness. Similar to the thickness fringes in Bragg scattering *(Pendellösung)*, the EMCD signal oscillates, going to almost zero for unfortunate choices of the specimen thickness. The theory to get all parameters right was fully established in 2007 [6]. Many interesting findings on magnetic phase transitions, EMCD on multilayers, nanoparticles, and ferrimagnets were obtained. For details on EMCD see [7].

In an idealized XMCD experiment, the magnetic quantum number of the target electron changes by $\pm 1$, because it absorbs a left- or -right circularly polarized photon. In EMCD, the probe electron exchanges a *virtual* left- or right- circularly polarized photon with the target. By conservation laws it follows that the electron must have changed its angular momentum by $\mp 1$. Essentially, it becomes a vortex. This observation opens new possibilities for EMCD with electron vortices. A vortex filter tells whether an electronic transition was spin polarized or not. A proof-of-principle experiment performed in 2019 [8] shows radial profiles of the $m=\pm 1$ vortices in the $L_{23}$ edges of a 70 nm thick Fe sample **(Fig. 2)**. With this technique, there is no need for crystalline samples in order to tune the phase shift, and there are no *Pendellösung* fringes in the EMCD signal. However, for applications, the current signal-to-noise ratio is too low. The new generation of single electron detectors potentially brings vortex EMCD on single atoms within reach. ■

**ACKNOWLEDGEMENTS**

*Naming all colleagues that contributed to the success of EMCD would fill more place than was accorded to me. Many thanks to all of them, especially (in chronological order, as far as I remember) to Klaus Leifer, El Kebir Hlil, Cécile Hébert, Stefano Rubino, Jan Rusz, Joe Zweck, Hannes Lichte, Elvio Carlino, Michael Stöger-Pollach, Michel and Nicolas Jaouen, Andreas Hütten, Inga Ennen, Jo Verbeeck, Stefan Löffler, Walid Hetaba, Thomas Schachinger, and the EELS groups in Dresden, Oak Ridge, Toulouse and Uppsala.*

## References

1. C. Hébert, P. Schattschneider, Ultramicroscopy, 96 (3-4), 463 (2003).
2. P. Schattschneider, S. Rubino, C. Hébert et al., Nature 441, 486 (2006).
3. P. Schattschneider, M. Stöger-Pollach, S. Rubino et al., Phys. Rev. B 78,104413 (2008).
4. P. Schattschneider, B. Schaffer, I. Ennen et al., Phys. Rev. B 85, 134422 (2012).
5. Z. Wang, A. H. Tavabi, L. Jin et al., Nature Mater. 17, 221 (2018).
6. J. Rusz, S. Rubino, P. Schattschneider, Phys. Rev. B 7, 21 (2007).
7. P. Schattschneider (Ed.), Linear and Chiral Dichroism in the Electron Microscope. Pan Stanford Publishing (2012).
8. T. Schachinger, Electron Vortex Beams: Production and Application. Doctoral Thesis, TU Wien (2019).

**Peter D. Nellist**
Department of Materials, University of Oxford, Oxford OX1 3PH, UK

# **Optical sectioning** in the scanning transmission electron microscope

The development of aberration correction has allowed for much larger numerical apertures in electron microscopy than those that were previously limited by spherical aberration. In the scanning transmission electron microscope (STEM), probe semi-angle of convergences of 30 mrad are routine and larger angles have been demonstrated. Prior to aberration-correction, images in the conventional transmission electron microscope (CTEM) and the STEM were generally regarded as being projections of the sample. The depth of field in imaging is, however, dependent on the inverse square of the numerical aperture and so in an aberration corrected microscope the depth of field can drop to a value smaller than the thickness of the sample. This creates the opportunity to retrieve three-dimensional information by selectively focusing at various depths in a sample – a process referred to as optical sectioning. In this short summary, we explain how the reduced depth of focus manifests itself in CTEM, STEM and also in the emerging area of 4D-STEM and in particular ptychography.

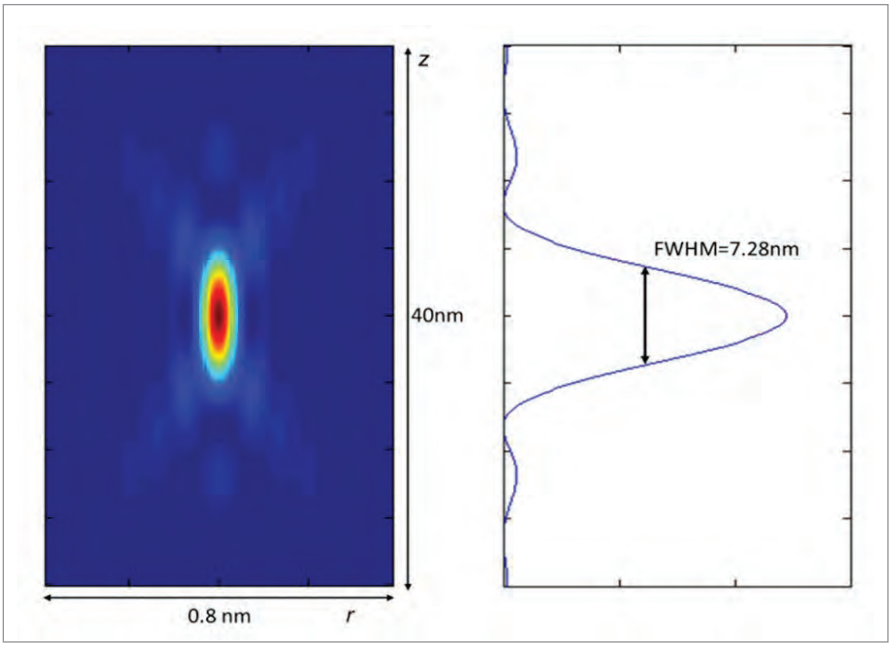


**Figure 1. (left) A cross-section of the intensity in a focused STEM probe and (right) an intensity line profile along the optic axis (*z*) at the centre of the probe. Beam energy 100 keV with semi-angle of convergence of 30 mrad.** *Reprinted from Reference[3] under a Creative Commons CC-BY license.*

Defocus is referred to as the distance that the lens object plane is from the sample. From a wave optical point of view, it can be incorporated into a mathematical model of the microscope simply by adding a phase shift into either the back-focal plane (for CTEM) or the front focal-plane (for STEM) that depends on the square of the scattering angle. This phase shift is also sometimes referred to as the Fresnel propagator. In the CTEM configuration, for example if we are considering high-resolution TEM, diffracted beams at a specific angle repeatedly come into phase with the direct beam as the focus is changed, and images can appear to come repeatedly into focus. This process does not provide effective optical sectioning. An alternative

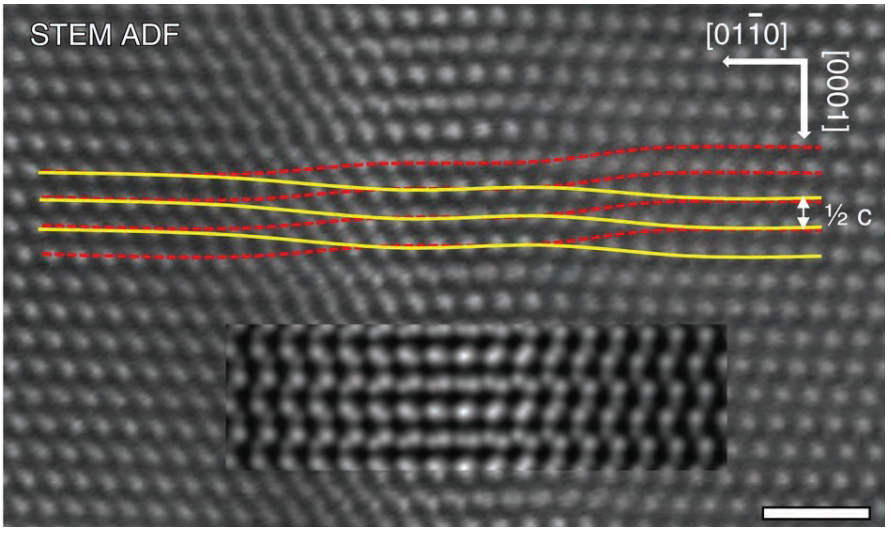


**Figure 2. Experimental and (inset) simulated ADF image of a dissociated dislocation lying perpendicular to the electron beam. The screw displacements associated with each of the partial dislocations can be observed, as indicated by the overlaid solid and dashed lines following the closer-to-focus stronger-intensity peaks and further-from-focus weaker-intensity peaks, respectively.** *Reprinted from Reference [3] under a Creative Commons CC-BY license.*

way of visualizing this is through the concept of the 3D transfer function. In the case of the CTEM, the 3D transfer function is actually a part of the Ewald sphere. Because it is thin in the z-direction, it does not offer good transfer in the third-dimension. For the remainder of this discussion, we therefore concentrate on STEM – both 2D and 4D.

Moving now to the STEM, we start with a discussion of optical sectioning in annular dark-field (ADF) imaging. Because ADF STEM is an incoherent imaging mode, the three-dimensional point-spread function is simply the intensity of the illuminating beam **(Figure 1)**. A line plot of the intensity of the probe along the optic axis shows a clear central maximum, which allows for optical sectioning. The full-width at half-maximum of this central maximum offers a measure of depth resolution, which is given by:

$$\Delta z = 1.77 \frac{\lambda}{\alpha^2}$$

where $\lambda$ is the wavelength of the electrons and $\alpha$ is the semi-angle of convergence for the probe-forming optics [1]. For a 200 kV microscope with a convergence angle of 25 mrad, the depth resolution is 5 nm. As discussed in more detail in [2], the optical sectioning effect is more accurately characterized using the 3D optical transfer function, which is essentially the 3D Fourier transform of the probe intensity. In cross-section, the transfer function has a "propeller"-like shape. The width of the transfer function in reciprocal space but parallel to the optic axis gives a measure of the depth resolution. At low lateral spatial frequencies, the depth resolution is poor, but improves at higher lateral spatial frequencies. An equivalent statement is that it is hard to detector when large, diffuse objects are defocused, but much easier for smaller objects. Using this approach, **Figure 2** shows how the displacements associated with a screw dislocation lying in the plane of a sample of GaN can be imaging by focusing close to the plane of the dislocation. The nature of the dislocation dissociation can be directly determined [3].

The poor resolution of larger and more diffuse objects can be overcome by using a confocal arrangement which is possible in instruments that are fitted with both probe forming and post-sample aberration correctors. This

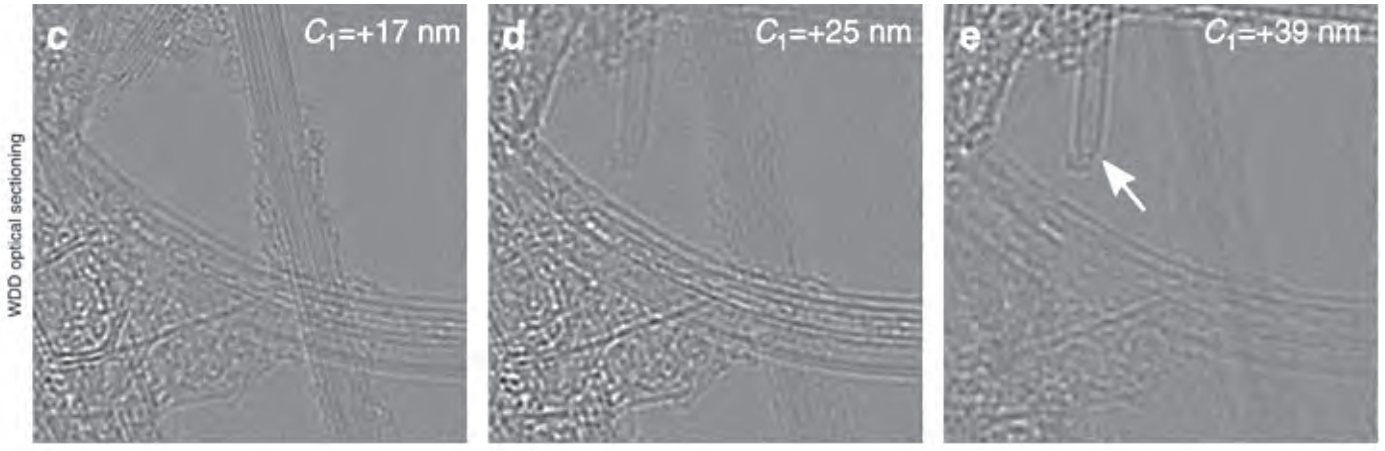


**Figure 3. Reconstructed ptychography phase image using the indicated defocus value in the reconstruction process. All these images were reconstructed from a single scan at one physical focus value. Note how different features appear and disappear at the different reconstruction focus values.** *Reprinted from Reference [4] under a Creative Commons CC-BY license.*

approach can fill the missing cone in the transfer function, but only for scattering which is inherently incoherent such as energy-loss events. An application of energy-filtered scanning confocal electron microscopy is discussed in Reference [1].

The emergence of 4D-STEM has also created opportunities for optical sectioning. The term, 4D-STEM, refers to the use of fast-pixelated detectors, usually direct electron detectors, that allow for the fully detector plane in STEM to be recorded for each probe position. The four dimensions associated with 4D-STEM are therefore the two real-space dimensions associated with the probe position and the two reciprocal space coordinates in the diffraction pattern. Using techniques such as electron ptychography or integrated Centre of Mass (iCOM), phase images not unlike HRTEM can be formed. Unlike HRTEM, however, they do show optical sectioning capabilities with bounds of three-dimensional transfer that are similar to those for ADF STEM [4]. In the case of ptychography, the optical sectioning process can take place in post-acquisition data processing – only a single scan at one physical focus value is required. **Figure 3** shows how carbon nanotubes at different heights can be selectively images using this approach and more recently work has shown that the depth sectioning approach can be used for more strongly scattering samples.

In conclusion, a perhaps unexpected outcome of aberration correction is the ability to optically section samples. Although the depth resolution is not nearly as high as the lateral resolution, and cannot achieve atomic resolution, the depth resolution is often a smaller distance than the thickness of the sample and can therefore be a useful way to provide information at specific depths from the sample [5].

## References


1. P.D. Nellist and P. Wang, *Annu. Rev. Mater. Res.* **42** (2012) 125.
2. E.C. Cosgriff et al., *Adv. in Imaging and Electron Phys.* **162** (2010) 45.
3. H. Yang et al., *Nat. Comm.* **6** (2015) 7266.
4. H. Yang et al., *Nat. Comm.* **7** (2016) 12532.


5. The author acknowledges funding from the EPSRC (grant numbers EP/M010708/1, EP/K032518/1 and EP/K040375/1). Financial support was also received from the EU H2020 Grant Number 823717 ESTEEM3. The technical assistance of JEOL Ltd and JEOL (UK) Ltd is also gratefully acknowledged.

**Jian-Min Zuo**[a,b]

[a] Department of Materials Science and Engineering, University of Illinois at Urbana-Champaign, Urbana, IL 61801, USA
[b] Materials Research Laboratory, University of Illinois at Urbana-Champaign, Urbana, IL 61801, USA

# The Coming Data Age of **Electron Diffraction**

**ABSTRACT**

**An emergent trend in electron microscopy is to collect large datasets of diffraction intensities for diffraction imaging using data mining. In this case, the microscope is used more like a diffractometer for the collection of diffraction data. A major advantage of this type of data-driven electron microscopy is being able to form direct images of crystal structural properties by decoding the diffraction signals and thus solves the perennial problem of image interpretation in transmission electron microscopy. This review captures this new development within the perspective of historical developments in electron diffraction and highlights the revolutionary potential of electron diffractive imaging.**

## Historical Background

Transmission electron diffraction using a focused beam has long been recognized as a powerful probe of crystal structure. The focused-beam mode produces so-called "convergent-beam" electron diffraction (CBED) patterns, as first demonstrated by Möllenstedt [1]. CBED led to the study of electron dynamical diffraction effects [2] and the development of the most sensitive methods for crystal symmetry determination and accurate structure factor measurement. Throughout the late 1970s and early eighties, Cowley together with Spence in Arizona were developing the coherent CBED method using subnanometer probes [3]. Remarkable CBED patterns using the Vacuum Generators HB5 instrument were produced from regions of crystal smaller than the unit cell [4]. Similar work on nanodiffraction, including the use of imaging energy filters and novel detectors, was later developed by Brown and co-workers in Cambridge, U.K. Both groups subsequently developed techniques for the study of defects in crystals and small nanoparticles using sub-nanometer probes [5].

The recent developments of electron diffraction are entwined with the development of electron microscope technologies. They are further helped with the development of computer algorithms for data analysis. The development of field emission guns (FEG) in the 70's and their adoption in conventional and scanning transmission electron microscopes (S/TEM) brought high source brightness, smaller probe size and improved coherence to electron diffraction. Electron energy filters, such as the in-column $\Omega$-energy-filter, allow the inelastic background from plasmon, or higher electron energy losses, to be removed from recorded diffraction patterns with an energy resolution of a few eV. The development of array detectors, such as CCD cameras, enables parallel recording of diffraction patterns and quantification of diffraction intensities over a large dynamic range, and thus overcoming a major limiting factor in the early efforts in electron diffraction. The move from the film age to digital age led to the development of quantitative CBED [6].

## Four-dimensional STEM and large data

With recent developments in fast electron detectors and efficient computer algorithms, it now becomes possible to collect unprecedently large datasets of diffraction patterns (DPs) and process DPs to extract crystallographic information to form direct images or tomograms based on crystal structural properties, giving rise to data-driven

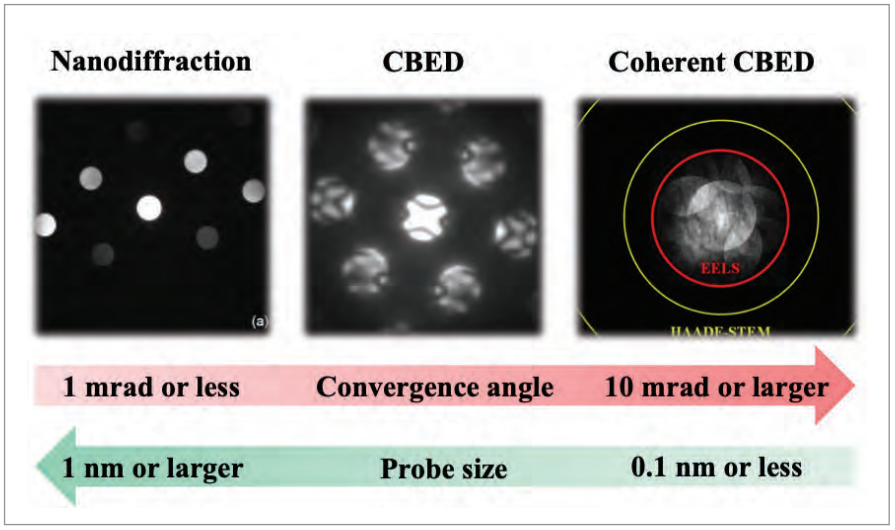


**Figure 1.** **Electron probe size, convergence angle and types of diffraction patterns recorded using a coherent illumination.**

electron microscopy. Diffraction patterns are collected in a STEM for every probe position in analogous to STEM imaging, but rather than integrating diffraction signals using prefabricated detectors, the whole diffraction pattern is recorded in the form of $I(S, x, y)$, with $I$ for diffraction intensity, $x$ and $y$ for the detector coordinates, and $S$ for the sampling points.

In a rectilinear STEM scan, the data is four-dimensional (4D) with the $S=(p_x, p_y)$ for probe position. For this reason, this approach is popularly known as 4D-STEM. The type of diffraction and the information collected changes the probe size. The same probe used for high-resolution STEM imaging produces coherent CBED patterns, or ronchigrams, that were explored by Cowley and Spence in the late 1970s and early 1980s. With a nm-sized probe, nanodiffraction patterns are recorded using the scanning electron nanodiffraction (SEND) [7], and scanning precession electron diffraction (SPED) techniques [8]. In between, scanning convergent beam electron diffraction (SCBED) [9] are used to collect rocking curve information **(Fig. 1)**.

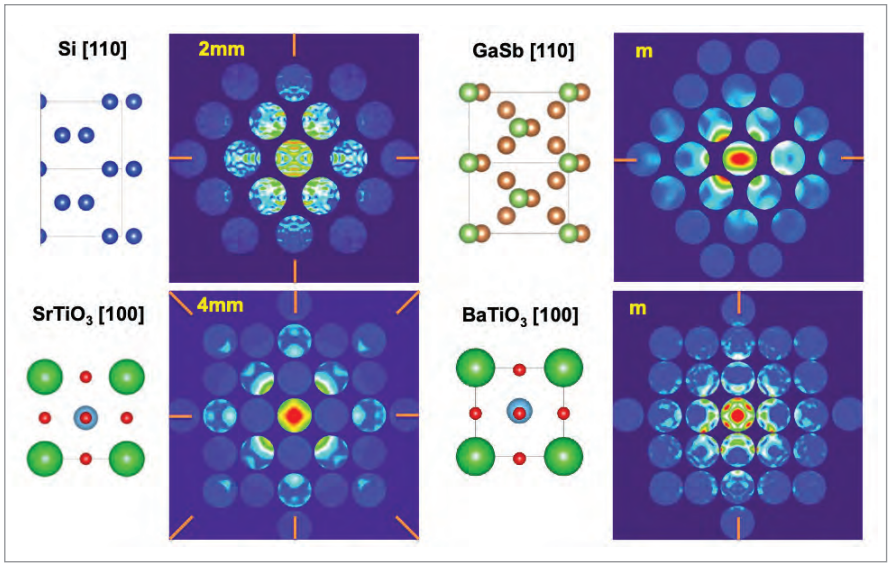


**Figure 2.** **Experimental CBED patterns obtained from centrosymmetric (left column) and noncentrosymmetric (right column) crystals using the SCBED method. Provided by Yu-Tsun Shao.**

The amount of collected data is easily in the range of gigabytes or more. For example, with a readout speed of $10^3$ frames per second, 256x256 pixels per frame, 16 bits in dynamical range and a 256x256 pixel scan, the data size comes to 17 gigabytes, acquired in above a minute. The amount data is more than 10^4 than typical electron images or diffraction patterns captured in a single exposure. The data size will increase as the detector size and readout speed increase.

## Data mining for structural information

Using diffraction patterns, the structure of materials can be interrogated at multiple levels. At Å scale, ptychography using coherent CBED achieves the spatial resolution beyond the diffraction information limit [10, 11]. At nm to micron scales, orientation, phase and strain mapping provides critical information about microstructure, including lattice rotation and deformation in the presence of defects and interfaces. Electron diffuse scattering recorded in DPs also provides information about local disorder, from short-range order (SRO) to the presence of dislocations and stacking faults [12]. Ultimately, grain boundary and orientation imaging at mesoscopic scale can be combined with atomic and nanoscopic structural information for a complete determination of materials' atomic structure.

For data mining, a variety of methods can be brought to bear for the extraction of crystallographic information and for the integration of current knowledge with advancements in data science and machine learning (ML). Dynamical inversion provides the utmost solution for crystals [13]. Electron diffraction simulations using kinematical and dynamical theories developed over past decades play a critical role in building databases for ML [14].

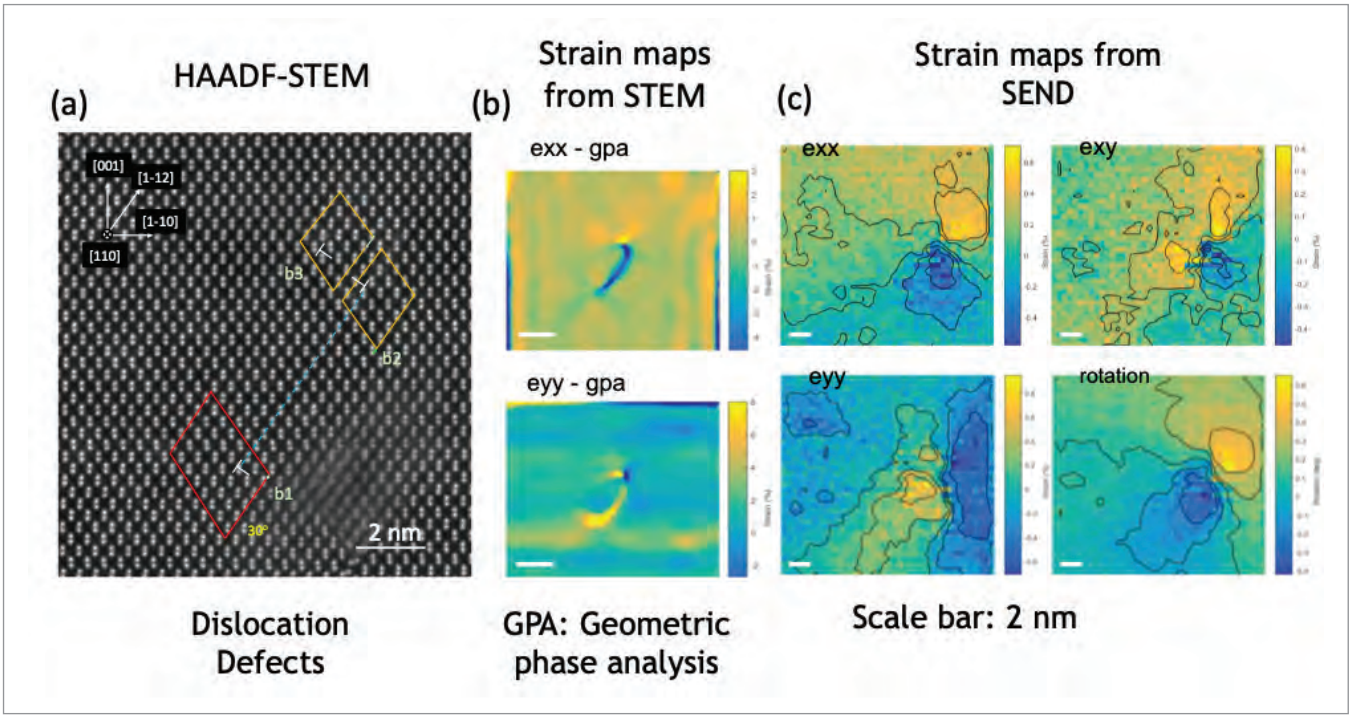


**Figure 3.** Strain mapping of a complex dislocation defect in SiGe. **(a)** A HADDF image of the defect. **(b)** and **(c)** Strain maps measured experimentally using GPA and SEND. Here, x is along [1-10] and y along [001], and the scale bar is 4 nm.

## Impact on Materials Research

### Mapping local crystal symmetry

Scanning CBED combines the most sensitive probe for determining crystal point and space group symmetry [15-18] with STEM. Local crystal symmetry and polarization nanodomains, for example, can be determined this way [19-21]. By comparing a diffraction pair or diffraction pairs, the symmetry of the CBED patterns can be quantified for symmetry mapping. CBED patterns from regions of high symmetry can be averaged to determine local symmetry. Figure shows examples using the symmetry quantification algorithm for CBED patterns obtained from two sets of centrosymmetric and noncentrosymmetric crystals, Si, GaSb, $SrTiO_3$, and $BaTiO_3$ (regions outside the disks being quantified in the CBED pattern are being masked off). The observed symmetry and the measured $\gamma$ values are marked on the CBED patterns.

## Determination of Lattice Strain Fields

Lattice strain broadly affects the properties of materials and there is a long history in imaging strain field using diffraction contrast in TEM based on the effects of strain on diffraction intensities. The lattice strain is measured in 2D projection using SEND with a nm-sized probe. By measuring the well-separated Bragg peaks in the recorded DPs [22], the 2D strain tensor can be calculated. This approach overcomes a major difficulty of electron diffraction contrast imaging, namely, the strain field can be imaged by not measured quantitatively. The precision of strain mapping is determined by the measurement precision of the position of diffraction disks, which is generally higher than the image-based methods [23].

**Figure 3** shows the strain field around misfit dislocations at the interface of two SiGe layers of different composition. The atomic resolution HAADF image reveals a stacking fault bounded by two 30° partial dislocations and a perfect dislocation $b_3$ found near $b_2$. The measured strain fields feature dipole-like features in $\epsilon_{xx}$ and rotation components, while complex features in $\epsilon_{yy}$ and $\epsilon_{xy}$ are observed. Compared with GPA based image analysis, the experimental strain maps demonstrates the good precision, sensitivity, and resolution of the SEND-based strain mapping technique that can be extended for general study of atomic defects.

## Imaging molecular microstructure

Low-dose electron diffraction is generally required for the study of molecular crystals. In electron diffraction imaging, a weak beam or multiple weak beams can be selected from the recorded DPs and by integrating the intensity of the selected beams for each pixel, a weak-beam diffraction image (WBDI) is formed. By recording DPs directly and processing them digitally, WBDI avoids the usual setup involved in diffraction contrast imaging and allows the use of virtual objective apertures of different shapes and sizes, as well as possibility to remove the background intensity, which is simply not possible with direct imaging in a TEM.

A recent example of WBDI is the observation of defect nanodomains in defect-engineered metal–organic

frameworks (MOFs) of UiO-66(Hf) exhibiting a blocky lamellar morphology [24] **(Fig. 4)**. The structure of MOFs is typically characterized by their periodic structure without information about defects and microstructure. The work by Johnstone et al. [24] demonstrated that defect analysis in MOFs can be carried out at nm resolution.

## Fluctuations in diffuse scattering and Patterson function of distortive potential

Elastic diffuse scattering is formed from structural and chemical imperfections that can be explored for imaging. The nature of diffuse scattering depends sensitively on its origin [12]. For this reason, the study of diffuse scattering is used to determine crystal imperfections by traditional methods. However, the interpretation of diffuse scattering is a challenging problem in both X-ray and electron diffraction [25]. Another issue is that electron diffuse scattering is weak, their detection requires a detector with a large dynamic range and good sensitivity to low electron signals. The advance of direct electron detection technology now opens the possibility to map electron diffuse scattering intensities and measure their fluctuations at nm spatial resolution.

In a nanodiffraction pattern obtained using a coherent electron beam, the diffuse scattering is more like laser speckles. The speckle patterns can be analyzed [26] using the difference Cepstrum ($dC_p$)

$$dC_p = \left| FT\left\{ log\left[ \frac{I(\vec{k})}{I_{avg}(\vec{k})} \right] \right\} \right| 23()$$

where $I_{avg}(\vec{k})$ represents intensity in the area averaged pattern, while $I(\vec{k})$ is the intensity in a single pattern from DPs collected over a region of interest (ROI). The interpretation of $dC_p$ for electron diffraction can be made based on the separation of the fluctuating part of the scattering potential ($U_1$) from the average scattering potential ($U_{avg}$, where $U_1$ varies with the electron probe position. Shao *et al.* show that $dC_p$ approximately corresponds to the autocorrelation function, or Patterson function, of the distortive part of scattering potential ($U_1$) in a thin sample.

The sensitivity of $dC_p$ to the distortive part of potential is demonstrated in **Figure**, in which the dislocation core imaged in **Fig. 3a** is analyzed. Four areas (1-4) are identified in the dislocation core. Each of these four areas gives

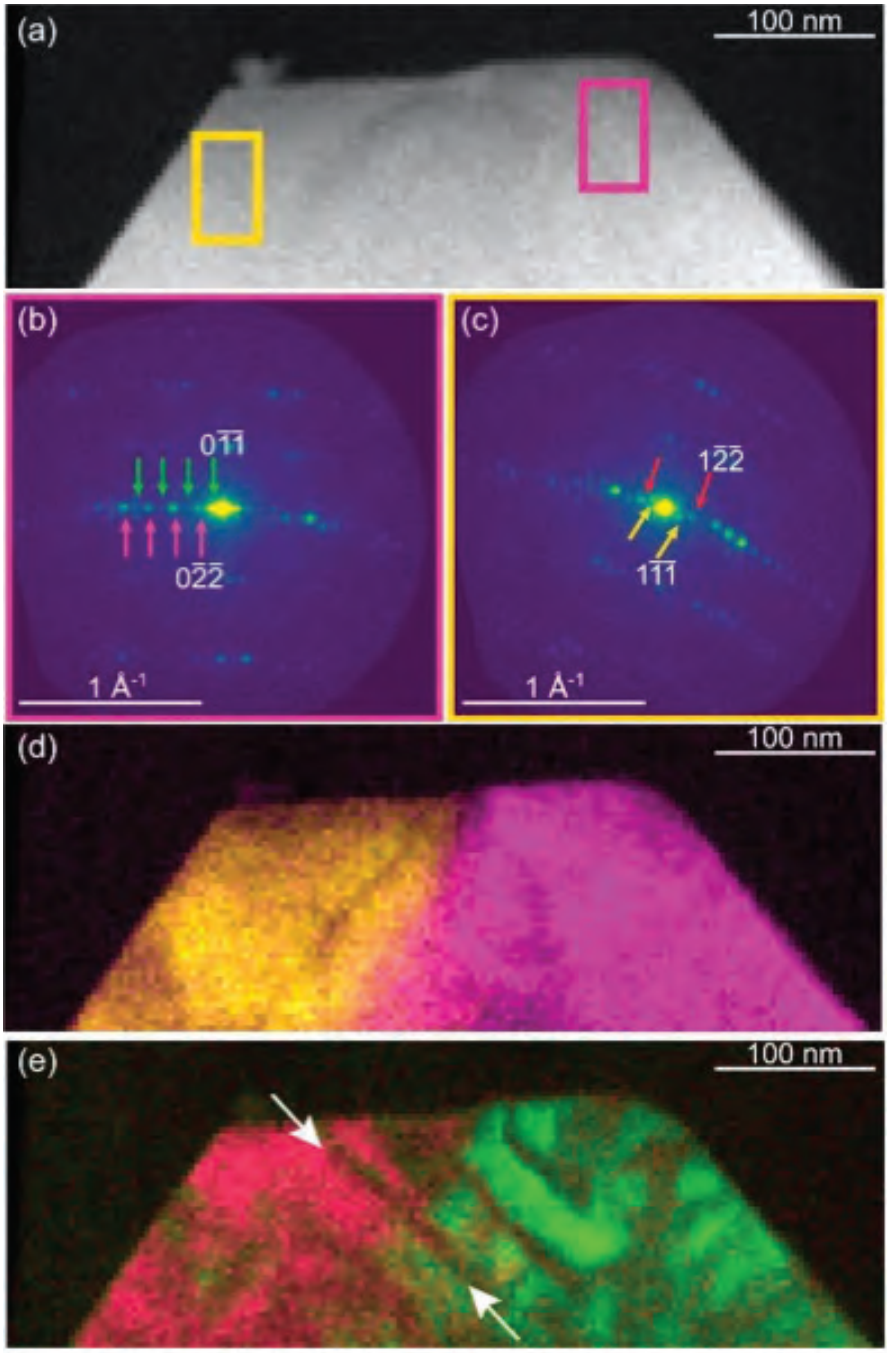


**Figure 4. Electron diffraction imaging analysis of a 6(Hf):5(BDC) UiO-66(Hf) particle with high defect density, containing a grain boundary. (a) ADF-STEM image indicating two marked regions, containing two different phases, where area averaged electron diffraction patterns (b, c) were obtained. The two phases differ by the presence of superlattice reflections. The two DPs also reveal a change in orientation between the left- and right-hand side of the particle. (d) Composite dark-field image formed using strong reflections. (e) Composite VDF image formed using weak superlattice reflections, green in b and red in c, revealing defect domains. (Figure taken from Ref. [24])**

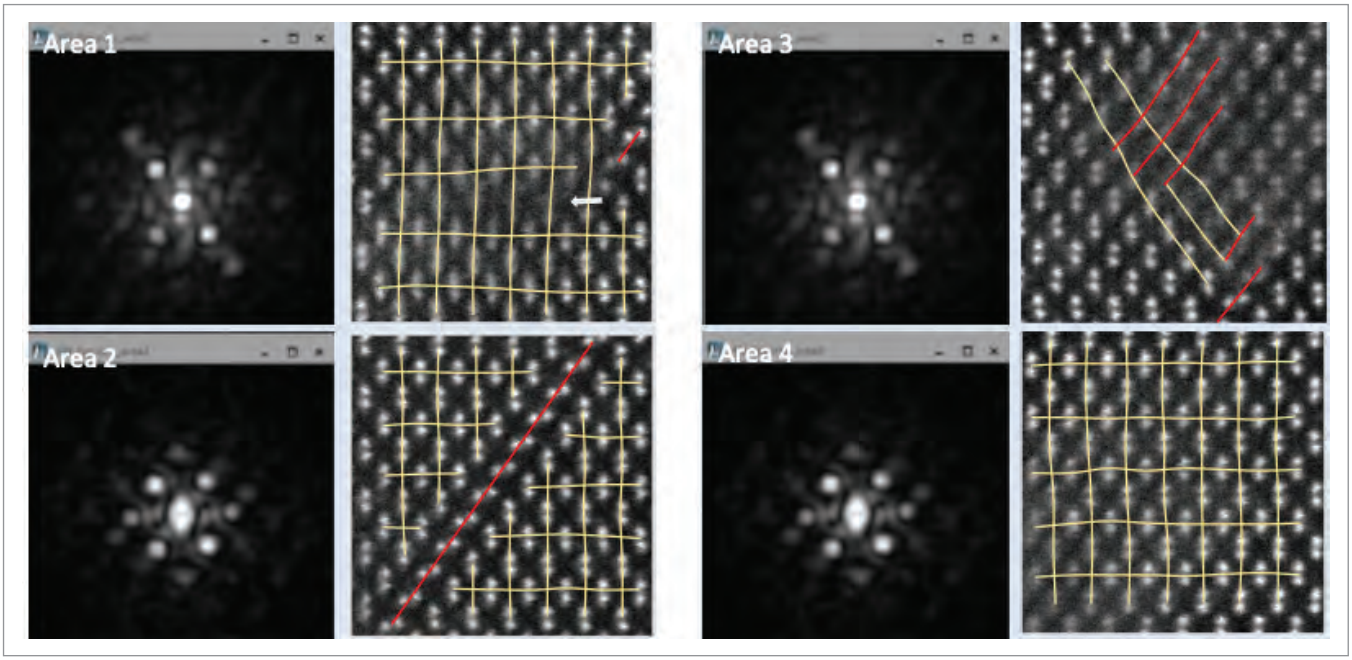


**Figure 5.** **Differential cepstral patterns from 4 areas of dislocation core in (Fig. 4a) and comparison with corresponding atomic resolution HAADF-STEM images**

distinct $dC_p$ pattern, which can be correlated directly with lattice distortions detected at the dislocation by atomic resolution HAADF image. Since diffuse scattering can be measured without the strict zone-axis condition requirement for atomic resolution imaging, the dCp method can be used to detect lattice change in the highly distorted regions or in high-index zone axis orientations for automatic detection of defects.

## Outlook

Since the first TEM was demonstrated by Max Knoll and Ernst Ruska in 1931, the field of electron microcopy has rapidly grown with technological innovations from electron optics to detectors. However, quantitative electron imaging is a rather recent development, starting with HREM and continuing with aberration corrected STEM. Electron diffraction provides the strongest and most highly quantifiable signal. Thus, we expect the development of electron diffraction imaging will accelerate the trend toward diffraction based quantitative analysis and the increasing role of electron diffraction in materials research, where information about atomic structure and microstructure can be extracted with advances in theory and computer algorithms. The type of materials that can be characterized using diffraction imaging approach include both hard and soft materials.

## ACKNOWLEDGMENTS

*This writing of this review was supported by Ivan Racheff Professorship of Materials Science and Engineering, University of Illinois and a Strategic Research Initiative grant from Grainger College of Engineering, University of Illinois.*

## Reference

1. Mollenstedt G (1989) MY EARLY WORK ON CONVERGENT-BEAM ELECTRON-DIFFRACTION. *Physica Status Solidi a-Applied Research* 116(1):13-22.
2. MacGillavry CH (1940) Examination of the dynamic theory of electron diffraction on lattice. *Physica* 7:329-343.
3. Spence JCH & Cowley JM (1978) Lattice imaging in STEM. *Optik* 50:129-142.
4. Cowley JM (1979) Coherent interference in convergent-beam electron-diffraction and shadow imaging. *Ultramicroscopy* 4(4):435-450.
5. Cowley JM (1996) Electron Nanodiffraction: Progress and Prospects. *Microscopy* 45(1):3-10.
6. Zuo JM (1998) Quantitative convergent beam electron diffraction. *Materials Transactions Jim* 39(9):938-946.
7. Tao J, *et al.* (2009) Direct imaging of nanoscale phase separation in $La_{0.55}Ca_{0.45}MnO_3$: Relationship to colossal magnetoresistance. *Physical Review Letters* 103(9):097202.
8. Midgley PA & Eggeman AS (2015) Precession electron diffraction - A topical review. *Iucrj* 2:126-136.
9. Zuo J-M (2019) Electron nanodiffraction. *Springer Handbook of Microscopy*, eds Hawkes PW & Spence JCH (Springer International Publishing, Cham), pp 905-969.

10. Rodenburg JM (2008) Ptychography and related diffractive imaging methods. *Advances in Imaging and Electron Physics, Vol 150,* Advances in Imaging and Electron Physics), Vol 150, pp 87-184.
11. Jiang Y, *et al.* (2018) Electron ptychography of 2D materials to deep sub-ångström resolution. *Nature* 559(7714):343-349.
12. Krivoglaz MA (1996) *Diffuse Scattering of X-Rays and Neutrons by Fluctuations* (Springer-Verlag Berlin Heidelberg).
13. Donatelli JJ & Spence JCH (2020) Inversion of Many-Beam Bragg Intensities for Phasing by Iterated Projections: Removal of Multiple Scattering Artifacts from Diffraction Data. *Physical Review Letters* 125(6):065502.
14. Yuan R, Zhang J, He L, & Zuo J-M (2021) Training artificial neural networks for precision orientation and strain mapping using 4D electron diffraction datasets. *Ultramicroscopy*:113256.
15. Goodman P & Lehmpfuhl G (1968) Observation of the breakdown of Friedel's law in electron diffraction and symmetry determination from zero-layer interactions. *Acta Crystallographica Section A* 24(3):339-347.
16. Buxton BF, Eades JA, Steeds JW, & Rackham GM (1976) The symmetry of electron diffraction zone axis patterns. *Philosophical Transactions of the Royal Society of London. Series A, Mathematical and Physical Sciences* 281(1301):171-194.
17. Morniroli JP & Steeds JW (1992) Microdiffraction as a tool for crystal-structure identification and determination. *Ultramicroscopy* 45(2):219-239.
18. Tanaka M & Tsuda K (2011) Convergent-beam electron diffraction. *Journal of Electron Microscopy* 60:S245-S267.
19. Kim K-H, Payne DA, & Zuo J-M (2015) Determination of 60 degrees polarization nanodomains in a relaxor-based ferroelectric single crystal. *Applied Physics Letters* 107(16):162902.
20. Shao Y-T & Zuo J-M (2017) Nanoscale symmetry fluctuations in ferroelectric barium titanate, $BaTiO_3$. *Acta Crystallographica Section B* 73(4):708-714.
21. Tsuda K, Sano R, & Tanaka M (2013) Observation of rhombohedral nanostructures in the orthorhombic phase of $KNbO_3$ using convergent-beam electron diffraction. *Applied Physics Letters* 102(5):051913.
22. Yuan R, Zhang J, & Zuo J-M (2019) Lattice strain mapping using circular Hough transform for electron diffraction disk detection. *Ultramicroscopy* 207:112837.
23. Zuo JM & Spence JCH (2017) *Advanced Transmission Electron Microscopy, Imaging and Diffraction in Nanoscience* (Springer, New York).
24. Johnstone DN, *et al.* (2020) Direct imaging of correlated defect nanodomains in a metal–organic framework. *Journal of the American Chemical Society* 142(30):13081-13089.
25. Welberry TR (2010) *Diffuse Scattering and Models of Disorder* (Int. Union of Crystallography, Oxford University Press).
26. Shao Y-T, *et al.* (2021) Cepstral scanning transmission electron microscopy imaging of severe lattice distortions. *Ultramicroscopy* 231:113252.

Annick De Backer, Sara Bals, Sandra Van Aert

# A decade of **atom-counting** in scanning transmission electron microscopy

**In this contribution, we provide a concise overview of the atom-counting methodologies and their applications over the past decade. Counting the number of atoms and retrieving the 3D atomic structure of nanoparticles plays an important role to understand the structure-property relation of materials. Therefore, materials characterisation resulting in precise structural information is a crucial point to study nanomaterials at the atomic scale.**

In the field of atomic resolution electron microscopy, annular dark field scanning transmission electron microscopy (ADF STEM) is extensively exploited due to its Z- and thickness contrast. Many efforts have been made to push atomic resolution ADF STEM toward precise measurements of unknown structure parameters.

To reach this goal, statistical parameter estimation theory was introduced. This approach enables quantifying atomic column positions and the total intensity of scattered electrons for each atomic column. The latter is the so-called scattering cross-section which is robust to defocus, source size, magnification, and small sample mistilt[1,2]. Furthermore, these scattering cross-sections increase monotonically with thickness and the atomic number Z. When further analysing the distribution of the scattering cross-sections with advanced quantification procedures, the number and/or type of atoms can be measured.

## Statistical parameter estimation theory

Using statistical parameter estimation theory, the experimental observations are considered as a data plane from which the unknown structure parameters are estimated. The key to the successful application of this approach is the availability of a parametric model which describes the pixel values in the ADF STEM image. Since the intensity is often sharply peaked at the atomic column positions, atom resolution (S)TEM images are modelled as a superposition as Gaussian peaks. The locations of the Gaussian peaks correspond to the atomic column positions and the volume under the Gaussian peaks equals the scattering cross-section. The parametric model consisting of a superposition of Gaussian peaks is fitted to the experimental ADF STEM image using the uniformly weighted least squares criterion. This criterion quantifies the similarity between the experimental data and the model. An efficient implementation of this algorithm is available in the StatSTEM software package[3].

## Atom-counting in homogeneous nanoparticles

To count the number of atoms in each atomic column of homogeneous nanoparticles, different methods were introduced in the past years. Here, the statistics-based atom-counting procedure[4] is illustrated for a Pt nanoparticle illustrated in **Fig. 1**. Based on the estimated parameters, the scattering cross-sections are determined for each atomic column. The distribution of the scattering cross-sections can be represented in a histogram. Ideally, the histogram of scattering cross-sections would consist of isolated components where each component corresponds to a set of atomic columns having the same number of atoms in it (in **Fig. 1** the columns containing, e.g., 7 atoms are coloured orange). In practice, however, the components are smeared out due to a combination of experimental detection noise and the environment. Therefore, the results cannot be interpreted directly in terms of the number of atoms in a column.

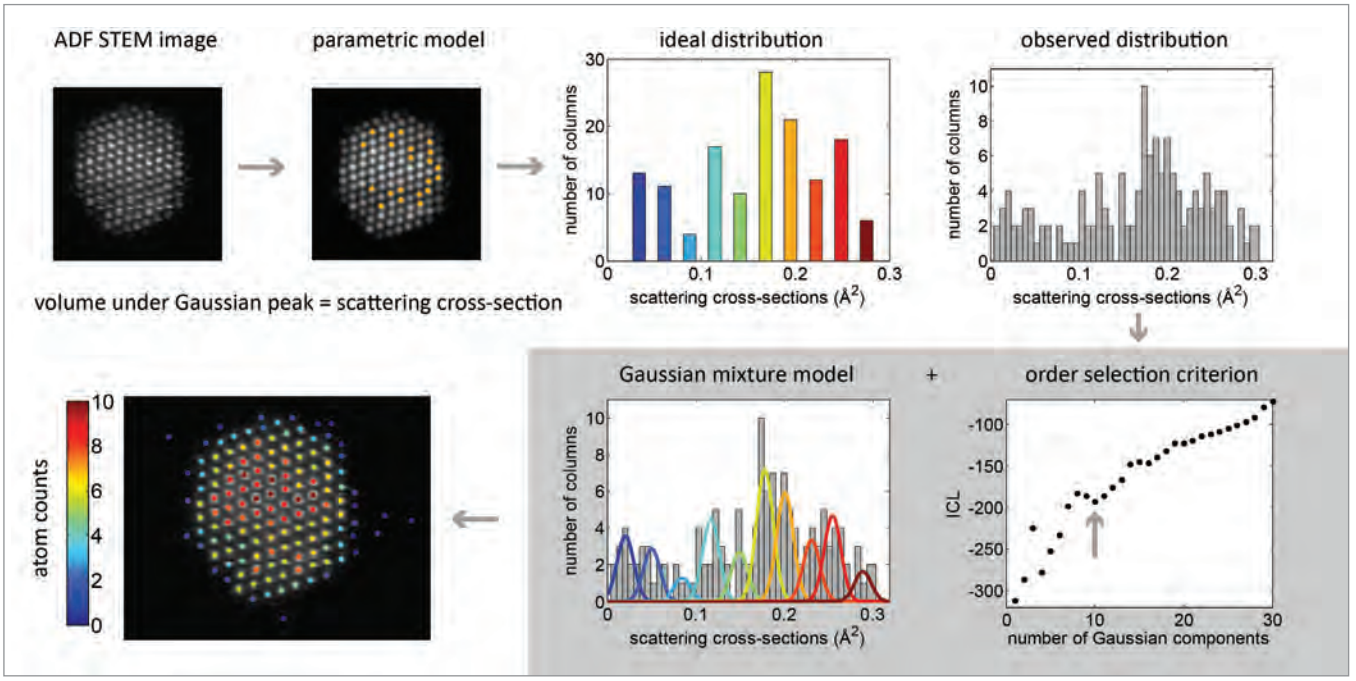


**Figure 1.** Procedure to count the number of atoms in a homogeneous crystalline nanoparticle.

To retrieve the number of components and their locations, a combination of a so-called Gaussian mixture model and an order selection criterion is used. The order selection criterion indicates the number of statistically relevant components in the underlying scattering cross-section measures. The number of components corresponds to a minimum in the evaluation of this criterion as a function of the number of components. For the Pt nanoparticle in **Fig. 1**, 10 components are present, suggesting that the number of atoms varies from 1 up to 10 atoms. The Gaussian mixture model analysis defines the positions, the width, and the proportion of each Gaussian component. The scattering cross-section of each atomic column can then be assigned to the component having the largest probability for this scattering cross-section, leading to a map reflecting the number of atoms for each atomic column.

## From homogeneous to heterogeneous

**Fig. 1** discussed atom-counting for nanoparticles consisting of a single type of element. However, many relevant materials consist of more than one chemical element tailoring specific electronic, optical, or catalytical properties. For this purpose, HAADF STEM imaging can be combined with energy dispersive X-ray spectroscopy [5]. In addition to the HAADF STEM image, at each probe position the resultant X-ray emission spectrum is recorded. These spectra can be used to construct elemental maps from which EDX scattering cross-sections can be estimated. A simple linear scaling between the STEM and EDX scattering cross-sections can be assumed, which has been confirmed theoretically and experimentally. The monotonic increase of both EDX scattering cross-sections and HAADF STEM scattering cross-sections can be used to count the number of atoms. For this purpose, the measured scattering cross-sections are matched to simulated library values, while estimating two scaling parameters for the EDX scattering cross-sections of the two types of elements. In this manner, the number of Ag and Au atoms in a Au@Ag core-shell nanoparticle was determined as illustrated in **Fig. 2**.

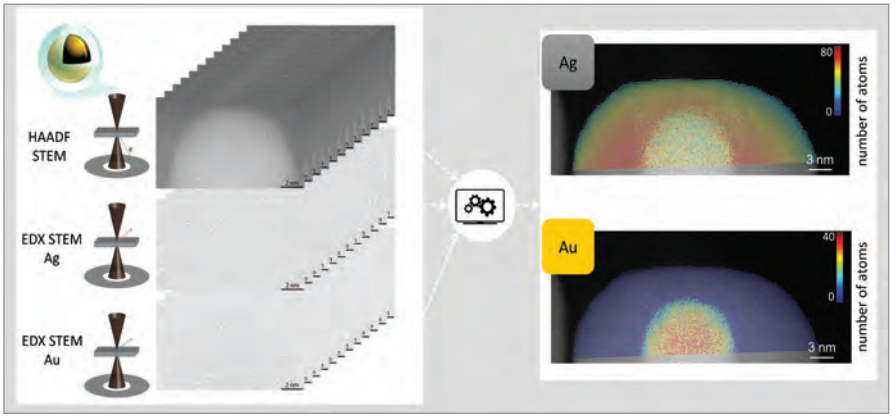


**Figure 2.** Counting the number of Ag and Au atoms in a Au@Ag core-shell nanoparticle by combing HAADF and EDX STEM.

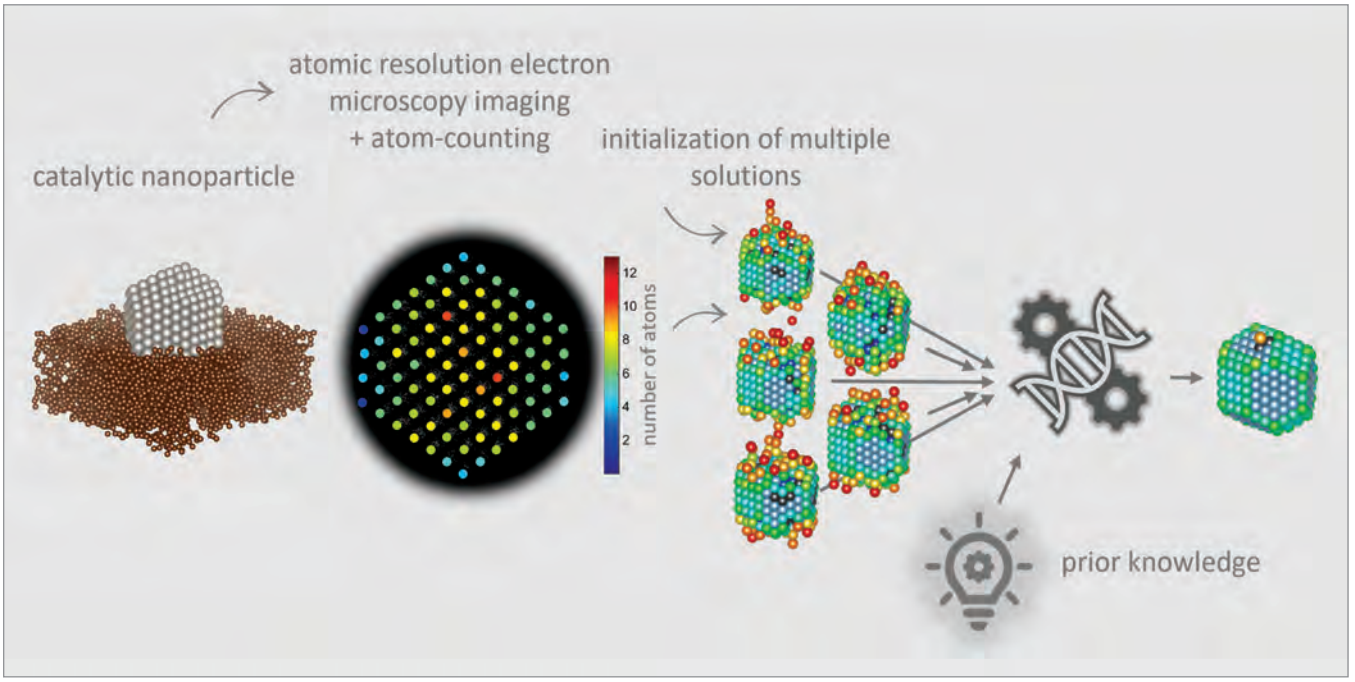


**Figure 3.** Reliable 3D atomic models are obtained based on the atom-counting results using he Baysesian genetic algorithm.

## From 2D to 3D

Using the atom-counting results, it is furthermore possible to retrieve a 3D atomic model from a single projection. For this purpose, the atom-counting results are used to create an initial 3D atomic model. Next an energy minimisation procedure can then be applied to obtain a relaxed 3D reconstruction of the nanoparticle. The traditional energy minimisation schemes, i.e. Monte Carlo approach or full molecular dynamics simulation to relax the nanoparticle's structure, often show some limitations. Either the finite atom-counting precision is ignored, or the final reconstruction ends up in a global energy minimum while the nanoparticle's structure deviates from a ground state configuration. To overcome these limitations, a Bayesian genetic algorithm [6] **(Fig. 3)** was developed. Bayesian methods are powerful tools to rationally combine a priori information with observed data and genetic algorithms are typically used for solving large optimization problems.

Our method enables to minimize the nanoparticle's energy while utilizing a priori information about the finite precision of the atom-counting results and neighbour-mass relations. A significant improvement is observed when including more relevant prior knowledge, especially at lower doses. Therefore, the method is very promising for obtaining reliable reconstructions of beam-sensitive nanoparticles during dynamical processes from images acquired with lower incident electron doses, or where the acquisition of a tilt series is impossible. One of the applications of a 3D atomic reconstruction based on atom-counting results is the quantification of the refaceting of Pt nanoparticles with atomic resolution during various oxidation–reduction cycles [7] **(Fig. 4)**.

The methodologies for atom-counting and 3D atomic modelling, showcased in this contribution, have successfully been applied to a variety of nanoparticles over the past decade [8]. Such results are essential to obtain a deeper understanding in the structure-property relationship of materials and will assist the design of materials with interesting properties which are predictable and producible. ■

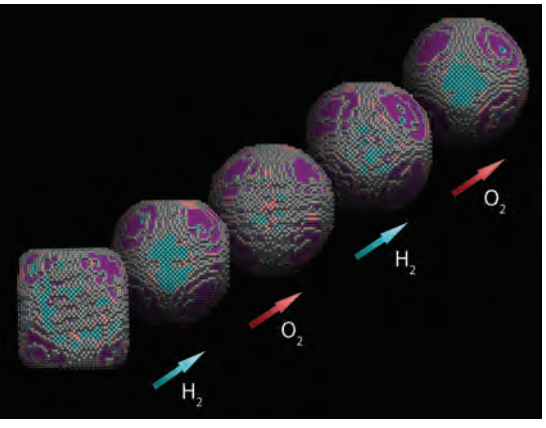


**Figure 4.** Refaceting of a Pt nanoparticle under the flow of different gases.

## References

1. S. Van Aert et al., Ultramicroscopy 109 (2009) 1236.
2. H. E et al., Ultramicroscopy 133 (2013) 109.
3. A. De Backer et al., Ultramicroscopy 171 (2016) 104.
4. S. Van Aert et al., Phys. Rev. B 87 (2013) 064107
5. A. De Backer et al., Small Methods 6 (2022) 2200875
6. A. De Backer et al., npj Comput. Mater. 8 (2022) 215.
7. T. Altantzis et al., Nano Lett. 19 (2018) 477.
8. A. De Backer, S. Bals and S. Van Aert, Ultramicroscopy 247 (2023) 113702.

**Hannes Lichte**
Faculty of Physics, Technische Universität Dresden, Germany - Hannes.Lichte@Triebenberg.de

# **Electron Holography** – in short

In 1924, Louis de Broglie showed that particles hence electrons are waves. His ideas were so mind-blowing that, at first, his PhD-dissertation was rejected by the Physics Faculty at Sorbonne University – yet accepted after intervention of Albert Einstein – but finally, in 1929 he was awarded the Nobel Prize in Physics. Since then, electron optics was increasingly developed as wave optics, in particular in those realms approaching high performance. For example, in TEM particle optics did not allow understanding electron diffraction or the subtleties of image contrast such as Fresnel fringes detected by Boersch [1], or CBED developed by Kossel and Möllenstedt [2]. As a visionary about seeing atoms, in 1949 Scherzer [3] showed that wave optics is indispensable for TEM: He considered atoms as phase objects bending the object wave and initiated wave optical transfer theory of information. He derived that atoms will be visible optimally at Scherzer Focus, because then the wave aberration of the objective lens approaches as closely as possible a Zernike phase plate for optimum phase contrast.

Wave optics seems more demanding, because waves need at least two quantities for a comprehensive description, i.e., local distribution of amplitude $a$ and phase $\varphi$, as

$$\psi(\vec{r}) = a(\vec{r}) \exp\left[i\varphi(\vec{r})\right]$$

After passage through an object, an initially plane wave is modulated both in amplitude and phase forming the object exit wave. Amplitude modulation comes about, e.g., by loss of electrons due to scattering into angles larger than the acceptance angle of the objective lens, and by inelastic interaction, which ejects the respective electrons from the inherent wave into a different one. Phase modulation arises from local variations of the index of refraction, i.e., electric potentials and magnetic fields originating from the object, which are indispensable for understanding properties and function.

The image recorded by a detector shows the intensity distribution of the wave given by

$$I(\vec{r}) = \psi(\vec{r})\psi^*(\vec{r})$$

where the asterisk denotes the complex conjugate wave. Evidently, the intensity depicts only the squared amplitude $a^2$, whereas the phase $\varphi$ is lost. This loss of phase information means a considerable loss of object information. By means of the wave equation, this loss relates to the famous Phase Problem of Diffraction found at first with X-ray diffraction; it says that the real space structure of an object can only be determined from its far-field diffraction pattern, if the phases of all reflections are known [4]. With his work, Wolfke stimulated a row of efforts for a solution, which is finally achieved in general by holography.

## Electron Holography

In face of the early results of Scherzer [5] showing that aberrations cannot be avoided with the usual round electron lenses, Dennis Gabor brooded about a solution by lens-less imaging: No lens, no aberrations. Of course, Gabor was aware of the fact that a wave propagates in space according to the wave equation; therefore, one can determine the wave everywhere, if one knows it completely by amplitude and phase on an – ideally closed – surface; the solution is the Kirchhoff-Diffraction Integral mathematically representing Huygens-principle. As well-established in light optics, phases are best recorded by interference of the object wave with a known reference wave.

However, it is extremely cumbersome to determine a phase distribution over an extended area at a density of sampling points sufficient for obtaining a good lateral resolution. It was the ingenious mind of Gabor to understand and utilize an interference pattern as a highly complex diffraction grating, where contrast and position of the interference fringes encode amplitude $a$ and phase $\varphi$, respectively. In his pioneering paper [6], at the example of light waves, he showed that one of the waves, resulting from diffraction of a copy of the reference wave

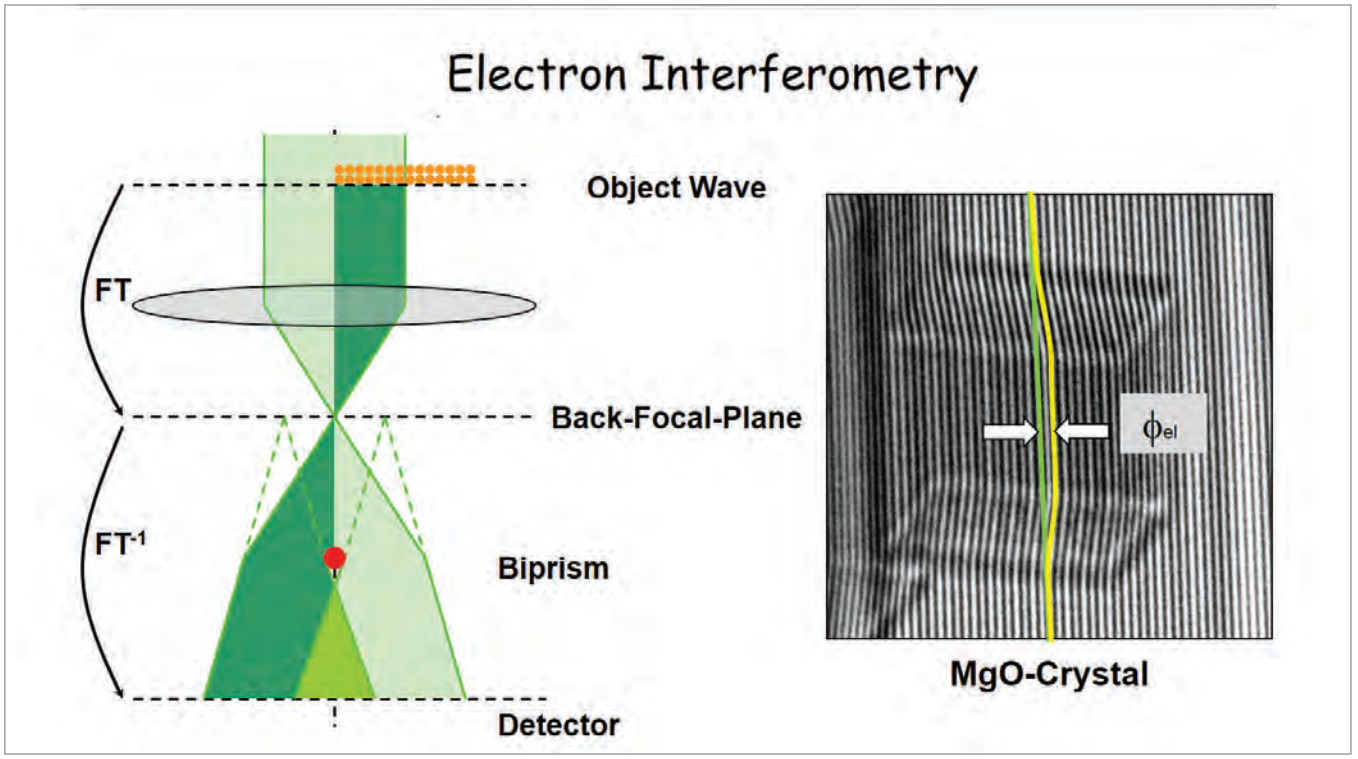


**Figure 1.** **Electron Biprism Interferometry. By means of the electron biprism, in the image plane an unmodulated part is superimposed off-axis on the object wave in the bright green area. In the interferogram recorded on the detector, the deflection of the interference fringes shows the object-related phase shift $\Phi_{el}$, which is evaluated by means of a ruler. Usually, the fringe contrast variations exhibiting the object amplitude modulations are not considered.**

at a hologram, is the desirable object wave reconstructed; the other one is the "twin-image", i.e., the conjugate object wave. After all, the original wave is revived for further handling and evaluation.

In this sense, every interference pattern is a hologram. In principle, it does not matter, where in the path of rays it is recorded, because, by means of the wave equation, the reconstructed wave may be propagated to any plane of interest, e.g., to the object exit face or to Fourier space.

However, since in contrast to a LASER, the coherence of electrons is severely limited, optimum results in terms of resolution and field of view of the reconstructed wave are achieved only, if the hologram is recorded close to the object or its image plane.

Another restriction comes about because of the twin image overlapping with the object wave. Rather than under in-line superposition of reference wave to the object wave as proposed by Gabor, only in the case of an off-axis scheme superimposing the two at an angle, the twin images are separable because they are propagating in different directions; consequently, they can be separated in Fourier space. At the end, of the many thinkable realizations of holography, the most successful one for electrons is Image Plane Off-Axis Holography pioneered by Möllenstedt and Wahl.

## Electron interferometry – the precursor of image plane off-axis electron holography

In order to record the phases of electron waves, Möllenstedt and Düker [7] developed electron biprism interferometry **(fig.1)**.

The biprism divides a plane wave front into two coherent partial waves, one of them propagates through the object resulting as object wave $\psi = a\ exp\ [i\ \varphi]$

The other one remains a plane reference wave $r=1$. Then the interference pattern reads as

$$I_{int}=(\psi+r)(\psi+r)^* = 1+a^2+2|\mu|a\ cos(2\ \pi k\beta x + \varphi)$$

with wavenumber $k=1/\lambda$, angle of superposition $\beta$, and degree of coherence $0 \leq |\mu| \leq 1$. The cosine-term allows determining the amplitude $a$ from local contrast and the phase $\varphi$ from local position of the interference fringes. The phase is given by the electric and magnetic properties of the object as

$$\varphi(x,y) = \frac{e}{\hbar v} V_{proj}(x,y) - \frac{e}{\hbar}\Phi(x,y)$$

with "projected electric potential"

$$V_{proj}(x,y) = \int V(x,y,z)dz$$

integrated through the object, and the magnetic flux

$$\Phi(x,y) = \oint \vec{A}(x,y,z)d\vec{s}$$

embraced by the two superimposed waves; $\nu$ is the electron velocity. Evidently, an interferogram represents all data needed for determining the object wave. Alas, people were not yet aware about the fact that these interferograms indeed are image plane off-axis holograms.

## Electron holography – further development

The first electron holograms were Fresnel in-line holograms recorded in 1952 by Haine and Mulvey [8]. Essentially, these were Fresnel diffraction patterns, i.e., defocused images of the very coherently illuminated object, showing high-contrast Fresnel interference phenomena. The holographic principle was proven for electrons, but the reconstructed light wave was heavily disturbed by the twin-image. In 1968, Tonomura et al. [9] published experiments in Fraunhofer-in-line holography hoping to avoid the twin image problem.

They recorded the hologram in the far-field of the object, because then the mutual axial distance of the reconstructed wave from its twin image is so large that the latter contributes only an unstructured background. Unfortunately, to meet the Fraunhofer condition, the object must be very small and a poor lateral resolution results.

Following the idea of Leith and Upatnieks [10], also in 1968, Möllenstedt and Wahl [11] for the first time recorded Fresnel Off-axis electron holograms using an electron biprism, they showed that the off-axis technique is the final solution of the twin-image problem. Stimulated by these findings aiming at atomic resolution, Wahl found out that the holograms have to be taken as image plane off-axis holograms, i.e., in the image plane of the object; only then the coherence limits of electrons would not restrict lateral resolution. In profound investigations, both experimental and theoretical, he laid the foundation for the so far most successful method of electron holography still to date [12].

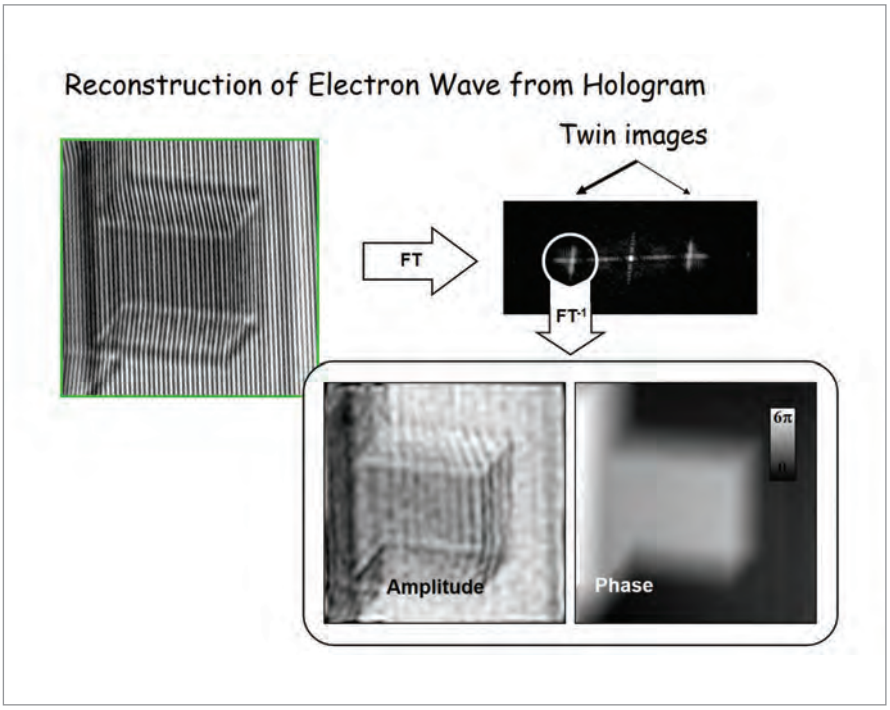


**Figure 2. Electron off-axis image plane holography. From the interferogram in fig.1 considered as a hologram, the object wave is reconstructed as follows: The waves diffracted at the hologram are determined by Fourier Transform FT. There are three waves, i.e., from left to right, object wave, zero beam plus autocorrelation, and conjugate object wave (twin image). After masking out the object wave, by inverse FT one finds the object wave, i.e., amplitude and phase distribution, in real space. Here, the scheme developed by Wahl for light-optical reconstruction on an optical bench, is performed numerically by image processing.**

## Image plane off-axis electron holography

For his pioneering works in the early 1970s, Wahl had at his disposal only comparably old-fashioned equipment, namely an Elmiskop I, operated with not very stable electronics with electronic valves for currents and voltages; for higher brightness, he equipped it with a tipped thermionic emitter.

Despite all the technical insufficiencies, he developed the physics and showed the holographic potential: applying light optical reconstruction and evaluation of the reconstructed light wave, for example by Zernike phase contrast and holographic interferometry. Interestingly, he already proved the possibility of aberration correction in that he reconstructed a light optical focal series from one hologram.

The subsequent development to high performance concerns first of all the improvement of the holograms according to the criteria field of view, lateral resolution (fringe spacing) and signal resolution (fringe contrast and definiteness). Signal resolution describes the discernibility of tiny phase differences between adjacent pixels; the phase shift of a single Oxygen atom of $2\pi/50$ may serve as an orientation value. Finally, atomic resolution was achieved [13]. Interestingly, all three above criteria together form a figure of merit, which we call Holographic Information Content. It is determined by quality factors such as brightness of electron beam, stability of lenses

and deflectors, MTF and DQE of the detector, strength of AC-stray fields and mechanical disturbances of the environment of the TEM – as well as skill and patience of the operator [14].

Nowadays, the electron wave is reconstructed numerically by image processing using the procedures developed by Wahl. An example is shown in **fig. 2**. The advantages of numerical vs. light-optical reconstruction are overwhelming: Once the hologram is fed into the computer, all thinkable processing steps are possible; they are precise, reproducible, and most flexible, e.g., for taking measures for correction of arbitrary aberrations, and finally, all data are given in terms of amplitude and phase quantitatively.

Today, after 50 years of development, the quality of holographical amplitude and phase images matches the one of highest performance TEM images; these conventional images, however, – in particular at aberration correction – do not reveal the phases. By holography, electric and magnetic fields in and around objects are accessible in the range between several µm down to fractions of nm **(figs. 3 and 4)**. Atomic resolution is reached with electric fields, in particular after fine-tuning of aberrations **(fig. 5)**. Since atomic phase shift depends on the atomic number, it allows discriminating the different atom species, for example in GaAs. Alas, atomic details of magnetism cannot yet be analyzed, because their phase shifting effects, by orders of magnitude, are smaller than the today best reachable phase resolution of $2\pi/300$ under atomic lateral resolution.

The object wave in real space allows determining the complex Fourier spectrum, again complete with amplitudes and phases. Therefore, all imaginable variants of Small Area Diffraction are possible for structure determination; the other way around, one can extract arbitrarily selected areas in Fourier space for determining their

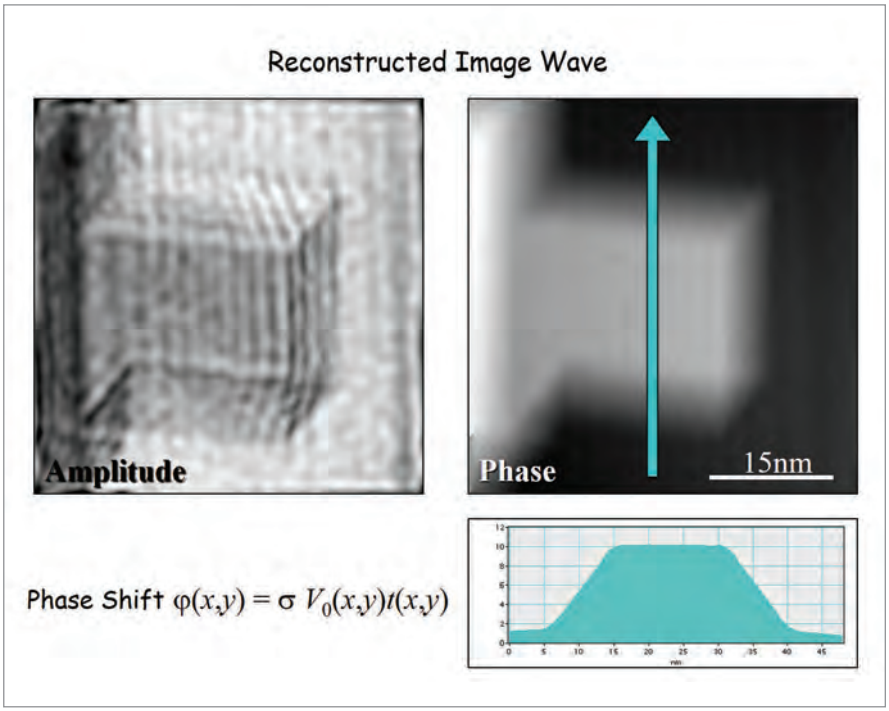


**Figure 3.** Reconstructed amplitude and phase image. The slightly tilted MgO-cube is seen in the amplitude like a wire-frame structure, in the phase image under large-area phase contrast (ideal Zernike phase contrast) in its projected potential. The quantitative phase distribution allows measuring the Mean Inner Potential $V_0$ from the known thickness distribution $t(x,y)$ where $\sigma = e/\hbar\upsilon$ with $\upsilon$ electron velocity.

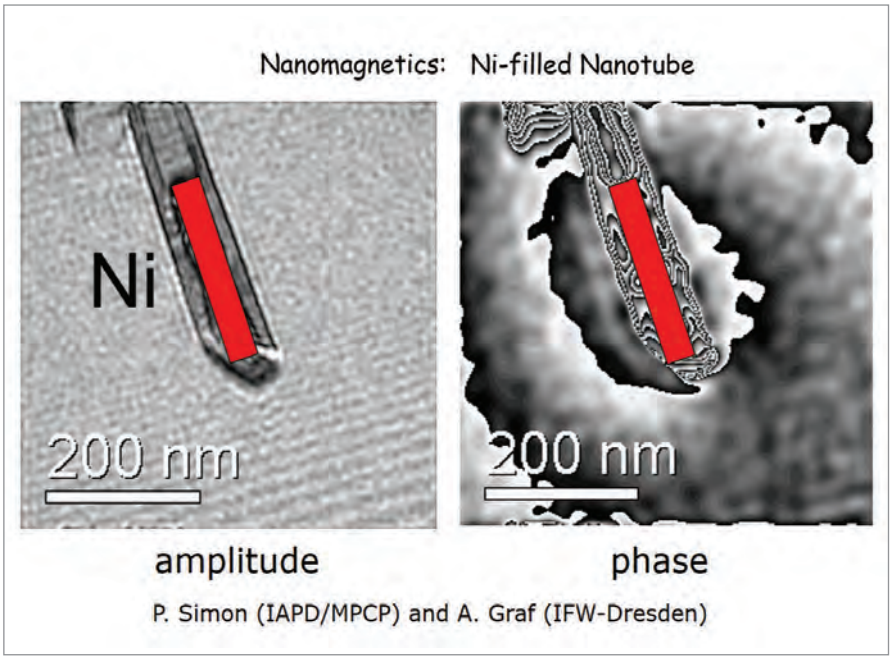


**Figure 4.** Magnetic phase shift around a Ni-rod embedded in a Nanotube. The contrast reversal bright to dark describes phase jumps from $2\pi$ to 0. Note that the magnetic phase increases from left to right on both sides of the rod, instead of increasing on one side and decreasing on the other one, as found for electrostatic phase shift. The curling in the phase line stems from small electrostatic contributions by the granular carrier foil. Example from a cooperation of Paul Simon and Andreas Graf.

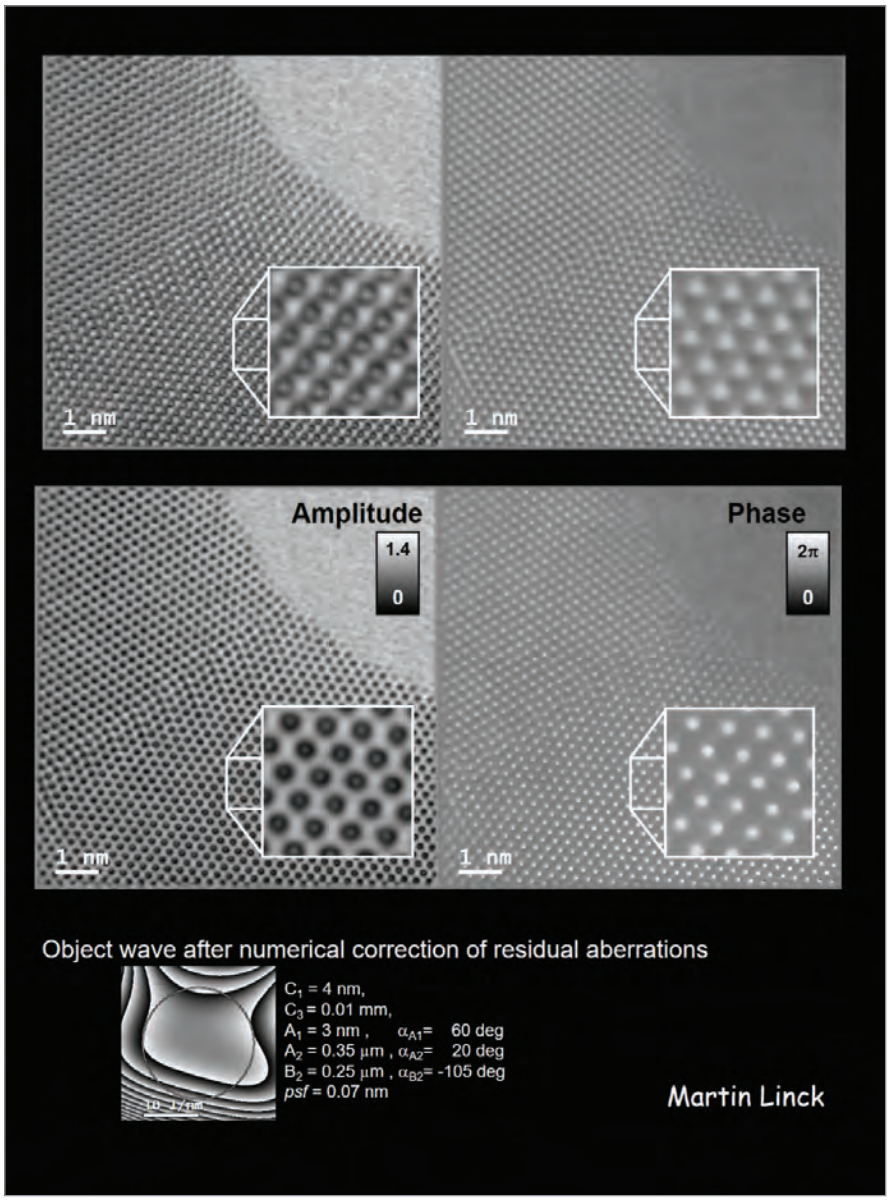


**Figure 5.** Atomic resolution holography of a (110)-oriented Gold crystal [15]. **Top:** Wave reconstructed from a hologram recorded in an aberration-corrected TEM. Violation of symmetry in the atomic structures visible in the inserts suggest effects of residual aberrations. **Middle:** Wave reconstructed after holographic fine-tuning of aberrations during reconstruction. Now the symmetry and the atoms appearance in both amplitude and phase are perfect. At the edge to the hole at top right, single gold atoms are clearly seen producing a phase peak of $2\pi/12$ . **Bottom:** Phase plate used for fine-tuning of aberrations on the reconstructed Fourier spectrum.

contributions to the real space structure. Since all the acquired data stem from the very same hologram, they jointly represent exactly the same object state and hence are mutually relatable. This is not possible with any of the other methods such as focal series restoration, etc., probably recording different object states.

These amazing results show todays possibilities of holography for unprecedented comprehensive analysis of materials structure, properties and fields. Interestingly, combination of hardware correction aberration and holography gives most benefits to both sides in that aberration correction improves hologram quality, and holography allows analyzing the phase information from the object.

This state of the art of electron holography is the achievement of many. Unfortunately, in such a short report, one cannot retrace the diverse, entangled paths of development and attribute the merits to the deserving persons. Therefore, at least, reference is given to review articles authored by the contributors [16-21].

## Novel developments in image plane off-axis holography

Because of the reached high performance, there is increasingly more room for further development. The final goal is the comprehensive analysis of all details in situ and even in operando. Some of these are on the way:

### Holographic Tomography

One problem stems from the fact that the reconstructed phase shows three-dimensional electric potentials and magnetic fields only in 2D projected along the electron trajectory $z$ and hence their distribution in $z$ is lost for evaluation. For solution, holography is combined with tomography: For each tilt of a tilt series a 2D-hologram is recorded; all the reconstructed 2D-phase images are combined in a 3D-phase volume by specific algorithms. Slicing through the 3D-volume allows determining the phase distribution across arbitrary areas or along any path through the object [22]. For scalar fields such as potentials, one tilt series is enough, however, vector fields such as magnetic fields need two series about independent axes [23]. As an example, **fig. 6** shows the 3D-structure of Skyrmions.

### Time resolved holography

The exposure time averages the time variations of object structures hence gives the achievable time resolution of several seconds. Consequently, in a dynamically operated object system, the switching behavior in electric

devices cannot be analyzed appropriately. For this purpose, Lehmann et al. have developed the method of *Interference Gating* [24]. Switching the contrast synchronously in a pump-probe scheme, e.g., pumping an applied potential and probing by gating interference with some delay, they create holographic time series of processes allowing time resolution as good 5ns.

### Inelastic holography

As mentioned above, inelastically scattered electrons are ejected from their inherent wave forming the elastic image, where their loss dampens the amplitude. Of course the inelastic electrons are still in the beam, but now in a wave newborn by the inelastic process. The question arises, how these electrons contribute to a detected image or an EELS-spectrum. For understanding, most decisive are the coherence properties both inside the newborn wave and with respect to the elastic ones, for the manifold excitations occurring. Examples are found in [25]; more novel insights and new results are under preparation. ■

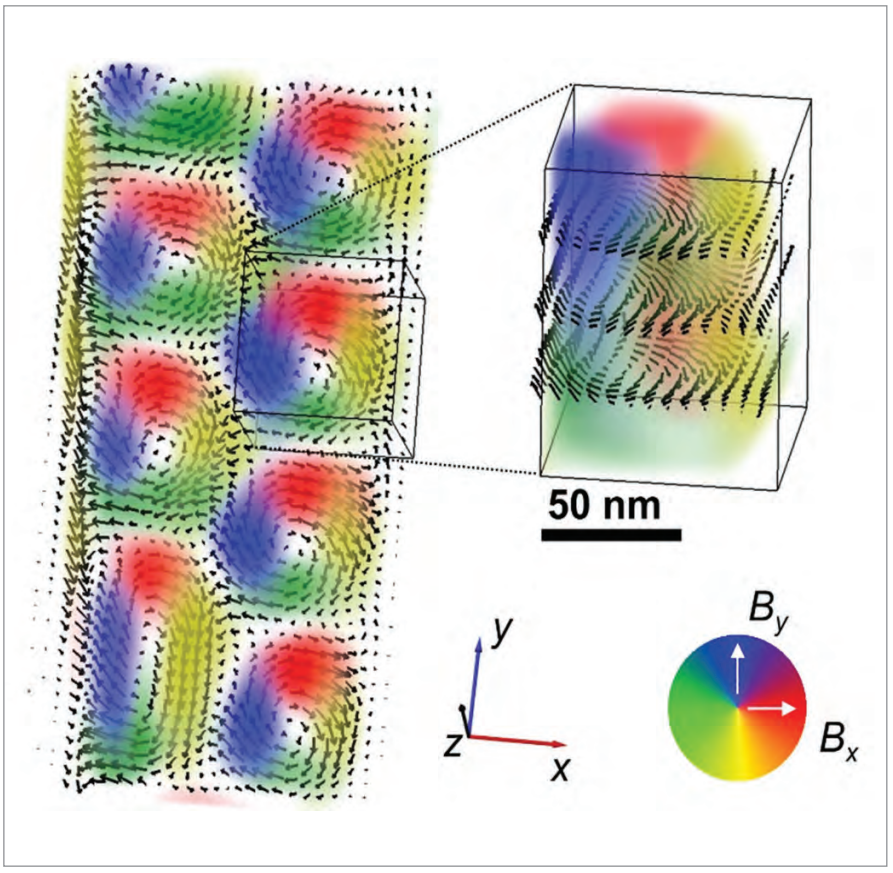


**Figure 6. Holographic Tomography. 3D magnetic induction of Skyrmions in a FeGe sample (courtesy of Daniel Wolf). Left: Color-coded components $B_x$ and $B_y$ with arrow plots show the direction and magnitude of the magnetic field. Right: Extracted single Skyrmion tubes with arrow plots at a top, middle and bottom plane.**

## References


1. H. Boersch (1940), Naturwissenschaften 28, 709
2. W. Kossel and G. Möllenstedt (1939), Annalen der Physik 428(2), 113-140
3. O. Scherzer (1949), J. Appl. Phys 20,20
4. M. Wolfke (1920), Physikalische Zeitschrift, 21, 495-7
5. O. Scherzer, (1936) *Z. Physik*, **101**, 593-603
6. D. Gabor (1948), *Nature* 161, 563–4
7. G. Möllenstedt and H. Düker (1956), *Z. Phys.* 145 377–97
8. M.E. Haine and T. Mulvey (1952) *J. Opt. Soc. Am.* 42 763
9. A. Tonomura, A. Fukuhara, H. Watanabe and T. Komoda (1968), Jpn J Appl. Phys. 7,295
10. E.H. Leith and J. Upatnieks (1962), *J. Opt. Soc.* Am. 52 1123–30
11. G. Möllenstedt and H. Wahl (1968) *Naturwissenschaften* 55 340–1
12. H. Wahl (1975), *Bildebenenholographie mit Elektronen*, Thesis, University of Tübingen
13. H. Lichte (1991) *Adv. Opt. Electron. Microsc.* 12 25–91
14. H. Lichte and M. Lehmann (2008), Annu. Rev. Modern Physics 71, 016102
15. M. Linck, B. Freitag, S. Kujawa, M. Lehmann and T. Niermann (2012), Ultramicroscopy 116, 13-23
16. A. Tonomura (1999), *Electron Holography*, Series in Optical Sciences, Springer, Berlin, Heidelberg
17. M. Beleggia, G. Pozzi, A. Tonomura (2010), Ultramicroscopy, 110 (11), 1428-1433.
18. Dunin-Borkowski RE, Kovács A, Kasama T, McCartney MR, Smith DJ (2019), Electron holography. Chapter 16 in 2nd edition of "Springer Handbook of Microscopy", pp. 767-818, edited by P W Hawkes and J C H Spence.
19. K. Harada (2021), Microscopy 70, 3 – 16.
20. M.R. McCartney, R. E. Dunin-Borkowski, David J. Smith (2019), Ultramicroscopy 203, 105–118
21. H. Lichte and M. Lehmann (2016), chapters 7 and 8 in *Transmission Electron Microscopy*, C. Barry Carter and David B. Williams eds, Springer ISBN 978-3-319-26649-7
22. D. Wolf , A. Lubk, F. Röder, H. Lichte (2013), Current Opinion in Solid State and Materials Science 17 (2013) 126–134
23. D. Wolf *et al.* (2022), *Nat. Nanotechnol.*. 17, 250
24. T. Wagner, T. Niermann, F. Urban, M. Lehmann (2019), Ultramicroscopy 206, 112824.
25. F. Roeder, H. Lichte (2011), Eur. Phys. J. Appl. Phys. 110, 33504.

**Joachim Frank**

Department of Biochemistry and Molecular Biophysics and Department of Biological Sciences, Columbia University, New York, USA

## SINGLE-PARTICLE CRYO-EM

# My lab's contributions to the revolution of structural biology in the past 25 years

I would like to start these reminiscences by recalling that in my lab, starting as early as 1981 with the first demonstration of 2D single-particle averaging (Frank et al., 1981), we adopted the ribosome as the "poster molecule" with which we tried out every new technique of data processing -- but at the time without much appreciation for the ribosome's pivotal role in all life processes. Its large size, high contrast and stability was just what we needed to get started. It became of course much more than that: new knowledge emerged as we obtained the first 3D images that could not have been obtained by any other technique of visualization.

Twenty-five years brings us back to the time when single-particle cryo-EM was just past its *Kinderkrankheiten*, its childhood diseases, and thought to be a nice technique of visualization, adding some dearly needed information of motion to the static pictures created by protein X-ray crystallography -- but without a chance of ever being able to compete with the latter in spatial resolution. Just three years before that, the *E. coli* ribosome had emerged for the first time in beautiful clarity in three dimensions (Frank et al., 1995) but at a resolution (25 A) still far away from the level required to discern and understand its actions. From that time on, my lab was on a double-track: the continued development of single-particle cryo-EM on the one hand, and the pursuit of research on the structural basis of protein synthesis on the other. Rajendra Agrawal, one of my postdocs at the time, helped me set up a wetlab specialized in ribosome biochemistry after I became a full HHMI investigator in 1998.

I remember 1998-2000 as the exciting time when we (Rajendra Agrawal and I) discovered the ratchet-like inter-subunit rotation of the ribosome (Agrawal et al., 1999; Frank and Agrawal, 2000) -- a gigantic motion on the molecular scale, where every Angstrom counts. We discovered it by comparing the 3D maps obtained from two *E. coli* ribosome samples, one with and one without EF-G in the presence of a nonhydrolyzable GTP analog. The existence of this motion was later confirmed in real time by bulk FRET (Ermolenko et al., 2007) and smFRET (Cornish et al., 2008; Fei et al., 2008), and was recognized as a motion instrumental for mRNA-tRNA translocation during each cycle of protein elongation (Horan et al., 2007). I recently had occasion to point out (Frank, 2021), in a tribute to Alexander Spirin, that he had the early insight to attribute ribosome function during the polypeptide elongation cycle to the action of a thermally-driven ratchet (Spirin, 2002; 2009).

As we found ourselves unable to compete in the race for the first atomic-resolution structure of the ribosome – or, for that matter, of any molecule lacking symmetry, it was nevertheless gratifying to see that we were able to make an important contribution toward the phasing of the X-ray structure of the large ribosomal subunit (Ban et al., 1998; Penczek et al., 1999; Ban et al., 2000).

(The pursuit of research on structure and function of the ribosome is difficult to cover in a short essay as it became ever more multi-faceted as the resolution advanced, so I will confine this account to our continued work on cryo-EM methodology.)

The view that emerged at that time was that the marriage of the two techniques – one contributing high-resolution structural information of a macromolecule, the other providing crucial information on its domain motions – was the best way to leverage the power of cryo-EM. Consequently, the methods development in our lab, as in the work of others, concentrated on techniques for interpreting cryo-EM maps in terms of existing atomic structures: by rigid-body fitting (real-space refinement; Gao et al., 2003; Gao and Frank, 2005) or flexible fitting (normal mode analysis, Tama et al., 2003; molecular dynamics flexible fitting (MDFF), Trabuco et al., 2008) for several years. In this way, functionally important domain motions could be precisely described and traced back to their presumptive structural origins. At this point I should acknowledge our collaborations with specialists of algorithm developments, whose experience was pivotal in carrying out this work: Michael Chapman, Charles Brooks III and the late Klaus Schulten, respectively. Obviously, these techniques have become less important after the introduction of electron detecting cameras in 2012, but they are still in use.

A unique opportunity offered by cryo-EM is the extraction of homogeneous subpopulations from a heterogeneous mixture of molecules present in the electron micrograph – "Story in a Sample" was the catchword I coined at the time (Frank, 2013). Initially, this was accomplished by supervised classification via template matching; an example for its application was the discovery of the twisted, deformed conformation that tRNA assumes in the A/P state during the tRNA section process (Valle et al., 2002; Yarus et al., 2003). Later much superior maximum likelihood algorithms were introduced (Scheres et al., 2007; Scheres, 2012) which offered a quantitative basis for 3D classification, foregoing the need for templates. In this latter development my lab had a relatively minor role, in supplying a large dataset of ribosome images previously sorted by supervised classification (Scheres et al., 2007). Today, of course, a number of packages offer an abundance of choices to analyze and sort molecule projections into classes, among them neural network-based approaches showing great promise.

In the years after the "resolution revolution," following the introduction of direct electron detecting cameras around 2012, methods for the collection and processing of data matured and spatial resolutions approached 1A, and it became quite clear that understanding life processes or drug discovery would not likely be advanced by further improvements in resolution. I found that instead, two new directions of cryo-EM development would be worth pursuing: (1) time-resolved cryo-EM, to follow reactions in real time, and (2) the analysis of large data sets from molecules in thermal equilibrium, toward characterization of occupancies in a continuum of states.

Let me briefly elaborate on these two new directions. Given the long (> 5s) duration of the sample preparation -- from pipetting of a sample to the procurement of the EM grid with the sample in vitrified ice – it is impossible to follow biomolecular reactions in real time with normal methods of cryo-EM. Time-resolved methods, in contrast, make use of microfluidic chips to start a reaction of two components, by mixing them, letting them react, and depositing the reaction product onto the EM grid. We have used this technique in several recent studies to determine intermediate states during translation (Fu et al., 2016; Fu et al., 2019; Kaledhonkar et al., 2019; Bhattacharjee et al., 2023).

The second direction of development has been the result of a close collaboration with Abbas Ourmazd and Peter Schwander, at the University of Wisconsin at Milwaukee. Methods of geometric machine learning are applied to massive amounts of cryo-EM data in efforts to map the continuum of states of a biomolecule in the thermal equilibrium (Dashti et al., 2014; Frank and Ourmazd, 2016; Seitz et al., 2022). To date, we have applied this method to the ribosome (Dashti et al., 2014), Ryanodine receptor (Dashti et al., 2020) and SARS Cov2 spike protein (Sztain et al., 2021). In each case, the energy landscape of the molecule was retrieved, revealing the rationale for its functional behavior.

In conclusion, the past 25 years have demonstrated the surprising power of single-particle cryo-EM to yield data far exceeding the visualization of single, static states but going to the heart of functional information, answering the question of "What makes a biological molecule tick?" ■

## ACKNOWLEDGMENTS

*This work was supported by NIH grant R35GM139453.*

## References


1. Agrawal, R.K., Heagle, A.B., Penczek, P., Grassucci, R.A., and Frank, J. (1999). EF-G-dependent GTP hydrolysis induces translocation accompanied by large conformational changes in the 70S ribosome. *Nat. Struct. Biol.* 6, 643-647.
2. Ban, N., Freeborn, B., Nissen, P., Penczek, P., Grassucci, R.A., Sweet, R., Frank, J., Moore, P.B., and Steitz, T.A. (1998). A 9 Å resolution X-ray crystallographic map of the large ribosomal subunit. *Cell* 93, 1105-1115.
3. Ban, N., Nissen, P., Hansen, J., Moore, P.B., Steitz, T.A. (2000). The complete atomic structure of the large ribosomal subunit at 2.4 A resolution. *Science* 289, 905-920.
4. Bhattacharjee, S., Feng, X., Maji, S., Dadhwal, P., Zhang, Z., Brown, Z.P., and Frank, J. (2023). Time resolution in cryo-EM using a novel PDMS-based microfluidic chip assembly and its application to the study of HflX-mediated ribosome recycling. *Biorxiv* doi.org/10.1101/2023.01.25.525430.
5. Cornish, P. V., Ermolenko, D. N., Noller, H. F., and Ha, T. (2008). Spontaneous intersubunit rotation in single ribosomes, *Mol. Cell*, 30, 578-588.
6. Dashti, A., Schwander, P., Langlois, R., Fung, R., Li, W., Hosseinizadeh, A., Liao, H.Y., Pallesen, J., Sharma, G., Stupina, V.A., Simon, A.E., Dinman, J., Frank, J., and Ourmazd, A. (2014). Trajectories of the ribosome as a Brownian nanomachine. *Proc. Natl. Acad. Sci. USA* 111, 17492-17497.
7. Dashti, A., Mashayekhi, G., Shekhar, M., Hail, D.B., Salah, S., Schwander, P., des Georges, A., Singharoy, A., Frank, J., and Ourmazd, A. (2020). Retrieving functional pathways of biomolecules from single-particle snapshots. *Nat. Comm.* 11, 4734.
8. Ermolenko, D. N., Majumdar, Z. K., Hickerson, R. P., Spiegel, P. C., Clegg, R. M., and Noller, H. F. (2007). Observation of intersubunit movement of the ribosome in solution using FRET, *J. Mol. Biol.*, 370, 530-540,
9. Fei, J., Kosuri, P., MacDougall, D. D., and Gonzalez, Jr., R. L. (2008). Coupling of ribosomal L1 stalk and tRNA dynamics during translation elongation, *Mol. Cell*, 30, 348-359.
10. Frank, J., Verschoor, A., and Boublik, M. (1981). Computer averaging of electron micrographs of 40S ribosomal subunits. *Science* 214, 1353-1355.
11. Frank, J., and Ourmazd, A. (2016). Continuous Changes in Structure Mapped by Manifold Embedding of Single-Particle Data in Cryo-EM. *Methods* 100, 61-67.
12. Frank, J., and Agrawal, R.K. (2000). A ratchet-like inter-subunit reorganization of the ribosome during translocation. *Nature* 406, 318-322.
13. Frank, J. (2013). Story in a Sample – the potential (and limitations) of cryo-electron microscopy applied to molecular machines. *Biopolymers* 99, 832-836.
14. Frank, J. (2015). Generalized single-particle cryo-EM – a historical perspective. *Microscopy* 65, 3-8.
15. Frank, J. (2021). Alexander Spirin's vision of the ribosome as a thermal ratchet machine. *Biochemistry (Moscow)* 86, 910-912.
16. Fu, Z., Kaledhonkar, S., Borg, A., Sun, M., Chen, B., Grassucci, R.A., Ehrenberg, M., and Frank, J. (2016). Key Intermediates in Ribosome Recycling Visualized by Time-Resolved Cryoelectron Microscopy. *Structure* 24, 2092–2101.
17. Fu, Z., Indrisiunaite, G., Kaledhonkar, S., Shah, B., Sun, M., Chen, B., Grassucci, R.A., Ehrenberg, M., and Frank, J. (2019). The structural basis for release factor activation during translation termination revealed by time-resolved cryogenic electron microscopy. *Nat. Comm.* 10, 2579.
18. Gao, H., Sengupta, J., Valle, M., Korostelev, A., Eswar, N., Stagg, S.M., Van Roey, P., Agrawal, R.K., Harvey, S.C., Sali, A., Chapman, M.S., and Frank, J. (2003). Study of the structural dynamics of the *E. coli* 70S ribosome using real-space refinement. *Cell* 113, 789-801.
19. Gao, H., and Frank, J. (2005). Molding atomic structures into intermediate-resolution cryo-EM density maps of ribosomal complexes using real-space refinement. *Structure* 13, 401-406.
20. Horan, L. and Noller, H.F. (2007). Intersubunit movement is required for ribosomal translocation. *Proc. Natl. Acad. Sci. USA* 104, 4881-4885.
21. Kaledhonkar, S., Fu, Z., Caban, K., Li, W., Chen, B., Sun, M., Gonzales, R.L., and Frank, J. (2019). Late steps in bacterial translation initiation visualized using time-resolved cryo-EM. *Nature* 570, 400-404.
22. Penczek, P., Ban, N., Grassucci, R.A., Agrawal, R.K., and Frank, J. (1999). ***Haloarcula marismortui*** 50S subunit-complementarity of electron microscopy and X-Ray crystallographic information. *J. Struct. Biol.* 128, 44-50.
23. Scheres, S.H., Gao, H., Valle, M., Herman, G.T., Eggermont, P.P., Frank, J., and Carazo, J.M. (2007). Disentangling conformational states of macromolecules in 3D-EM through likelihood optimization. *Nat. Methods* 4, 27-29.
24. Scheres, S.H. (2012) A Bayesian view on cryo-EM structure determination. *J. Mol. Biol.* 415, 406-418.
25. Seitz, E., Acosta-Reyes, F., Maji, S., Schwander, P., and Frank, J. (2022). Recovery of Conformational continuum from single-particle cryo-EM images: optimization of ManifoldEM informed by ground truth. *IEEE Trans. Comp. Im.* 8, 462-478.
26. Spirin, A. (2002). Ribosome as a molecular machine, *FEBS Lett.*, 514, 2-10,
27. Spirin, A. S. (2009). The ribosome as a conveying thermal ratchet machine, *J. Biol. Chem.*, 284, 21103-21119.
28. Sztain, T., Ahn, S.-H., Bogetti, A.T., Casalino, L., Goldsmith, J.A., Seitz, E., McCool, R.S., Kearns, F.L., Acosta-Reyes, F., Maji, S., Mashayekhi, G., McCammon, J.A., Ourmazd, A., Frank, J., McLellan, J.S., Chong, L.T., and Amaro, R.E. (2021). A glycan gate controls opening of the SARS-CoV-2 spike protein. *Nat. Chem.* 13, 963–968.
29. Tama, F., Valle, M., Frank, J., and Brooks, C.L., 3rd (2003). Dynamic reorganization of the functionally active ribosome explored by normal mode analysis and cryo-electron microscopy. *Proc. Natl. Acad. Sci. USA* 100, 9319-9323.
30. Trabuco, L.G., Villa, E., Mitra, K., Frank, J., and Schulten, K. (2008). Flexible fitting of atomic structures into electron microscopy maps using molecular dynamics. *Structure* 16, 673-683.
31. Valle, M., Sengupta, J., Swami, N.K., Grassucci, R.A., Burkhardt, N., Nierhaus, K.H., Agrawal, R.K., and Frank, J. (2002). Cryo-EM reveals an active role for aminoacyl-tRNA in the accommodation process. *EMBO J.* 21, 3557-3567.
32. Yarus, M., Valle, M., and Frank, J. (2003). A twisted tRNA intermediate sets the threshold for decoding. *RNA* 9, 384-385.


**Prof. Yuichi Ikuhara & Prof. Naoya Shibata**

(Institute of Engineering Innovation, The University of Tokyo)
Japan Academy Prize (2023)

# Development of State-of-the-Art Electron Microscopy and Contribution to **Nano Interface Technology**

Prof. Yuichi Ikuhara has been a leading figure in the field of advanced electron microscopy and nanomaterial science in the 21st century. He has made numerous world-leading contributions, and has ascended to an international leadership role in the field. Specifically, he has pioneered the state-of-the-art development of transmission electron microscopy for more than a quarter of a century. Consequently, he has established innovative methods for the quantitative characterization and analysis of local atomic structures, elemental distributions, and local electronic states at nanointerfaces and lattice defects, both experimentally and computationally.

One of his specific research achievements is the direct observation of atoms related to material functions, such as dopants and impurities at the material interface, using ultra-high resolution scanning transmission electron microscopy (STEM). This study has facilitated a major breakthrough in the field of material science. He was the first in Japan to introduce spherical aberration-corrected STEM for analyzing material interfaces. In addition, he proposed a method that combined electron energy loss spectroscopy (EELS) at the atomic-resolution level with first-principles calculations, and established a quantitative analysis method for atomic structures and electronic states, such as interfaces and dislocations.

In 2017, Prof.Ikuhara collaborated with with JEOL Ltd. to achieve a spatial resolution of 40.5 pm for STEM, thus setting a world record for the highest performance of a STEM at that time. They also proposed and developed a new annular bright-field (ABF)-STEM technique that facilitated selective capture of electrons transmitted and/or scattered at low angles. This method enabled the first direct observation of lithium atoms in lithium-ion battery materials and hydrogen atom columns in hydrogen storage materials, which have attracted attention as energy and environmental materials. This research led to the worldwide diffusion of this method as a new analytical technique that originated from Japan, which is now routinely used as a general method in overseas research institutes.

Prof. Naoya Shibata has led the world in the advancement of atomic-resolution STEM and its application to the study of material interfaces. Specifically, he has pioneered the development of a method for the direct visualization of electromagnetic field distribution at an atomic scale, which has been extensively used as a new electron microscopy technique in the field of materials and devices. He has reported numerous research results that have contributed to the true and deeper understanding of the mechanisms of interface-originated properties in various materials.

A specific example of Prof. Shibata's research is the development of segmented STEM detector for atomic-resolution imaging. This detector has been used to observe the electric field at the interface of a semiconductor p-n junction and the magnetic field inside a magnetic skyrmion using the differential phase contrast method. Furthermore, he modified this method to precisely measure the slight deflection of the electron beam caused by the existing electric field between the positively charged atomic nucleus and

negatively charged electron cloud. Due to his novel discovery the electric field distribution inside an atom can be directly observed in real space for the first time in the world. This is an innovative achievement that is expected to facilitate the use of electron microscopes for real-space observation of intra- and interatomic structures, rather than only observe atomic arrangements.

In 2019, in collaboration with JEOL Ltd., Prof. Shibata successfully developed a new objective lens that realized the atomic-resolution observation while maintaining a sample in magnetic-field-free conditions, which had been a relatively unexplored area of electron microscopy. For the first time, a spatial resolution of less than 1 angstrom was achieved in a magnetic field-free environment, thus rendering the observation of the atomic structure of magnetic materials possible. Furthermore, using this electron microscope, he also realized real-space visualization of the intrinsic magnetic field of an antiferromagnet for the first time in 2022. These achievements are considered groundbreaking breakthroughs in the field of electron microscopy and have received high international acclaim.

Prof. Ikuhara and Prof. Shibata have been conducting research to elucidate various material phenomena that have been previously considered black boxes through the appropriate development of state-of-the-art electron microscopy techniques developed in a complementary and collaborative manner. Their studies have been focused on the correlation between interfacial atomic and electronic structures and functional properties; identification of atomic positions of light elements in inorganic materials and their relationship to physical properties; clarification of dislocation cores and lattice defect structures; understanding material deformation and fracture mechanism via *in situ* observation; revealing segregation mechanism at ceramic grain boundaries; studying heterogeneous catalytic interface structures; and discovery of one-dimensional ordered crystals formed at the grain boundary triple point. Based on the results of such studies, they have designed and created new materials that utilize the functions of interfaces and lattice defects. These results have been published in more than 900 original papers in international journals, and have received extensive appreciation worldwide. Thus, these achievements demonstrate the significant contributions made by them to the fields of advanced electron microscopy and nanomaterial science. ■

## References


1. T. Futazuka, R. Ishikawa, N. Shibata, Y. Ikuhara, "Grain boundary structural transformation induced by co-segregation of aliovalent dopants," Nature Communications,13, 5299 (2022).
2. Y. Kohno, T. Seki, S.D. Findlay, Y. Ikuhara and N. Shibata, "Real-space visualization of intrinsic magnetic field of an antiferromagnet," Nature 602, 234-239 (2022).
3. J. K. Wei, B. Feng, R. Ishikawa, T. Yokoi, K. Matsunaga, N. Shibata, and Y. Ikuhara, "Direct imaging of atomistic grain boundary migration," Nature Materials, 20, 951-955(2021).
4. D. Q. Yin, C. L. Chen, M. Saito, K. Inoue, and Y. Ikuhara, "Ceramic phases with one- dimensional long-range order," Nature Materials, 18, 19-23 (2019).
5. S. Kondo, A. Ishihara, E. Tochigi, N. Shibata, and Y. Ikuhara, "Direct observation of atomic-scale fracture path within ceramic grain boundary core," Nature Communications, 10, 2112 (2019).
6. N. Shibata, Y. Kohno, A. Nakamura, S. Morishita, T. Seki, A. Kumamoto, H. Sawada. T. Matsumoto, S.D. Findlay and Y. Ikuhara, "Atomic resolution electron microscopy in a magnetic field free environment," Nature Communications, 10, 2308 (2019).
7. S. Morishita, R. Ishikawa, Y. Kohno, H. Sawada, N. Shibata, and Y.Ikuhara, "Attainment of 40.5 pm spatial resolution using 300 kV scanning transmission electron microscope equipped with fifth-order aberration corrector," Microscopy, 67[1] 46-50 (2018).
8. S. Kondo, T. Mitsuma, N. Shibata and Y. Ikuhara, "Direct observation of individual dislocation interaction processes with grain boundaries", Science Advances, 2 (11), e1501926 (2016).
9. C. Chen, Z. Wang, T. Kato, N. Shibata, T. Taniguchi, and Y. Ikuhara, "Misfit accommodation mechanism at the heterointerface between diamond and cubic boron nitride", Nature Communications, 6, 6327 (2015).
10. R. Ishikawa, N. Shibata, F. Oba, T. Taniguchi, S. D. Findlay, I. Tanaka, and Y. Ikuhara, "Functional Complex Point-Defect Structure in a Huge-Size-Mismatch System", Physical Review Letters, 110[6], 065504(2013).
11. I. Sugiyama, N. Shibata, Z. Wang, S. Kobayashi, T. Yamamoto, and Y. Ikuhara, "Ferromagnetic dislocations in antiferromagnetic NiO", Nature Nanotechnology, 8[4], 266-270(2013).
12. N. Shibata, S.D. Findlay, Y. Kohno, H. Sawada, Y. Kondo and Y. Ikuhara, "Differential phase-contrast microscopy at atomic resolution," Nature Physics, 8, 611-615 (2012).
13. Y. Ikuhara, "Grain boundary atomic structures and light-element visualization in ceramics: combination of Cs-corrected scanning transmission electron microscopy and first-principles calculations," Journal of Electron Microscopy, Review paper, 60(Supplement 1), S173 -S188 (2011).
14. Z. Wang, M. Saito, K. P. McKenna, L. Gu, S. Tsukimoto, A. L. Shluger, and Y. Ikuhara, "Atom-resolved imaging of ordered defect superstructures at individual grain boundaries", Nature, 479[7373], 380-383(2011).
15. S. D. Findlay, T. Saito, N. Shibata, Y. Sato, J. Matsuda, K. Asano, E. Akiba, T. Hirayama, and Y. Ikuhara, "Direct Imaging of Hydrogen within a Crystalline Environment", Applied Physics Express, 3[11], 116603(2010).
16. Y. Ikuhara, "Nanowire design by dislocation technology", Progress in Materials Science, 54[6], 770-791(2009).
17. N. Shibata, M. F. Chisholm, A. Nakamura, S. J. Pennycook, T. Yamamoto, and Y. Ikuhara, "Nonstoichiometric dislocation cores in alpha-alumina", Science, 316[5821], 82-85(2007).
18. J. P. Buban, K. Matsunaga, J. Chen, N. Shibata, W. Y. Ching, T. Yamamoto, and Y. Ikuhara, "Grain boundary strengthening in alumina by rare earth impurities", Science, 311[5758], 212-215(2006).
19. Y. Ikuhara, H. Nishimura, A. Nakamura, K. Matsunaga, and T. Yamamoto, "Dislocation structures of low-angle and near-Sigma 3 grain boundaries in alumina bicrystals", Journal of the American Ceramic Society, 86[4], 595-602(2003).
20. A. Nakamura, K. Matsunaga, J. Tohma, T. Yamamoto, and Y. Ikuhara, "Conducting nanowires in insulating ceramics", Nature Materials, 2[7], 453-456(2003).

**Frances M. Ross**
MIT Department of Materials Science and Engineering, fmross@mit.edu

# Electron Microscopy of Crystal Growth in Liquid and **Ultra High Vacuum Environments**

Ever since the first electron microscopes were constructed, microscopists have dreamed of recording not just static images but movies: viewing dynamic processes as they take place with good spatial and temporal resolution. The last few decades have seen dramatic progress in this field of *in situ* microscopy. It has become clear that placing a sample in a well-controlled environment – gas at a range of pressures, water or other liquids – presents rich opportunities. Such experiments extend the range of scientific problems that can be addressed by TEM to include, for example, phenomena of nanostructure growth and dynamic structure-property relationships in catalysts and energy storage materials. Advances in instrumentation and data handling have driven rapid development of environmental experiments that enable us to achieve ever greater precision in understanding materials behavior. I find that the extreme ends of the environment spectrum provide particularly exciting insights: electron microscopy of samples in liquids and in ultra high vacuum illuminate basic physics while also being deeply relevant to real-world applications such as batteries and catalysts.

**Liquid-mediated processes** underlie key phenomena in electrochemistry, crystal growth, catalysis and biological functions. Imaging liquid samples appears incompatible with the vacuum requirements of the microscope column: water would evaporate instantly. The liquid must therefore be encapsulated between membranes that are mechanically robust yet reasonably transparent to the electron beam. This 'closed liquid cell' strategy was proposed in electron microscopy literature but was impractical until the advent of modern microfabrication methods that enable controlled formation of thin silicon nitride membranes. Confining a liquid in this way enables imaging with good time resolution and reasonable spatial resolution, a unique combination that is not offered by scanning probe or light microscopy [1, 2].

Our interest in liquid cell electron microscopy was motivated by the importance of electrochemical deposition of the copper interconnects during microelectronics fabrication [3]. Our liquid cells were constructed by fabricating silicon window chips and gluing them face to face by hand. Liquid was added using a syringe through ports on one chip and lids were glued over the ports. The initial chips were filled with acidified $CuSO_4$ electrolyte and contained one Au electrode extending over the window on one chip, with other electrodes formed by gluing thin Cu and Au wires into the ports. Only one in 20 of these early cells yielded results (mostly due to leaks in the glue layers) - but when data emerged it was rich (**Figure 1**). Copper nucleation sites, temporal and spatial correlations, diffusion-limited growth, dissolution, island faceting, growth front instability and dendrite formation could be correlated with current and voltage recorded simultaneously. Cyclic voltammetry, potentiostatic and galvanostatic Cu deposition yielded information on diffusion processes and additive effects [3-5]. The electron beam affected the result, and modelling efforts helped to link this to phenomena already understood by

radiation chemists [6]. The liquid cell technique has been extended to crystal growth, corrosion, batteries, biological materials in their native environment, and non-aqueous systems, imaging by both STEM and TEM, including analytical techniques [1, 2]. Commercial equipment with sophisticated designs, advances in the liquid enclosure (particularly the use of graphene as the window material), liquid flow, heating, control of liquid thickness, low-dose techniques, sensitive detectors, and optimized imaging modes now create a smoother experience for users [1, 2], even though liquid cell microscopy is never completely straightforward. Liquid cell microscopy smoothly adopts modern imaging and data handling innovations and continues to provide a unique view of otherwise inaccessible phenomena.

At the other end of the pressure spectrum, the importance of clean surfaces for growth and materials reactions has long been recognized by surface scientists, since uncontrolled contamination on the surface or in the gas environment alters the results of almost

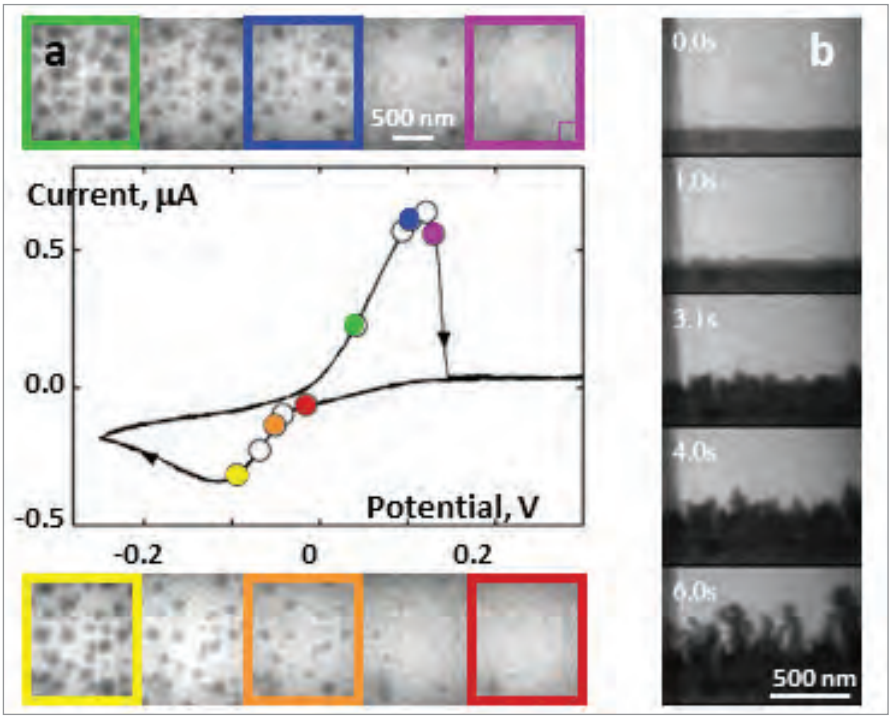


**Figure 1.** Electrochemical crystal growth imaged using liquid cell TEM. **(a)** Cyclic voltammogram and images from a bright field movie recorded simultaneously during deposition and stripping of copper (dark islands) on a polycrystalline Au electrode (grey background) from an electrolyte containing 0.1M $CuSO_4$ + 0.18M $H_2SO_4$. The colors indicate the times of the images shown. Adapted from [4]. **(b)** Movie frames recorded during galvanostatic deposition of copper on a polycrystalline Pt electrode from the same electrolyte as in **(a)**. The average current density of 290A/m² results in a local average growth rate of 70nm/s. The growth front becomes dendritic after several seconds. Adapted from [5].

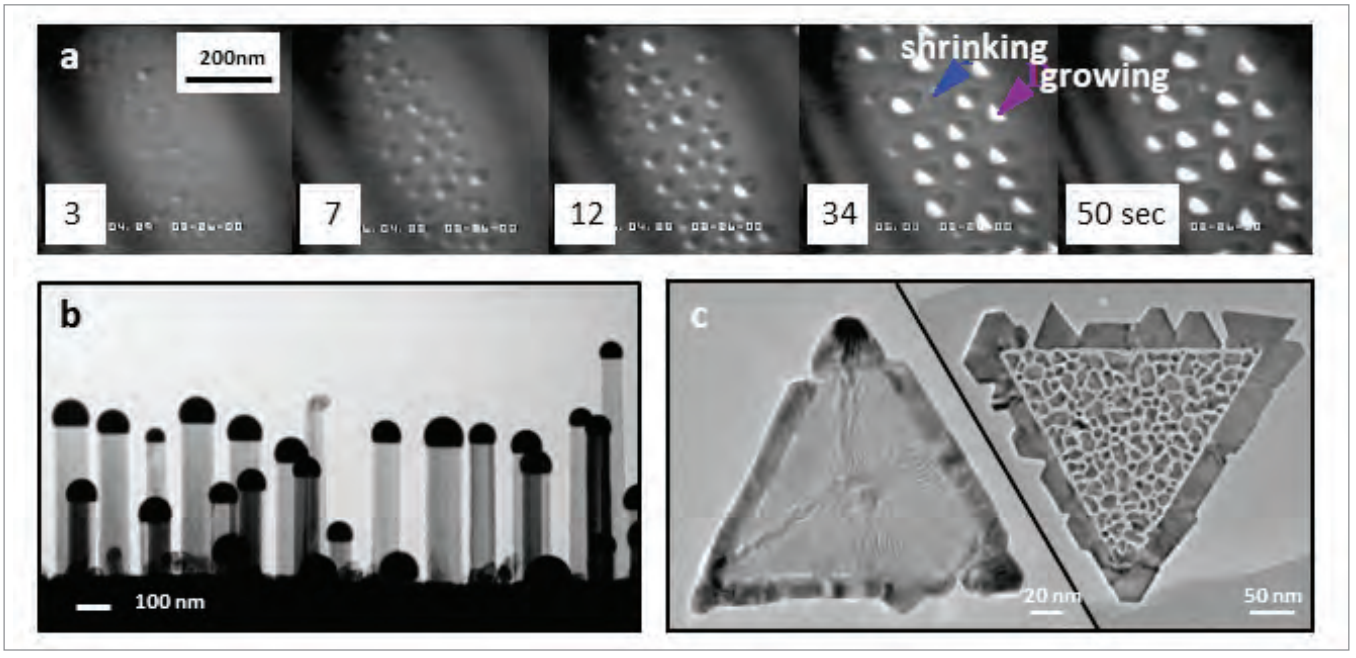


**Figure 2.** Vapor phase crystal growth imaged using UHVTEM. **(a)** Nucleation, growth and coarsening via Ostwald ripening of Ge islands during deposition of Ge on Si(001) at 650 °C from 2x10$^{-7}$ Torr $Ge_2H_6$. From [8]. **(b)** Silicon nanowires imaged during growth at 550 °C from 1×10$^{-6}$ Torr $Si_2H_6$. The droplets (dark semicircles) and faceted nanowire surfaces are visible. From [9]. **(c)** Deposition of Au on Ti on graphene, comparing UHV conditions **(left image)**, where growth is fully epitaxial, to conditions that included exposure to oxygen between Ti and Au deposition **(right image)**, where Au grows as islands without epitaxy on the oxidized Ti surface. Unpublished.

every process. In the electron microscopy community, interest in achieving an **ultra high vacuum environment** around the sample has motivated instrument designs in which increased pumping speed and bakeable components allow the sample to sit in a vacuum of around $10^{-10}$ Torr, rather than the $10^{-7}$ Torr found in conventional microscope columns [7]. The importance of reaching this vacuum level is evident if we think about the arrival rate of gas molecules from the vacuum. At $10^{-10}$ Torr, it takes several hours for a full monolayer to impinge and adsorb on the surface; at $10^{-7}$ Torr the surface may be covered after only a few minutes, affecting any experiment that attempts to probe surface processes on reactive samples.

Our interest in ultra high vacuum transmission electron microscopy was motivated by the fascinating epitaxial growth of Ge and SiGe alloys on Si. Growth of these materials by chemical vapor deposition underlies microelectronics device fabrication and is a model system for understanding the phenomena that control strained layer epitaxy. Chemical vapor deposition can be carried out by flowing the precursor gases in the UHVTEM and yields observations used to develop models for self-assembled island formation and coarsening and dislocation dynamics [8] (**Figure 2a**). Many related growth processes are also feasible *in situ*, particularly the self-assembly of nanowires via chemical vapor deposition in the presence of catalytic droplets [9] (**Figure 2b**). The experiments visualize the especially rich physics that governs nanowire growth, interface formation and metastability of catalyst phases. UHVTEM experiments can also probe crystal growth phenomena that control the deposition of conventional (3 dimensional) materials on two-dimensional van der Waals materials [10] (**Figure 2c**). The chemical mismatch and weak bonds at the 3D / 2D interface determine the growth morphology and epitaxy and lead to phenomena such as moiré pattern formation. 3D materials grown on 2D substrates also provide a versatile platform for probing surface processes such as oxidation and for examining strain relief during deposition of multilayers, with relevance for design of nanostructured functional materials.

The ability to carry out practical TEM observations in the 'extreme' environments of ultra high vacuum and atmospheric pressure liquids, while also applying stimuli such as voltage, current flow, temperature and gas composition changes, provides great power to TEM as a technique for solving materials problems. Challenges in these experiments include the complex equipment, the time required for setup, calibration, execution and analysis, and the need to understand artifacts such as beam-sample interactions. Modern techniques of data analysis and automation are helping to mitigate these issues and democratize the experiments. Ultra high vacuum and liquid cell microscopy have become a key part of the microscopy community's toolbox, and we anticipate amazing future outcomes. ■

## References


1. N. de Jonge and F. M. Ross, *Electron microscopy of specimens in liquid*, Nature Nanotechnology **6**, 695-704 (2011)
2. F. M. Ross, *Opportunities and challenges in liquid cell electron microscopy,* Science **350**, aaa9886 (2016)
3. M. J. Williamson, R. M. Tromp, P. M. Vereecken, R. Hull and F. M. Ross, *Dynamic electron microscopy in liquid environments*, Nature Materials **2**, 532-536 (2003)
4. A. Radisic, P. M. Vereecken, P. C. Searson and F. M. Ross, *The morphology and nucleation kinetics of copper islands during electrodeposition*, Surface Science **600**, 1817-1826 (2006)
5. N. M. Schneider, J. H. Park, J. M. Grogan, D. A. Steingart, H. H. Bau and F. M. Ross, *Nanoscale evolution of interface morphology during electrodeposition*, Nature Communications **8**, 2174 (2017)
6. N. M. Schneider, M. M. Norton, B. J. Mendel, J. M. Grogan, F. M. Ross and H. H. Bau, *Electron-water interactions and implications for liquid cell electron microscopy,* Journal of Physical Chemistry C **118**, 22373–22382 (2014)
7. K. Reidy, J. D. Thomsen and F. M. Ross, *Perspectives on ultra-high vacuum transmission electron microscopy of dynamic crystal growth phenomena,* Progress in Materials Science **139**, 101163 (2023)
8. F. M. Ross, J. Tersoff and R. M. Tromp, *Coarsening of self-assembled Ge quantum dots on Si(100),* Physical Review Letters **80**, 984-987 (1998)
9. F. M. Ross, *Controlling nanowire structures through real time growth studies*, Reports on Progress in Physics, **73**, 114501/1-21 (2010)
10. K. Reidy, J. D. Thomsen, H.-Y. Lee, V. Zarubin, Y. Yu, B. M. Wang, T. Pham, P. Periwal and F. M. Ross, *Mechanisms of quasi van der Waals epitaxy of three-dimensional metallic nanoislands on suspended two-dimensional materials.* Nano Letters **22**, 5849-5858 (2022)


**Leslie J. Allen[1] and Scott D. Findlay[2]**

[1]School of Physics, University of Melbourne, Parkville, Victoria 3010, Australia
[2]School of Physics and Astronomy, Monash University, Clayton, Victoria 3800, Australia

# Quantitative analytical microscopy at **atomic resolution**

The first aberration corrected electron microscopes, principally correcting spherical aberration, became available more than twenty-five years ago. However, contrast mismatches, often by a factor as large as three to five, persisted when comparing atomic resolution images between experiment and simulation in conventional transmission electron microscopy (CTEM).

A similar phenomenon was observed in scanning transmission electron microscopy (STEM) in the Z-contrast or high-angle annular dark field (HAADF) imaging mode. Despite much speculation as to the reason for these discrepancies, they remained unresolved for many years. The first major step towards absolute-scale, quantitative agreement between experiment and theory was made in 2008 for STEM HAADF imaging [1] (see **Fig.1**). The

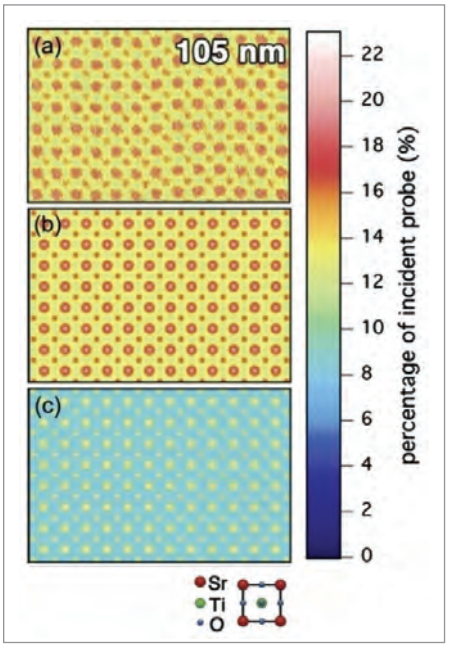


**Figure 1. (a) Experimental Z-contrast image of SrTiO3 along <100>[1]. (b) Simulation in quantum excitation of phonons model[11]. (c) Bloch wave simulation.**

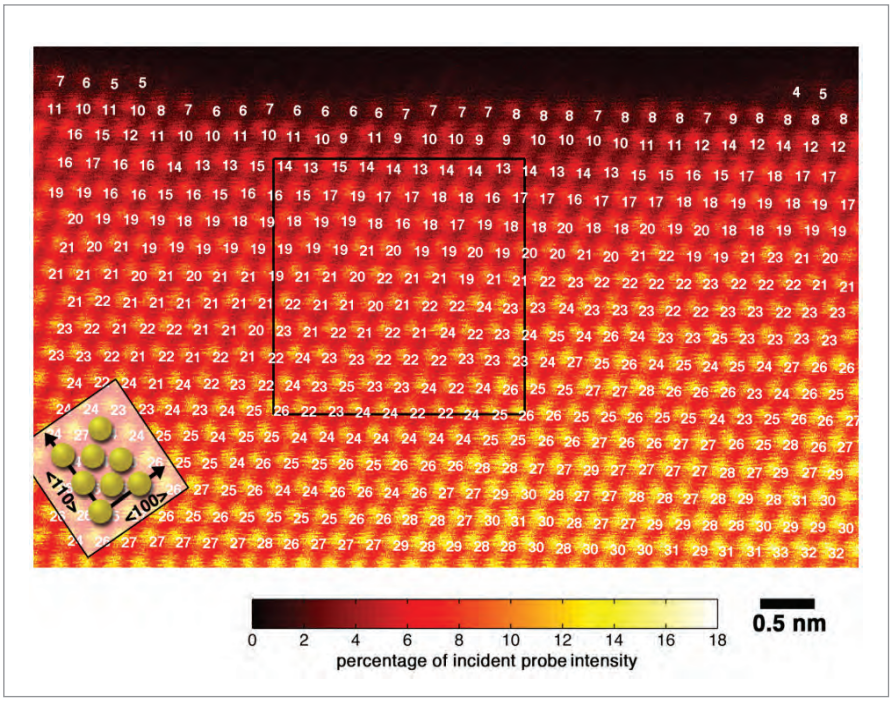


**Figure 2. Z-contrast image of a gold foil compared with simulations to give the number of atoms in each column[4].**

experimental issues that need to be addressed to achieve such agreement were elucidated in Ref. [2]. Shortly thereafter, substantial progress was also made in reconciling experiment and simulation in CTEM imaging [3].

This ability to be quantitative greatly increased the utility of atomic-resolution aberration corrected microscopy. For example, in STEM it enabled the counting of atoms [4] (see **Fig. 2**) and the three-dimensional imaging of individual dopant atoms within small clusters [5].

In CTEM, it facilitated the determination of the 3D shape of a nanocrystal with atomic resolution from a single image [6]. A review of quantitative annular dark-field imaging, paying attention to the methods of image quantification and the application of quantitative data to relate the properties of nanomaterials to atomic-level structure, was published recently [7]. A review of a statistics-based approach to atom counting that complements the absolute-scale approach and can reduce (and sometimes even eliminate) the need for both a well-characterised instrument and for comparison simulations is given in Ref. [8].

In STEM spectroscopic imaging, absolute-scale comparison between experiment and simulation has been achieved in core-loss electron energy loss spectroscopy [9] and energy dispersive x-ray spectroscopy [10] (see **Fig.3**), enabling element-specific counting of atoms.

Understanding of the physics of both the elastic and inelastic scattering of the probing fast electrons in a specimen [11,12] is an essential component of quantitative microscopy. ■

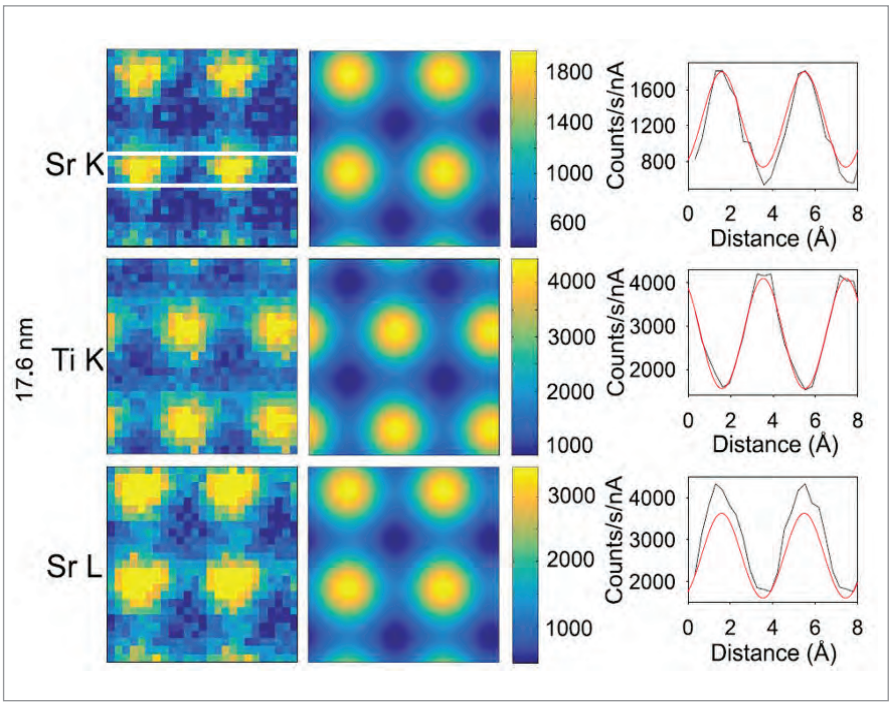


**Figure 3. Absolute-scale comparison of experimental and simulated EDX maps for a 17.6 nm thick specimen of SrTiO3. A 200 keV probe with a convergence angle of 19.5 mrad was used. An incoherent effective source was modelled using a Gaussian with 1.05 Å full-width-half-maximum. Line profiles are averaged across a 1.6 Å wide strip, e.g., that indicated by the white rectangle for the Sr K edge.**


## ACKNOWLEDGEMENTS

*We gratefully acknowledge the contributions to the work described here by several collaborators. We would particularly like to thank Adrian D'Alfonso, Jim LeBeau and Susanne Stemmer for their contributions and for many stimulating and helpful discussions over the years.*


## References


1. J.M. LeBeau, S.D. Findlay, L.J. Allen and S. Stemmer, Physical Review Letters 100 (2008) 206101.
2. J.M. LeBeau and S. Stemmer, Ultramicroscopy 108 (2008) 1653.
3. A. Thust, Physical Review Letters 102 (2009) 220801.
4. J.M. LeBeau, S.D. Findlay, L.J. Allen and S. Stemmer, Nano Letters (2010) 4405-4408.
5. J. Hwang, A.J. D'Alfonso, L.J. Allen and S. Stemmer, Physical Review Letters 111 (2013) 266101.
6. C.L. Jia, S.B. Mi, J. Barthel, D.W. Wang et al., Nature Materials 13 (2014) 1044–1049.
7. C. Dwyer, Journal of Physics: Materials. 4 (2021) 042006.
8. A. De Backer, S. Bals and S. Van Aert, Ultramicroscopy 247 (2023) 113702.
9. H.L. Xin, C. Dwyer and D.A. Muller, Ultramicroscopy 139 (2014) 38–46.
10. Z. Chen, M. Weyland, X. Sang, W. Xu et al., Ultramicroscopy 168 (2016) 7–16.
11. B.D. Forbes, A.V. Martin, S.D. Findlay, A.J. D'Alfonso et al., Physical Review B 82 (2010) 104103.
12. L.J. Allen, A.J. D'Alfonso and S.D. Findlay, Ultramicroscopy 151 (2015) 11–22.

**Christian Colliex**

Laboratoire de Physique des Solides (UMR CNRS 8502), Bât. 510, Université Paris Sud XI, Université Paris Saclay, 91405 Orsay, France

# From the acquisition of early EELS spectra to undreamt recent achievements in the **exploration of the nanoworld**

## Introduction

Electron energy loss spectroscopy (EELS) has now been recognized as an essential complementary accessory to the well-established transmission electron microscope. Its first demonstration as an analytical technique providing local chemical and electronic information dates back from the sixties and early seventies, its superb potential as a powerful machine providing 2D elemental maps with atomic resolution was accepted as a routine tool in the early nineties for solving issues in materials science. As equipped with a parallel detector recording full EELS spectra for each probe position in a Scanning Transmission Electron Microscope (STEM), a "spectrum-image", it has demonstrated its unique capabilities in many cases of nanosciences, such as the atomic-level structure of singlewall-C, multiwall-C, mixed- (C-BN) nanotubes.

The ultimate goal of single atom identification as suggested in the mid of the seventies independently in Chicago [1] and in a collaboration Orsay-Cambridge [2], has finally been demonstrated in a paper published in Science [3]. In this later paper, it was shown that the sensitivity and spatial resolution of the used STEM-EELS machine were sufficiently powerful to identify single Gd atoms attached to $C_{80}$ molecules encapsulated in a single walled carbon nanotube.

## Developments in instrumentation

This was however only the beginning of a period very rich in innovative developments opening brand new fields of research in nanosciences. Breakthroughs were realized in advanced instrumentation, data acquisition and processing in multi-dimensional spaces, in opening multisignal information and specific coupling with the photonic domain.

Concerning the global field of spatial resolution accessible in the electron microscope, the success in the correction of the spherical aberration realized in parallel by a German [4] and a British [5] team has been decisive. The introduction of aberration correctors following the design proposed by these researchers has created an explosion of elemental and electronic mapping with an attainable spatial resolution of 50 pm at 200 kV and a current up to 1 nA in a probe of 150 pm. This success was officially reacognized very recently with the attribution of the 2020 Kavli prize to the two teams (Max Haider, Harald Rose and Knut Urban on one side, and Ondrej Krivanek on the other). As for the spectacular advances in spectral (or energy-loss) resolution, the introduction of a monochromator at the exit of the electron source, bringing it from the natural width of about 0.25 eV for a beam delivered by a FEG (field emission gun), down to the range of 10 meV and below. Different systems of electrostatic, of magnetic or of mixed type, have been developed and tested. The device developed by the Nion company, made of an alpha-shaped magnetic monochromator, has produced a 30-meV wide, atom-sized electron probe, giving access to vibrational spectroscopy in the electron microscope. The development over the years, of more and more performing detection units, measuring the flux of electrons in the dispersion plane of the spectrometer and transferring it to the digital acquisition and processing unit, constitutes a key component responsible for the success of these machines. Parallel EELS detection using an indirect electron-photon-electron conversion scheme has reached a high level of performance and has produced most of the spectral-images acquired over the past years. Recently, the progress in the realization and use of semiconductor devices has generated the production of CMOS multipixel detectors over 1 Mégapixels of small lateral size typically 5-10 $\mu$m detecting and counting

individual electrons. Rates higher than $10^5$ spectra per second are achieved opening the way to "Fast spim" modes. These major instrumental progress in STEM-EELS techniques over the past decades, generated improvements in both spatial and energy resolution, which are illustrated in the following scheme:

## The original information produced by this new generation of instruments

What do we learn from the EELS spectra? They reflect the spectrum of excitations created by the fast electron of the electron microscope transferred through the specimen, and one of its extreme richness is that it covers a very broad spectral range from a few meV up to a few keV, in optical terms from the IR to the X-Ray domain. In its high energy part, typically from 50 eV up to a few kV, the fine structures on the characteristic edges are generated by the excitation of the core shell electrons of the individual atoms. They constitute a rich source of information beyond the atom identity (elemental maps) and on its immediate environment, its bonding, ionic state, and its crystalline environment (chemical and electronic maps). These 2D atomically resolved maps have become a common approach to solve condensed matter issues [6] following the first demonstration of their impact about fifteen years ago [7].

As the low energy loss domain (from 1 to 50 eV), it constitutes the major part of an EELS spectrum acquired across a thin foil or at glancing incidence on a surface or interface, the contributions to this spectral domain have been extensively studied from the earlier times, see the two reference books due to Raether [8] and to Egerton [9]. The collective response of the free or quasi-free electron gas of the specimen, the plasmons, are made of longitudinal oscillations of the electrons, and the associated energy loss function is fully described in terms of its dielectric function ε (ω,q) where ω is the frequency and q the wave vector of the excitation. Over the past twenty years, two specific aspects have been more specifically developed : (i) individual transitions from unoccupied states to occupied ones and band gap measurements through a detailed study of the imaginary part of ε, $\varepsilon_2$ ; (ii) collective excitations at surfaces and interfaces associated to the zero value of the real part of the dielectric function $\varepsilon_1$. With the progress in instrumentation in spatial as in energy resolution, it has become possible to monitor ultrafine changes in EELS spectra recorded when scanning the probe at the apex of surfaces or interfaces, and in general around specimens in the field of nanostructures: silicon nanospheres in $SiO_2$ matrix, carbon nanotubes, metallic nanowires.

The strong correlation between the movement of charges and the generation of electromagnetic fields has generated the growth of abundant experimental and theoretical studies. Boundary conditions such as surfaces or interfaces between metallic and dielectric materials, generate localized or propagating surface charge oscillations, surface plasmons (SP) associated with electric fields. Their mapping at unraveled sub-nm spatial, together with the parallel rapid progress of theoretical and numerical tools has become a field of intensive research giving rise to the emergence and rapid development of "nanoplasmonics".

The recent easy access, with an energy resolution of 10 meV and nm- spatial resolution offered by the

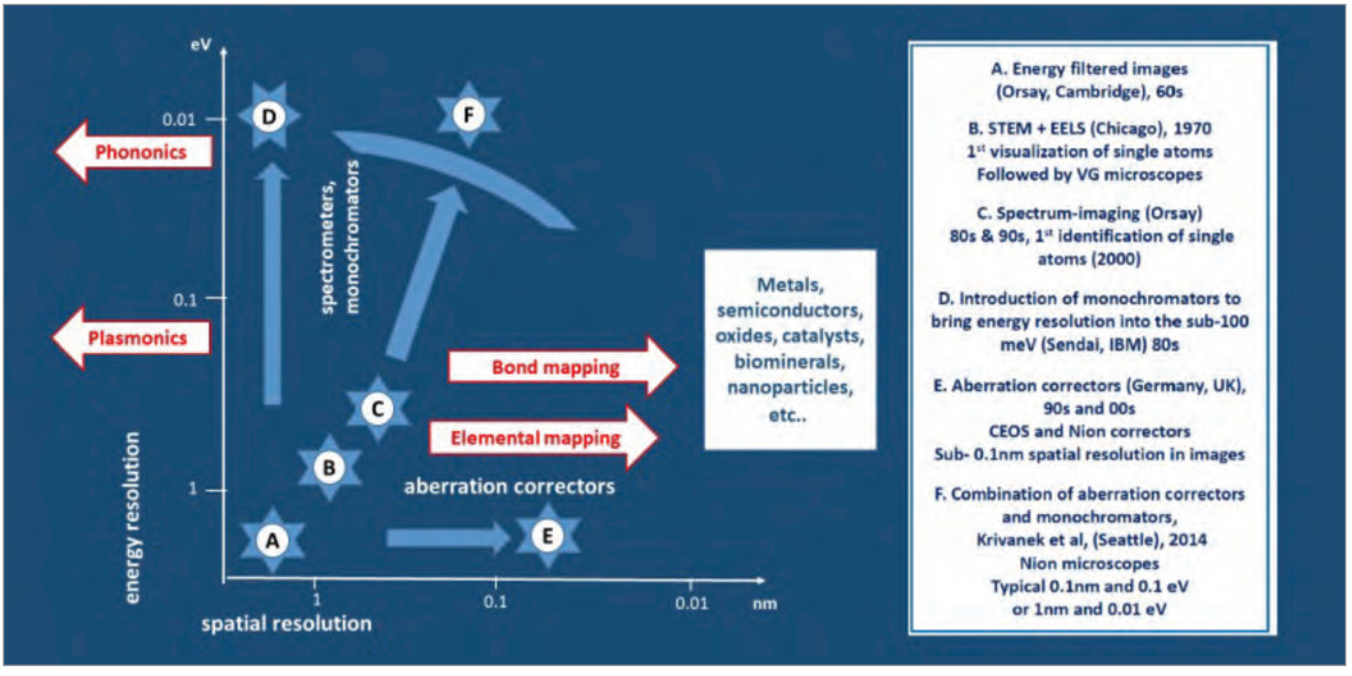


**Figure 1.** Illustration of the major instrumental progress generating improvements in both spatial and energy resolution in STEM/EELS techniques over the past decades, giving thus access to new domains of research

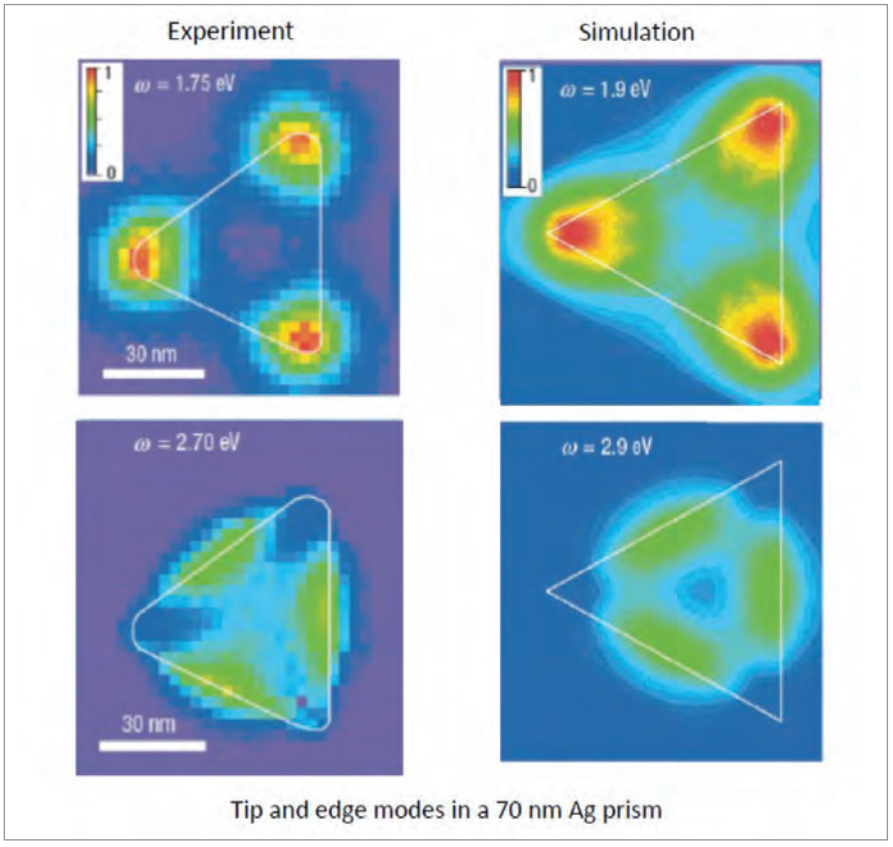


**Figure 2. The energy filtered images of a thin triangular Ag nanoplatelet show clearly at different energy loss values the localized tip and edge surface plasmon modes in agreement with their numerical simulation [10].**

monochromators [11] has opened the way to the recording and study of new types of excitations of very low energy, surface phonons [12], vibrational stretching modes in molecules [13]. Considering only the exploration of the basic physics of condensed matter over the whole spectral I-to-IR range, this new generation of STEM-EELS has definitely contributed to our knowledge of the excitation spectrum in condensed matter.

## Towards a multi-signal strategy

A complementary channel of information is carried in the desexcitation processes of the energy collected by the specimen in the primary event which has been responsible of the energy loss. In particular, this energy can be radiated back into the far-field. If it happens in the IR/Vis/UV range, the detection and analysis of the emitted photons is realized by a Cathodoluminescence (CL) system directly facing the surface of the specimen. For the X-ray range, a specific X-ray detector offers broader and broader angles of capture for the emitted photons.

The simultaneous acquisition and recording of the photons emitted in the desexcitation processes together with the relevant energy-loss constitutes a first example of the multi-signal strategy for collecting the maximum of information from the interaction of a single incident electron of high voltage kinetic energy Illustration of a with a thin sample [14].

The recent impact of the recording and interpretation of these associated signals has been enormous, in particular when mapping at nanometer scale the field configurations around a diversity of nanostructures produced by the most recently developed techniques of nanofabrication: multilayers, wires, cubes, spheres, fractals, and simultaneously imaged and analyzed. This has become known as “nanoplasmonics” and “nanophotonics”.

There are many other aspects of STEM/EELS techniques in rapid and important development. The generation and use of new sources of electrons stimulated by laser impact has opened the way to ultrafast electron microscopy (UEM) by the group of Zewail at Caltech [17]. Timed single-electron packets produced by the impact of laser pulses on the electron source of microscope can overlap with the evanescent electromagnetic field generated by an intense femtosecond pulse of light around a nanostructure. Practically the laser fs pulses are split into two arms, one generating the incident electron pulses, the second one creating the nanostructure excitation. The time delay can be controlled and opens access to time-dependent studies with ns time-resolution. As an interesting application, this set-up has produced spectra with both EELossSpectra and EEGainSpectra exhibiting lines symmetrically with respect to the zero line [18]. The detailed ratio between Loss and Gain lines has been used recently to measure the temperature [19] !!

To be fully exhaustive, this brief report of the STEM-EELS history should also mention the development of “nanolaboratories” with the installation around the specimen of variable environment setups (variable temperature, variable pressure, illumination by an external laser, friction device), the use of shaped electron beam such as the vortex-type one developed by Verbeeck [20] which gives access to an angular momentum information…

As a conclusion, when “photons and electrons team up” as mentioned by Garcia de Abajo [21] there is still for sure a rich field of experimental and theoretical science to be explored. As an example, the field of energy gains has only been observed now, after fifty years of work on energy gains!!

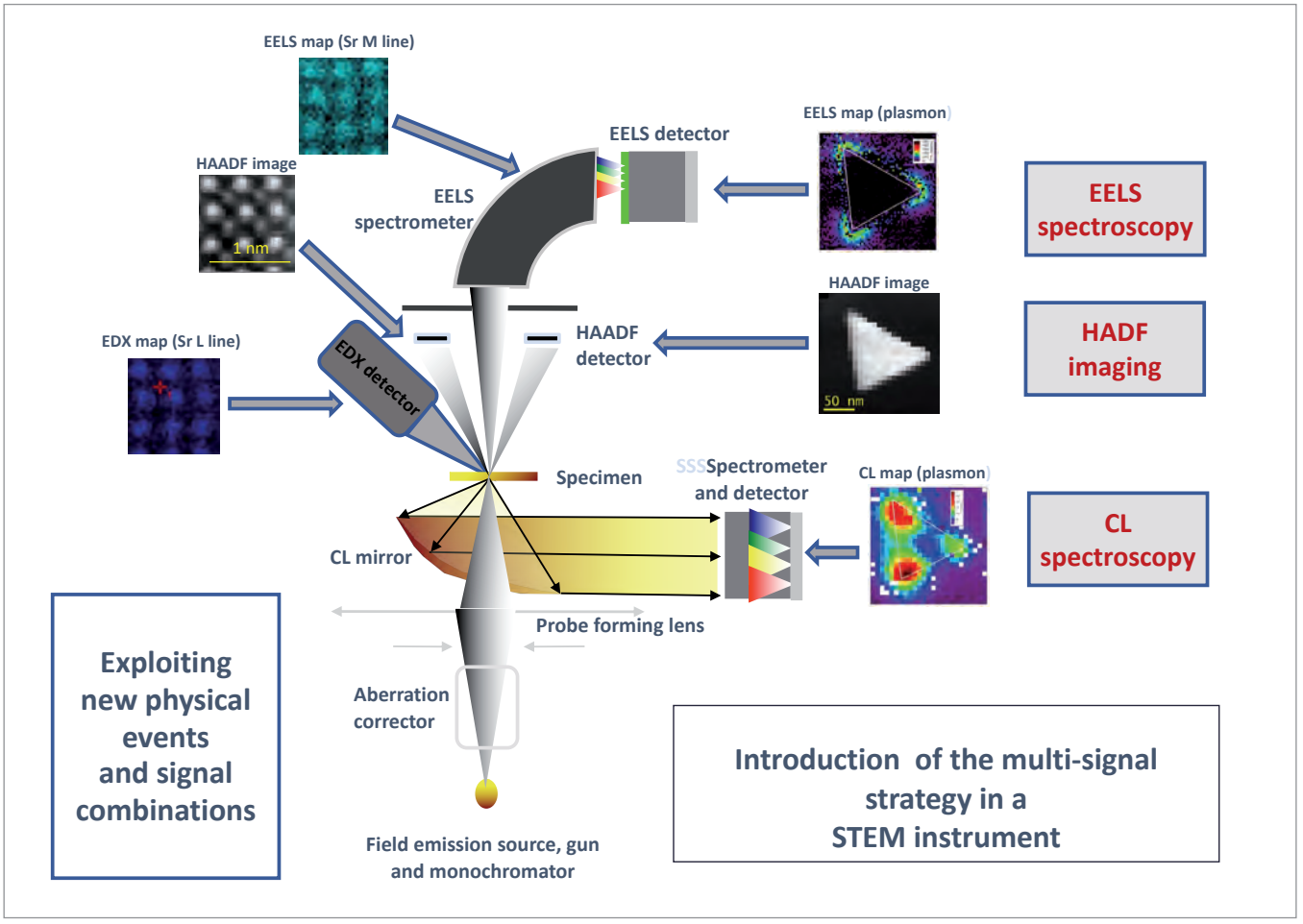


**Figure 3.** **Illustration of a multi-signal acquisition scheme on a most recent STEM instrument, simultaneously delivering an HADF dark field image, an EELS signal, and two different routes to carry out the emission of photons depending on the concerned wavelength : (i) an EDX detector collects the emitted EDX photon image complementary with the EELS core-loss image, with atomic resolution, as demonstrated by Suenaga[15]; (ii) a CL mirror transferring the photons in the broad visible-UV range towards an optical system (spectrometer, polarizer, filter, interferometer), see Kociak and Zagonel for a review[16].**

## POST-SCRIPTUM

*As a most recent contribution to the progress in our understanding of the pathway between the energy loss and the photon emission process, the paper "Cathodoluminescence excitation spectroscopy: Nanoscale imaging of excitation pathways, Science Advances 8, eabq4947, 2022. https://www.science.org/doi/10.1126/sciadv.abq4947 by Nadezda Varkentina*, Yves Auad*, Steffi Y . Woo, Albert , Laura Bocher, Jean-Denis Blazit, Xiaoyan Li, Marcel Tencé, Kenji Watanabe, Takashi Taniguchi, Odile Stéphan, Mathieu Kociak, Luiz H. G. Tizei, "has been awarded the EMS Outstanding Paper Awards (OPA) 2022 in the category Instrumentation and Technique Development.*

*On the 13 September 2023 during the 25th anniversary of the EMS, the recognition of the importance of a coincidence technique between both spectroscopies that confirms that there is a bright future for the STEM-EELS association.*

## References


1. M. Isaacson and D. Johnson, Ultramicroscopy, **1**, 33 (1975)
2. C. Colliex et al. Ultramicroscpy, **1**, 301 (1976)
3. K. Suenaga et al. Science **290**, 2280 (2000)
4. M. Haider et al. Nature **392**,768 (1998)
5. O.L. Krivanek et al. Ultramicroscopy **78**, 1 (1999)
6. A. Gloter et al. Mater. Sci. Semicond. Process. **65**, 2 (2017).
7. D.A. Muller et al. Science **319**, 1073 (2008)
8. H. Raether, Electron energy loss spectroscopy, Springer Tracts in Modern Physics 38, 85 (1965)
9. R.F. Egerton, Electron energy loss spectroscopy in the electron microscope, 1st edition,Plenum Press (1986), 3rd edition Springer 2011)
10. J. Nelayah et al. Nat. Phys. **3**, 348 (2007)
11. O.L. Krivanek et al . Nature **514**, 209 (2014)
12. M. J. Lagos et al. Nature **543**, 529 ( 2017)
13. P. Rez et al. Nature Comms. (2016) DOI: 10.1038/ncomms10945
14. C. Colliex et al. Microscopy and Analysis, 25th anniversary issue **26**, 33 (2012)
15. K. Suenaga et al. Nat. Photonics 6, 545 (2012)
16. M. Kociak and L.F. Zagonel, Ultramicroscopy **174**, 50 (2017)
17. A.H. Zewail, Science **328**, 187 (2010)
18. P.Das et al. Ultramicroscopy **203**, 44 (2019)
19. J.C. Idrobo et al. Phys. Rev. Lett. **120**, 095901 (2019)
20. J. Verbeeck et al. Nature **46**, 301 (2010)
21. F.J. Garcia de Abajo, Photons and electrons team up, Nature **462**, 861 (2009)

**Ondrej L. Krivanek[1,2], Niklas Dellby[1], Michael T. Hotz[1], Joel Martis[1], Ben Plotkin-Swing[1], Steve C. Quillin[1], Benedikt Haas[3], Zdravko Kochovski[4] and Tracy C. Lovejoy[1]**

[1]Nion R&D, 11511 NE 119th St., Kirkland, WA 98034, USA
[2]Department of Physics, Arizona State University, Tempe, AZ 85287, USA
[3]Department of Physics & IRIS Adlershof, Humboldt-Universität zu Berlin, 12489 Berlin, Germany
[4]Helmholtz Zentrum Berlin for Materials and Energy, 14109 Berlin, Germany

# **Advances** in atomic-resolution STEM, SEI and ultra-high energy resolution EELS

ABSTRACT

**We highlight three major advances made in scanning transmission electron microscopy (STEM) since EMS's founding 25 years ago: working aberration correctors that have improved STEM spatial resolution to 1 Å and better at beam energies as low as 20 keV; atomic-resolution secondary electron imaging (SEI) that allows single atoms to be imaged on surfaces, and newly developed monochromators and spectrometers that have opened up the study of atomic and molecular vibrations at the atomic scale as well as other investigations. We review the progress and illustrate it with practical examples.**

Microscopy has often been called "the eyes of science". EMS's core mission has been to make the eyes sharper, more sensitive and more versatile, and to promote their use. In this brief review, we summarize advances contributed to this effort by Nion and its collaborators.

The electron microscope (EM) was invented in 1931 [1], and it would not have been surprising if by 1998, the year of EMS's founding, EM technology had matured so much that only incremental improvements would have been left to do. In reality, however, a lot of fundamental progress has taken place, as described below. The spatial resolution improved greatly when aberration correctors managed to null the principal aberrations of electron lenses, and at the same time to make parasitic aberrations and instabilities as small as needed for the improved resolution.

Three generations of correctors led to the present, highly perfected state [2, 3]: i) proof-of-principle correctors, which showed that the electron-optical principles used by the correctors were sound, but did not manage to improve the resolution, ii) correctors which improved the resolution by correcting third-order spherical aberration as well as parasitic aberrations up to third order, and iii) more advanced correctors that corrected all geometric aberrations up to fifth order, and optionally also chromatic aberration.

**Fig. 1.** shows an image of graphene obtained at 20 keV using a fifth-order aberration corrector developed by Nion [3, 4]. Chromatic aberration limits the attainable spatial resolution at 20 keV primary energy even when using a cold field emission gun with 0.3 eV energy spread, as was done here, and this can be overcome by monochromating the energy spread of the beam to about 0.1 eV. The resultant high angle annular dark field (HAADF) image has captured spacings down to 1.07 Å [5], as shown by its FFT.

Carbon atoms bonded to 3 neighbors in graphene are typically not displaced at beam energies of 60 keV and lower [6], but atoms at graphene edges and defects can be displaced at energies as low as 40 keV. Being able to resolve such structures without damaging them at 20 or 30 keV should prove invaluable.

Atomic-resolution secondary electron imaging (SEI) was first demonstrated in 2009, at 200 keV beam energy [7]. It is greatly improved at lower keV operation and in UHV sample environment, available in Nion microscopes. **Fig. 2.** illustrates the possibilities opened up by the SE detector which we have developed [8], and by sensitive electron energy loss spectroscopy (EELS) that is also available in Nion microscopes.

The figure shows three different types of images of graphene with B and N atomic substitutions: a) high angle dark field (HAADF) image optimized for light atom imaging [9], b) secondary electron image (SEI), and c) elemental map obtained by atomic-resolution EELS spectrum-imaging [10]. All the images detect the single-atom substitutions, and provide further information. The HAADF image essentially "weighs" the atomic nuclei, the SE image allows atomic resolution to be reached on the surfaces of thick and even bulk samples, and the EELS maps demonstrate that the chemical species of individual atoms can be readily identified by using their energy loss signal.

Major advances have also been made in 4D STEM [11], such as deep sub-Å resolution via ptychography [12] and live processing of 4D STEM data [13]. This brief review unfortunately does not provide enough room to cover them.

Turning now to spectroscopy, vibrational EELS in the electron microscope, introduced in 2014 [14, 15], has progressed remarkably. In the form pioneered by Nion, it was made possible by two separate advances: the development of a high-performance monochromator placed at ground potential, i.e. monochromating the full-energy electron beam [16-18]; and the development of an ultra-stable electron energy loss spectrometer [19]. A key step in the progress was the realization that there are two types of vibrational signals available in the electron microscope [20]: dipole scattering, which occurs at scattering angles of the order of microradians (for 100 keV electrons), and probes materials in a delocalized way, and impact scattering, which occurs at scattering angles of the order of tens of milliradians, and is able to analyze vibrations with atomic resolution.

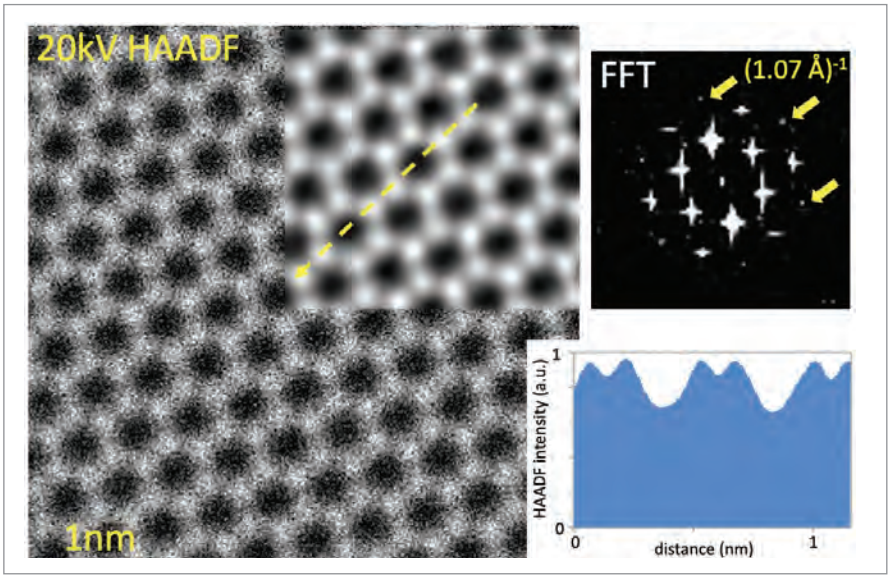


**Figure 1.** **HAADF image of monolayer graphene with low-pass filtered inset, Fourier transform (FFT) of the image, showing 1.07 Å contrast in 3 directions and line profile that shows the absolute contrast along the line marked in the filtered inset. $E_0$=20 keV, monochromated to δE=100 meV, probe half-angle= 55 mrad. Resolution/electron wavelength λ = 12.5.**

**Fig. 3.** shows work carried out at the Daresbury SuperSTEM laboratory, which demonstrates that vibrational spectroscopy performed with a STEM can analyze the vibrations of a single atom [21]. Dark field EELS, in which only electrons that have been scattered outside the bright field cone and thus carry high spatial resolution information, was used for the analysis. Spectra were collected with a 60 keV electron probe of about 1 Å in diameter, placed at various locations relative to a dopant Si atom in graphene, and the

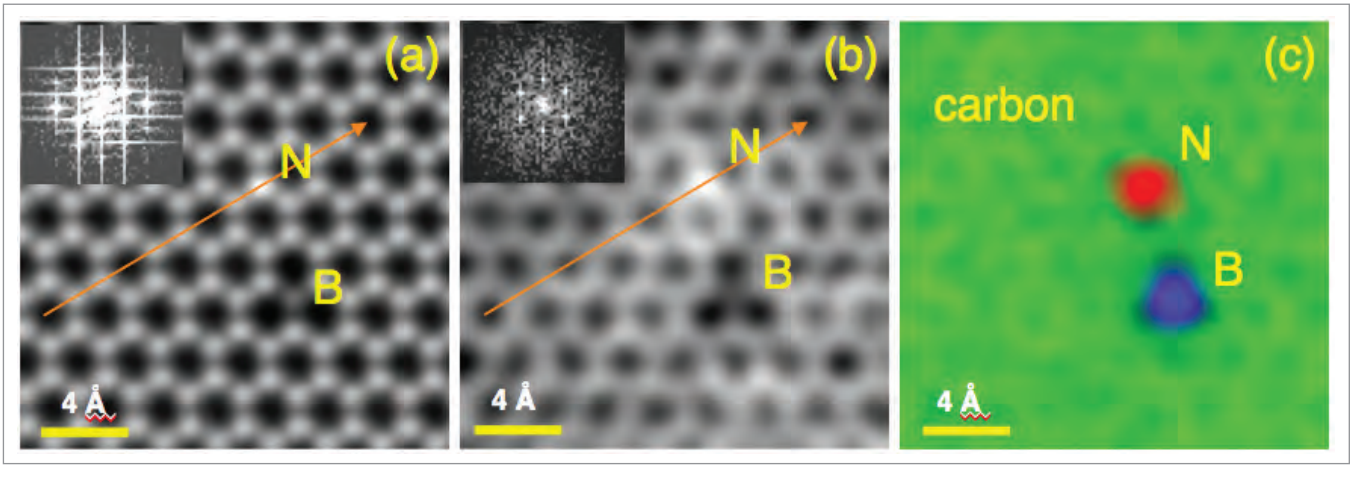


**Figure 2. a)** **HAADF image, b) secondary electron image (Gaussian filtered), c) EELS elemental maps of the same area of graphene with B and N substitutions. $E_0$ = 60 keV.**

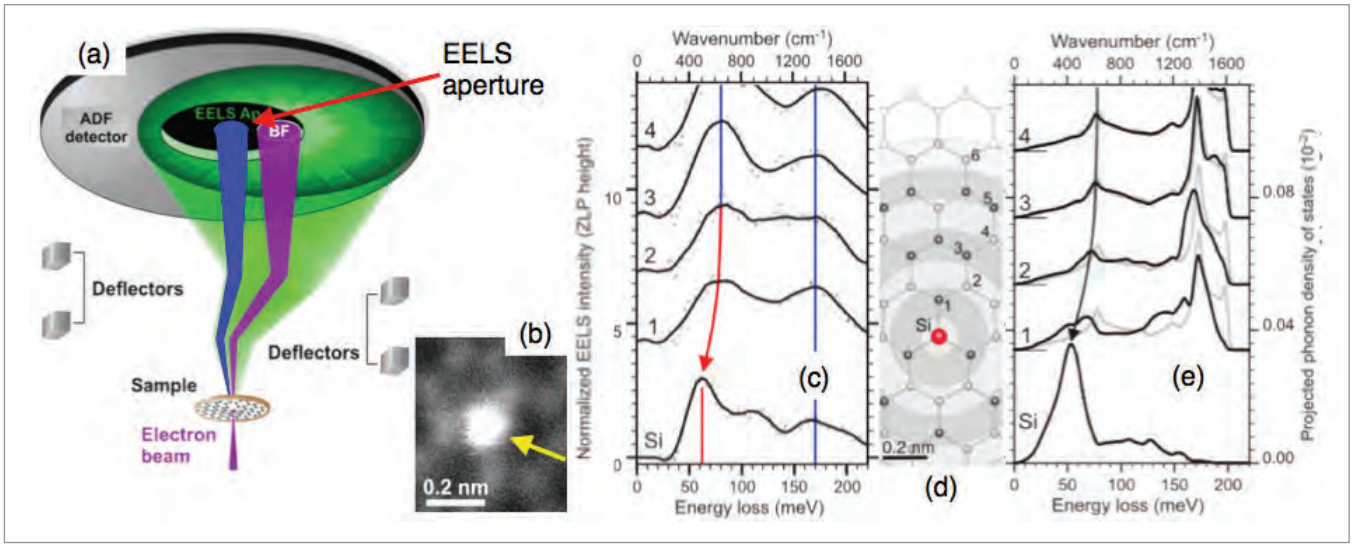


**Figure 3. a)** schematic of dark field EELS acquisition: only the scattered (blue) beam was admitted into the EELS aperture, **b)** HAADF image of a Si impurity atom in graphene, **c)** experimental spectra from sample points marked in **d)**, **e)** theoretical simulations showing the spectra at different sites in black and the graphene spectrum in grey. *Courtesy F.S. Hage et al., and Science.*

experimental results were compared to theoretical simulations. When the probe was on the Si atom, the dominant vibrational mode shifted to a lower energy, as expected for a heavier atom. When the probe was on the third nearest neighbor of the Si atom, the spectrum became essentially identical to spectra of perfect graphene. The experiment showed that STEM is now able to probe the vibrations in solid materials at atomic resolution, and the simulation indicated that when the experimental energy resolution (about 20 meV in this work) is improved further, detailed new information should become available.

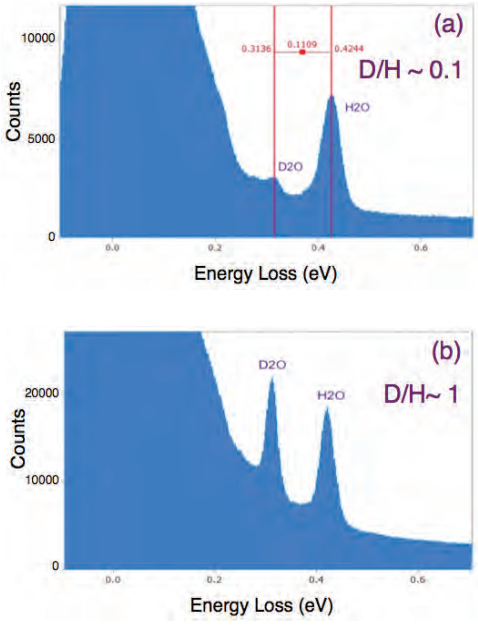


**Figure 4. a)** vibrational EELS of amorphous ice prepared in $H_2O$ humidifying atmosphere, **b)** EELS of ice prepared in $D_2O$ atmosphere.

The Daresbury advance stimulated further work probing the influence of individual defects and grain boundaries on phonon energies and propagation [22-30]. In a remarkable recent achievement, Yan et al. combined polarization sensitivity demonstrated earlier [31] with high spatial and energy resolution EELS imaging to analyze the vibration modes of the three atomic species in $SrTiO_3$, and to show that O atoms vibrate in different directions as a function of energy [32].

Another new capability introduced by vibrational EELS is that it can detect and map isotopic substitution in materials [22, 33-35]. This is illustrated in **Fig. 4**, which shows vibrational spectra obtained from frozen hydrated samples of apoferritin embedded in amorphous $D_2O$ (heavy water) ice. The embedding ice gives rise to two dominant spectral peaks, one at 424 meV, from H-O stretch vibration, and one at 314 meV, from D-O stretch. Similar to FTIR optical spectroscopy [36], a distinct peak due to HDO was not detected in the 300-450 meV energy region that covers ice stretch vibrations.

Sample preparation started with a solution of apoferritin in water, which was diluted 10:1 with heavy water, i.e. about 90% of the water's vibrations were expected to come from $D_2O$. The ice-covered sample grids were prepared in a ThermoFisher Vitrobot in two different ways: a) with $H_2O$ as the humidity-maintaining atmosphere, and b) with $D_2O$ as the atmosphere. The resultant spectra showed that when the humidifying atmosphere was regular $H_2O$, the sample's ice contained >90% $H_2O$, even though the initial sample (prior to blotting) was ~90% $D_2O$. But when the humidifying atmosphere was $D_2O$, the sample contained about 50% $D_2O$ bonds. This demonstrates that a vigorous molecular exchange takes place between the humidifying atmosphere and the water on the grid, in the few seconds needed for blotting the grid before plunging it into liquid ethane, and that the majority of the water molecules in the frozen sample come from the humidifying atmosphere rather than from the initial water layer spread on the grid. The fact that preparing the sample in the $D_2O$

atmosphere did not give the expected 90% $D_2O$ ice composition may be due to regular ice being picked up during the cryotransfer process from the Vitrobot to the EM.

Detecting and mapping isotopic substitution is useful for tracing the progress of atomic migration in inorganic samples and of metabolic pathways in biological specimens. We expect that the technique will become a versatile tool in the microscopy toolkit.

The delocalization of the dipole vibrational signal extends over tens to hundreds of nanometers, and this allows the vibrations of biological samples to be analyzed with the electron beam parked a few tens of nm outside the sample, thereby avoiding radiation damage [37]. In an alternate approach called "leapfrog scanning", the probe is advanced in discrete steps of tens of nm on a beam-sensitive sample, whereupon it drills a hole at each new location [38]. The radiation damage is greatly reduced once the hole is drilled, and this allows much larger exposure levels than if the probe was scanned continuously. These techniques worsen the spatial resolution to about 30-100 nm, but being able to analyze biological samples in the electron microscope without substantial radiation damage seems very promising.

The improved energy resolution has made possible a broad range of other fundamental developments. Key advances include:

i. mapping surface and bulk vibrational modes, including surface phonon polaritons, of nano-objects in simple projection [39], and in 3 dimensions [40],
ii. analyzing plasmons with resonant energies as low as 157 meV in perovskites [41],
iii. enhancing the vibrational response of materials by placing them in the plasmon-induced electric field of metallic nano-objects [42],
iv. comparing EELS with cathodoluminesce (CL) in $WS_2$ enclosed in h-BN in a way that reached similar energy resolution for the two techniques and led to a detailed elucidation of the photonic response of the material [43],
v. determining the sample temperature with a precision of a few degrees K, by comparing the strength of energy gains to corresponding energy losses [44, 45], at temperatures as low as 125 K [46],
vi. analyzing phonon dispersion in h-BN at temperatures up to 1300 K, and finding important discrepancies relative to standard theoretical treatments [47].

For more comprehensive compilations, see reviews by Yan et al. [48] and Lagos et al. [49].

In summary, there have been many revolutionary developments in electron microscopy and spectroscopy in the last 25 years, whose full impact is now being felt. It is an exiting time to be working in these fields, and the prospects for further major advances seem very bright indeed. ■

## References


1. E. Ruska, (1986) www.nobelprize.org/uploads/2018/06/ruska-lecture.pdf.
2. P.W. Hawkes, Ultramicroscopy **156** (2015) A1–A64.
3. O.L. Krivanek, N. Dellby and M.F. Murfitt, *in:* Handbook of Charged Particle Optics, 2nd edn (CRC Press, Boca Raton, J. Orloff, Ed.), 601–640.
4. N. Dellby, O.L. Krivanek and M.F. Murfitt, Phys. Procedia **1** (2008) 179–183.
5. N. Dellby et al., Microsc. Microanal. **29** (Suppl 1, 2023) 626–627.
6. C. Mangler and J.C. Meyer, Comptes Rendus Physique **15** (2014) 241–257.
7. Y. Zhu et al., Nature Materials **8** (2009) 808-812.
8. M.T. Hotz et al., Microsc. Microanal. **29** (Suppl 1, 2023) 2064–2065.
9. O.L. Krivanek et al., Nature **464** (2010) 571-574.
10. D.A. Muller et al., Science **319**, (2008) 1073-1074.
11. C. Ophus, Microscopy and Microanalysis **25** (2019) 563–582.
12. Z. Chen et al., Science **372** (2021) 826–831.
13. B. Haas et al., Microsc. Microanal. **27** (Suppl 1, 2021) 994-995.
14. O.L. Krivanek et al., Nature **514** (2014) 209–212.
15. T. Miyata et al., Microscopy **63** (2014) 377–382.
16. O.L. Krivanek, US patent #5,097,126.
17. O.L. Krivanek and N. Dellby, US patent #8,373,137 B2.
18. O.L. Krivanek et al., Phil. Trans. R. Soc. A **367** (2009) 3683–3697.
19. T.C. Lovejoy et al., Microsc. Microanal. **24** (Suppl 1, 2018), 446-447.
20. C. Dwyer et al., Phys. Rev. Letts **117**, (2016) 256101(1-5).
21. F.S. Hage et al., Science **367** (2020) 1124–1127.
22. A. Konecna et al, ACS Nano **15** (2021) 9890-9899.
23. X. Yan et al. Nature **589** (2021) 65-69.
24. R. Qi et al. Nature **599** (2021) 399-403.
25. Z. Cheng et al., Nature Commun **12** (2021) 6901(1-10).
26. C.A. Gadre et al., Nature **606** (2022) 292-297.
27. E.R. Hoglund et al., Nature **601** (2022) 556-561.
28. E.R. Hoglund et al., Adv. Mater. **35** (2023) 2208920 (1-9).
29. M. Xu et al., Nature Materials **22** (2023) 612-618.
30. B. Haas et al., Nano Lett. **23** (2023) 5975–5980.
31. G. Radtke et al., Phys Rev Letts **123** (2019) 256001 (1-5).
32. X. Yan et al. (2023) https://arxiv.org/abs/2312.01694.
33. J.R. Jokisaari et al., Adv. Mater. **2018** (2018) 1802702(1-6).
34. J.A. Hachtel et al., Science **363** (2019) 525–528.
35. R. Senga et al., Nature **603** (2022) 68-72.
36. I. Litvak, Y. Ankerac and H. Cohen, RSC Advances **8** (2018) 28472–28479.
37. P. Rez et al., Nature Comms **7** (2016) 10945 (DOI: 10.1038/ncomms10945).
38. R.F. Egerton, T. Aoki and P.A. Crozier, Micr. Microanal. **22** (Suppl 3, 2016) 960-961.
39. M.J. Lagos et al. Nature **543** (2017) 529-532.
40. Li et al., Science **371** (2021) 1364–1367.
41. H. Yang et al., Small **18** (2022) 2106897 (1-8).
42. L.H.G. Tizei et al., Nano Lett. **20** (2020) 2973–2979.
43. N. Bonnet et al., Nano Lett. **21** (2021) 10178–10185.
44. J.-C. Idrobo et al., Phys. Rev. Lett. **120** (2018) 095901 (1-4).
45. M.J. Lagos and P.E. Batson, Nano Lett. **18** (2018) 4556–4563.
46. S.C. Quillin et al., unpublished results (2023).
47. A. O'Hara et al., https://arxiv.org/ftp/arxiv/papers/2310/2310.13813.pdf.
48. X. Yan et al., Trends in Chem. **4** (2022) 76-90.
49. M.J. Lagos et al., Microscopy **71** (Suppl. 1, 2022) i174–i199.


**Knut W. Urban[1] and Maximilian Haider[2]**

[1] Ernst Ruska-Center for Microscopy and Spectroscopy with Electrons, ER-C 2, Forschungszentrum Jülich GmbH, 52425 Jülich, Germany
[2] CEOS GmbH, Englerstrasse 28, 69126 Heidelberg, Germany

# **Aberration corrected optics** and atomic-resolution imaging in transmission electron microscopy

The conventional transmission electron microscope (CTEM) was invented by Knoll and Ruska in 1931, and the scanning transmission electron microscope (STEM) was first described by von Ardenne in 1937. In both cases one was able to draw on studies on the lens properties of rotationally symmetric magnetic fields carried out by Busch in the nineteen-twenties. First estimates of the theoretically achievable resolving power of the electron microscope, made by Knoll and Ruska already in 1932, led them to atomic dimensions [1]. They commented: *"Whether this high resolving power can also be used to visualize structures of this or similar size cannot be decided at the present stage of the investigations and is left to a further development of the methodology, which must include an enhancement of the intensity of the electron source in addition to the detailed study of imaging errors".*

This cautious restraint proved more than appropriate, as we know today. It took nearly forty more years until 1970, when Crewe and his collaborators became the first to actually image individual gold and uranium atoms in molecules in a STEM equipped with a field emission source [2,3]. Crewe's microscope had a resolution of 2.5 angstroms, which was a world record at the time. Nevertheless, it was not possible to see all the atoms of a molecule. Only the particularly heavy and therefore strongly scattering atoms could be imaged. In contrast, in materials science one is interested in imaging individual atoms in solids, regardless of their chemical nature. This is especially true for investigations of crystal defects and internal interfaces. Here, in projection, atomic distances of fractions of an angstrom occur. To be able to measure these, a much higher resolving power is required.

The finer the object details to be imaged, the larger the diffraction angle of the electrons and thus the angle at which they enter the objective lens. And this is where the lens aberrations come into play. The aberrations of electromagnetic lenses had been theoretically described by Glaser [4], Brüche and Scherzer [5] as early as 1933, and Scherzer had shown in 1936 that for round lenses, it is basically impossible to avoid the two most important aberrations, chromatic and spherical aberration [6]. When an electron source with a low energy spread (e.g. a field emission source) is employed, the optical resolution is limited by the spherical aberration. As already described by Scherzer and Glaser in the 1940s, there are two strategies to reduce spherical aberration.

The first is to use higher accelerating voltages. The shorter electron wavelengths that can be achieved in this way lead to smaller diffraction angles for a given size of the object details to be imaged. This path led to the construction of the high-voltage electron microscopes, the "dinosaurs" of electron optics, which used electron accelerating voltages of up to 3 million volts [7].

The second strategy was to exploit the special property of the bell-shaped magnetic field distribution of electron lenses that the coefficient of spherical

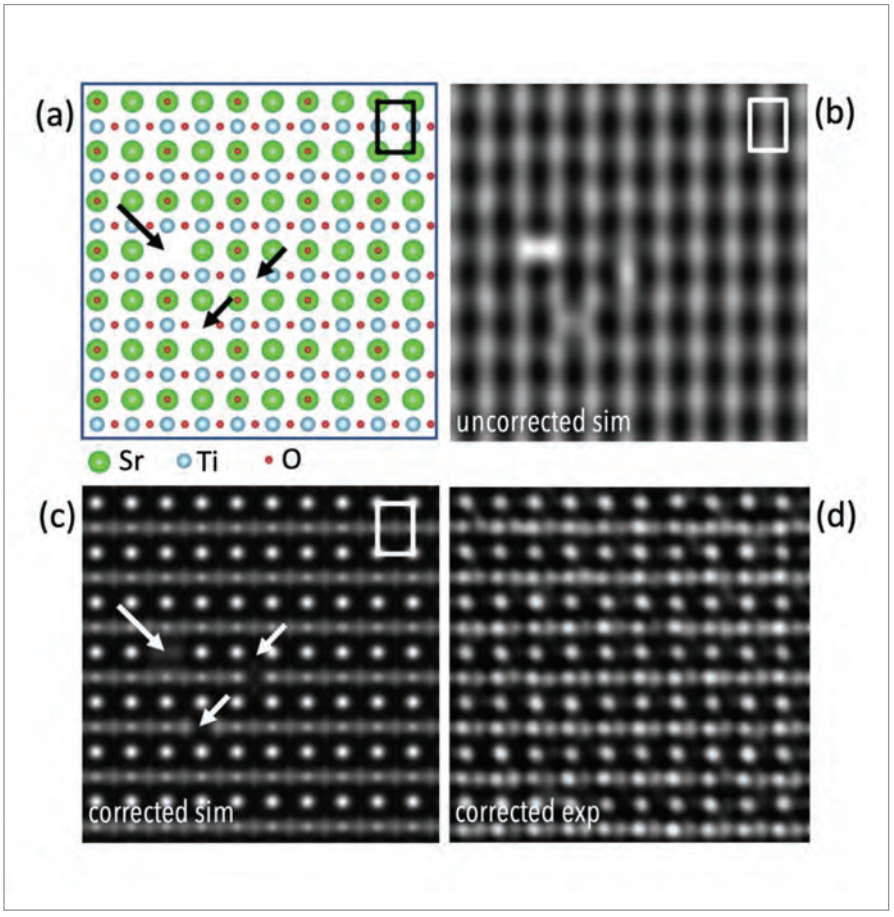


**Figure 1.**

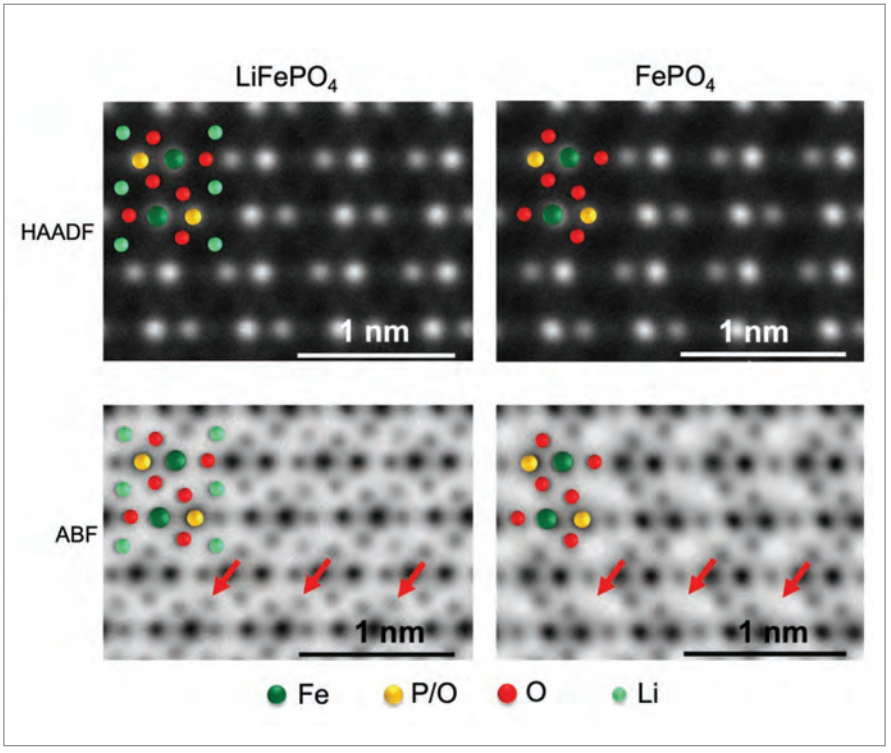


**Figure 2.**

aberration is proportional to the focal length [8]. By the early 1980s, it was clear that both strategies yielded inadequate results; in particular, the goal of imaging at single-atom resolution in solids remained out of reach. In addition to the special technical and electron-optical problems of high-voltage electron microscopy, the specimens were quickly destroyed by atom-displacement damage at the high electron energies. The way to reduce the spherical aberration by shortening the focal length was limited by the fact that the magnetic pole piece dimensions had to achieve very small values. This meant that there was no longer space at the specimen location for a double-axis goniometer with which the specimens could be appropriately tilted and crystallographically aligned with respect to the electron beam.

To construct aberration-corrected electromagnetic lens systems by combining a converging lens with a suitably calculated diverging lens, as Abbe did for light microscopy in the second half of the nineteenth century, is forbidden by Laplace's equation, which does not allow to construct diverging lenses. However, as already shown in the fundamental theoretical work of Scherzer in 1947, this restriction applies only to rotationally symmetric lenses, i.e. not to magnetic multipole lenses [9]. Although the work for an experimental and technical realization of the elimination of spherical aberration by systems of magnetic multipole lenses started early [10], it was to take another fifty years until it was possible in 1997 to realize the first aberration-corrected transmission electron microscope, whose resolving power was substantially increased, in fact doubled, compared to the uncorrected instrument (Haider et al. [11,12]). Thus, the atomic resolution Knoll and Ruska had hoped for was finally achieved. However, there is a fundamental difference between the first attempts to correct the spherical aberration as proposed by Scherzer [9] and the later successful aberration correction by employing

hexapole-fields. Scherzer proposed an astigmatic ray path with line-foci generated with the help of quadrupole fields, where the spherical aberration for a section can be compensated directly by an octupole field. Within the hexapole-corrector concept there are no strong quadrupole-fields needed.

The long development time was due, among other things, to the fact that the divergent action, which is independent of the azimuthal angle and analogous to the effect of a round diverging lens, is a second-order effect superimposed by the much stronger primary aberration of a multipole, a massive distortion of the electron beam. To compensate this distortion by a second multipole is technically very complex. The first successful aberration-corrected objective lens system, which is still by far the most widely used system in CTEM and STEM today [13], is based on a double-hexapole arrangement. The correction system theoretically calculated by Rose [14] after preceding work by Hawkes [15], Beck [16] and others uses a highly symmetrical arrangement of the elements, which facilitates the technical compensation or minimization of the unwanted aberrations of the double hexapole system. Another development is that of the quadrupole-octupole corrector for STEM by Krivanek et al. [17], which was successful in 2001 by demonstrating for the aberration-corrected microscope a substantial improvement of the resolution compared to the uncorrected instrument.

Modern materials research now benefits from electron microscopes that offer quasiroutine atomic resolution with Rayleigh resolution of better than 50 pm and a precision of the order of 1 pm in CTEM and STEM. Structural studies at true atomic resolution, atom by atom, are now standard in CTEM [18,19] and STEM [20,21]. In CTEM **(Fig. 1)** the standard imaging mode is NCSI [22]. Atomic resolution studies by EELS of electron states for chemical identification and for the investigation of low-energy electronic and vibronic excitations as pioneered by Krivanek et al. [23-25] have dramatically increased the interest in STEM. In fact about 80% of all aberration corrected transmission electron microscopes installed today are STEMs. These also allow the use of many new STEM investigation techniques that have been developed in recent years to be used in addition to the standard HAADF imaging technique [21]. This includes annular brightfield (ABF) technique, which allows imaging of both the strongly and weakly scattering atoms [26] **(Fig. 2)**.

Although the vast majority of atomic-resolution electron microscopes have only spherical aberration correction, there are also a few instruments, CTEMs, that have chromatic aberration correction in addition to spherical aberration correction. In addition to quadrupole-octupole elements, combined electrostatic-magnetic quadrupole correction elements are also necessary for this purpose [27-30]. This has allowed a new field of transmission electron microscopy to develop, low-energy electron microscopy, which operates at electron energies between 15 and 80 keV (Suenaga et al. [31], Kaiser et al. [32]). Finally, we would like to mention that in recent years aberration-corrected electron microscopes, which were, after all, originally developed for applications in materials science, are also finding their way into biological electron microscopy at atomic resolution [33]. ■

## References


1. M. Knoll, E. Ruska, Z. f. Physik 78, 318 (1932).
2. A. Crewe, J. Wall, J. Langmore, Science 168, 1338 (1970).
3. M.S. Isaacson, Ultramicroscopy 123, 3 (2012).
4. W. Glaser, Z. f. Physik 81, 649 (1933).
5. E. Brüche, O. Scherzer, Geometrische Elektronenoptik, Springer, Berlin (1934).
6. O. Scherzer, Z. f. Physik 101, 593 (1936).
7. G. Thomas, M.J. Goringe, Transmission Electron Microscopy of Materials, Wiley&Sons (1979).
8. W. Glaser, Z. f. Physik 117, 285 (1941).
9. O. Scherzer, Optik 2, 114 (1947).
10. R. Seeliger, Optik 8, 311 (1951).
11. M. Haider, S. Uhlemann, E. Schwan, H. Rose, B. Kabius, K. Urban, Nature 392, 768 (1998).
12. M. Haider, H. Rose, S. Uhlemann, E. Schwan, B. Kabius, K. Urban, Ultramicroscopy 75, 53 (1998).
13. In the literature, the acronyms CTEM and STEM are used for both the instruments and the mode of operation of these. For the sake of simplicity, we also follow this practice here.
14. H. Rose, Optik 85, 19 (1990).
15. P.W. Hawkes, Phil. Trans. R. Soc. A, 257, 479 & 523 (1965).
16. V.D. Beck, Optik 53, 241 (1979).
17. N. Dellby, O.L. Krivanek, P.D. Nellist, P.E. Batson, A.R. Lupini, J. Electron. Microsc. 50, 177 (2001).
18. K. Urban, Science 321, 506 (2008).
19. K.W. Urban et al., Prog. Mat. Sci. 133, 101037 (2023).
20. P.E. Batson, N. Dellby, O.L. Krivanek, Nature 418 (2002).
21. S.J. Pennycook, P.D. Nellist (Eds.) Scanning Transmission Electron Microscopy, Springer (2011).
22. C.-L. Jia, M. Lentzen, K. Urban, Science 299, 870 (2003).
23. D.A. Muller et al., Science 319, 1073 (2008).
24. O.L. Krivanek et al., Nature 464, 571 (2010).
25. O.L. Krivanek et al., Nature 514, 209 (2014).
26. S.D. Findlay, R. Huang, R. Ishikawa, N. Shibata, Y. Ikuhara, Microscopy 66, 3 (2017).
27. H. Rose, Optik 26, 289 (1967)
28. M. Haider, P. Hartel, H. Müller, S. Uhlemann, J. Zach, Microsc. Microanal. 16, 393 (2010).
29. U. Dahmen et. al., Phil. Trans. Roy. Soc. A 367, 3795 (2009).
30. L. Jin, J. Barthel, C.-L. Jia, K.W. Urban, Ultramicroscopy 176, 99 (2017).
31. T. Sasaki, H. Sawada, F. Hosikawa, Y. Sato, K. Suenaga, Ultramicroscopy 145, 50 (2014).
32. M. Linck et al., Phys. Rev. Lett. 117, 076101 (2016).
33. K.M. Yip, N. Fisher, E. Paknia, A. Chari, H. Stark, Nature 587, 157 (2020).

**David A. Muller**
School of Applied and Engineering Physics, Cornell University, Ithaca NY, USA

# Imaging beyond the diffraction limit with **electron ptychography**

**Electron microscopes use electrons with wavelengths of a few picometers, and are potentially capable of imaging individual atoms in solids at a resolution ultimately set by the intrinsic size of an atom. Until very recently, the best resolution was more than an order magnitude worse than this limit. This was caused by two things – first the intrinsic aberrations in electron lenses are much worse than for optical lenses – comparable to using a beer bottle as a magnifying glass. Second, electrons are multiply-scattered inside the sample – a process described by Hans Bethe over 90 years ago. It's been a limitation for electron microscopists ever since, but the recent advances described here for detector technology and reconstruction algorithms, the resolution of the electron microscope is now limited only by the dose to the sample, and thermal vibrations of the atoms themselves.**

Microscopists obsess over resolution. This one number has become the shorthand that describes the performance of a new instrument, even when it is only a proxy for the desired benefit, such as enhanced contrast or signal. **Figure 1** shows the improvement in diffraction-limited resolution over the past two centuries: optical microscopy reached its far-field diffraction limit a little over a century ago. Electron lenses are limited by intrinsic aberrations to relatively small numerical aperture, so electron microscope resolution initially improved by increasing the beam voltage in order to reduce the electron wavelength. Unfortunately, higher energy electron beams are also able to knock atoms around more effectively, so by the late 1980's that strategy had mostly been exhausted. Ways to correct lens aberrations in principle had been known since 1948. It was not until the 1990's that computer control of the microscope and the machining had developed to a point that these correction strategies became practical. From 1996 to 2008, aberration correctors saw rapid improvements in resolution, reaching 0.5 Angstrom resolution in 2008, with only incremental improvements since then as the complexity of correcting and stabilizing geometric and chromatic aberrations at higher angles increased.

In July 2018, we reported what was then the highest resolution image ever obtained using an electron microscope[1]. The images were obtained, not at the highest possible beam voltage, but rather at 80 keV, and with a point-to-point resolution, two-and-a-half times beyond the diffraction limit for those microscope conditions. This improvement in imaging conditions was made possible by a new detector design and a long history of algorithm development, and marked the first time ptychography, or any diffractive imaging method, had surpassed the resolution obtained by the best electron lenses. By 2021, we had further improved resolution by developing an approach to account for the multiple scattering in thicker samples, and demonstrated images where the instrumental blur was now reduced below 20 pm, and the thermal blur of individual atom columns became visible for the first time.

## Coherent Diffractive Imaging

There is a long history to diffractive electron imaging, in which image-forming optics are replaced or supplemented by an inverse calculation using scattered intensity data that is in principle limited only by the highest scattering angle at which useful data can be collected. Starting with Dennis Gabor's invention of holography in 1948 as an approach to overcome the aberrations

of the electron lens, is the recognition that phase information can be encoded in the amplitude of a wave, and also recovered to form an image[2]. Coherent diffractive imaging from objects of limited size again exploit this concept.

Originally conceived by Walter Hoppe as a way to solve the phase problem in crystallography[3], ptychography exploits the phase information encoded in the diffraction pattern from a localized electron beam. By focusing the beam to a spot of width $\Delta x$, the diffraction spots will blur out into disks of width $\Delta k$. When $\Delta x$ is made smaller than the atomic lattice spacing, then the diffraction disks become wide enough to overlap, and the interference between the wave functions from two adjacent scattered disks is captured in the overlap region. Moving the probe in real space, causes a phase shift in diffraction space, leading to a contrast change in the overlap. Ptychography (or "folded writing" from the German translation of convolutional imaging) seeks to recover the phase shifts, and by stepping out from disk to disk can build up the phase relationship between all the scattered beams, thus solving the crystal structure. John Rodenburg developed the theory to apply to general, non-crystalline objects, recognizing this was also a way to extend the resolution of the electron microscope well beyond the limits of the lens.[4] With his then student Peter Nellist, they demonstrated a proof of concept for a thin silicon sample almost 25 years ago, reaching a line resolution of 3.3 Å.[5] At the time, electron detector technology was really too primitive to do much more, and the arrival of aberration correctors provided a powerful alternative for high resolution imaging.

Instead, the x-ray community, which also had its own challenges with producing high-resolution lenses adopted these ideas. The weaker interactions of the x-ray beam with the sample, and the less severe drift requirements at much lower resolutions of synchrotrons made it a more tractable

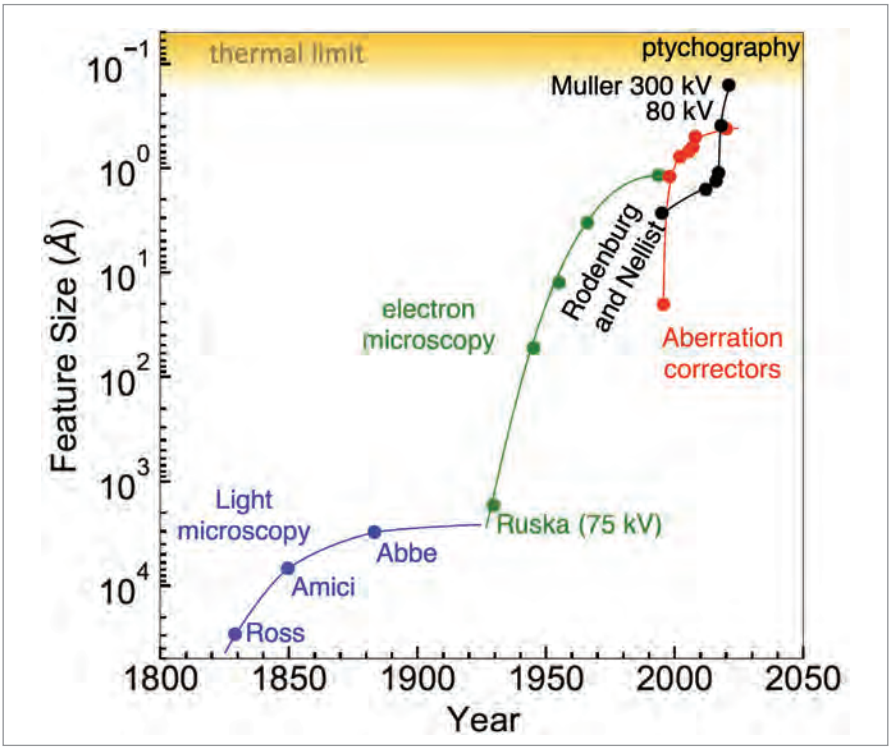


**Figure 1.** **Minimum Resolvable Feature Size vs Time.**

implementation, and it is widely used there today. The rebirth of electron ptychography has benefited from both the new generation of detectors, and also the ideal test samples in the form of 2D materials systems. Even with a limited dynamic range detector, ptychography shows promise for low-dose and light element sensitivity, and in the past few years interest had picked up again.

## Measuring Every Electron

The past three decades have seen the rapid development and maturation of aberration-corrected electron lenses. To match their improved resolution, manufacturers also had to improve the stability of microscope columns. It now made sense to also improve the quality of the measured signals. Direct electron detectors, with their better sensitivity and speed compared to the older generation of scintillators-coupled CCD or CMOS cameras have already revolutionized biological cryo-electron microscopy. These detectors were designed for recording images with very many pixels, but very few electrons per pixel – perfect for low-dose biological imaging, but very poorly suited to materials applications where larger doses are used and needed. Further, much materials work today in STEM mode with the detector is placed in the diffraction plane, where the usable scattered signal varies in intensity by about 6 orders of magnitude.

For over a decade, Sol Gruner and I had worked together on building, optimizing, and utilizing pixel array detectors for scanning transmission electron microscopy to overcome this problem.[6,7] Our first electron detector[6], adopted from a direct x-ray detector was promising - it had the speed and sensitivity, but lacked the dynamic range necessary for quantitative work. Learning from this, we developed a series of electron microscope pixel array detectors (EMPADs) that can collect every electron in the diffraction pattern (including those in the central beam) as the electron beam is rapidly scanned over the sample. [7] The resulting 4D dataset records the full position and momentum distribution of the transmitted electrons, from which any elastic imaging mode can

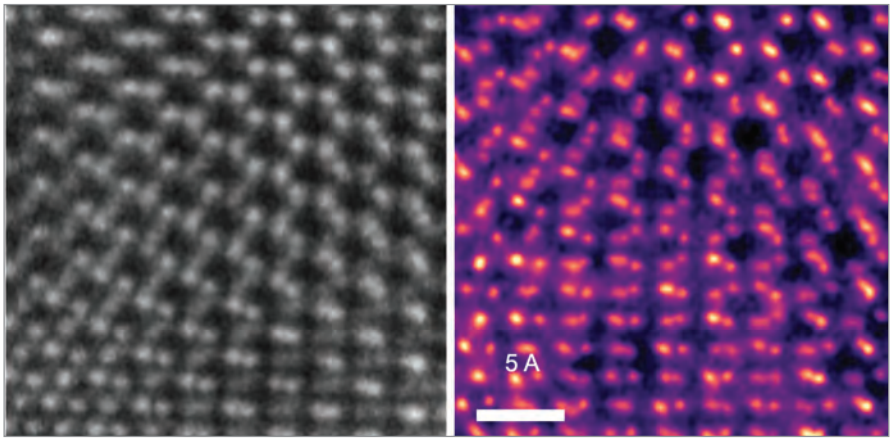


**Figure 2. (left)** A High-Angle annular dark field (HAADF) image of an AA-stacked $MoTe_2$-$WSe_2$ bilayer. **(right)** Electron ptychography of a similar region showing the misregistration between the two layers due to their lattice mismatch.

be reconstructed, including magnetic imaging and strain mapping. The precision of both these imaging modes depends most strongly on the dose, so being able to handle large currents meant sub-picometer (<0.3 pm) precision lattice and strain(< 0.2%) maps could be made from data sets recorded in about 1 minute[8]. A 2nd generation device, completed in 2020, framed almost 20x faster, with a 100x increase in saturation current, and commensurate improvements in performance[9].

By 2016, we had mounted the detector on an aberration-corrected tool and were ready to revisit using ptychography to improve the resolution of the microscope. Electron beams can be quite damaging, especially at higher energies, so much of the imaging of 2D materials is done at lower beam voltages, where the resolution is also considerably lower and also severely limited by chromatic aberrations. Here is where the combination of the new high-dynamic range detector and ptychography came into play. By collecting the momentum distribution out to scattering angles well beyond the numerical aperture of the lens - i.e outside the central disk -and using iterative ptychography[10] we were able to recover more phase information than from the lens alone.[1] In effect, creating a virtual aperture that is larger than what could be achieved with the lens. Provided sufficient signal can be collected, the resolution can be increased commensurately. As a practical matter, this boosted resolution about 2.5x over what the lens alone could do, and at 0.39 Å was even beyond the highest-resolution, highest-voltage, aberration-corrected tools.[1]

Testing resolution in real space is a challenge – there are no bond lengths below 0.5 Å. Surprisingly, 2D materials provided a perfect test sample - a twisted bilayer of two monolayer sheets of transition metal dichalcogenides stacked on top of each other, with the two sheets rotated a few degrees apart from each other. The resulting incommensurate moire pattern when viewed in project provides a range of atomic distance from a full bond length apart, to directly overlapping, with all possible spacings in between[1]. Following the patterns as the atoms shift in and out of registry reveals when pairs of atoms are no longer resolvable determined the resolution **(Figure 2)**.

## Multiple Scattering, Thick Samples and Depth-Sectioning

Electron imaging of thicker samples is severely hampered by multiple scattering that changes the probe shape and causes dechannelling effects

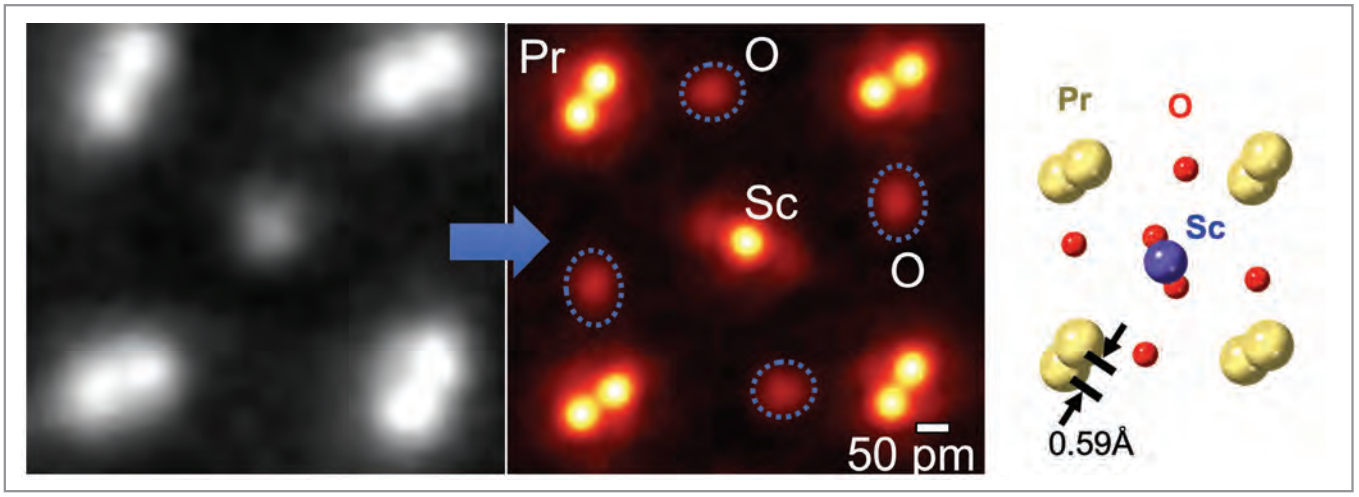


**Figure 3.** Improved resolution by electron ptychography. Left is a state-of-the-art HAADF STEM image of PrScO3 showing 0.5Å resolution. Right is the same region by ptychography at 0.16Å resolution. The elongation of the oxygen nuclei is from increased thermal vibration perpendicular to the Sc-O bonds, with reduced vibration along the bonds.

between neighboring atomic columns which reduces the interpretable resolution. Multiple scattering also leads to a complicated image contrast that is nonlinearly or even nonmonotonically dependent on the sample thickness, especially for phase-contrast imaging methods. Attempts at phase retrieval from both multi-slice electron ptychography and Bloch wave based scattering matrix approaches had been reported. However none of these early experimental demonstrations have been widely adopted due to limited resolution or image quality. By 2021 we had identified the numerical instability in the multi-slice approach and then demonstrated a robust experimental realization of inversion of the multiple scattering using a regularized implementation of multislice electron ptychography[11]. This approach provides ultra-high-resolution reconstructions for samples hundreds of Angstroms thick. More importantly, the contrast maintains a linear dependence on thickness over a wide thickness range. The linear phase-contrast can also greatly widen the applicable sample thickness and makes it possible to obtain three-dimensional structural information including the locations of single dopant and interstitial atoms.

Experimentally, the multislice reconstruction was demonstrated on a 210-Å thick $PrScO_3$ sample, showing an isotropic lateral information transfer down to 23 pm, with a depth resolution of 3.5 nm. Quantitative analysis of the atomic column width showed that the blurring from the instrument was smaller than 20 pm, which is also smaller than the intrinsic broadening from thermal fluctuations[11]. In other words, the resolution of the image was limited not by the instrument, but instead by the thermal vibration of the atoms, and closer examination showed the anisotropy of the vibrational blur of the oxygen atoms, along and perpendicular to their bonds. The method also allows for direct measurements of Debye-Waller factors of atoms near defects or interfaces.

The detectors have performed well in other areas, showing high sensitivity for imaging magnetic Skyrmions[12] and ferroelectrics, including polarization vortices[13,14]. The high-precision strain mapping in radiation-sensitive materials has already found application for solving 2D materials problems.[15] Even for imaging biological samples, early results show a better signal-to-noise ratio than energy-filtered TEM in thick samples.[16] While there is still much work to be done, ptychography and 4D-STEM are already fulfilling their earlier and hoped-for promises. We have entered a new era of electron microscopy in which new detectors, in combination with ptychography, makes it possible to achieve deep sub-Ångström resolution, and also enabling new imaging modes for measuring functional properties of materials. ■

## References


1. Jiang, Y., Chen, Z., Han, Y., Deb, P., Gao, H., S. Xie, Purohit, P., Tate, M. W., Park, J., Gruner, S. M., Elser, V. & Muller, D. A. Electron, "Ptychography of 2D Materials to Deep Sub-Ångström Resolution." *Nature* **559**, 343–349, (2018).
2. Dennis Gabor, Nobel Lecture (1971), https://www.nobelprize.org/prizes/physics/1971/gabor/lecture/
3. Hoppe, W. "Diffraction in inhomogeneous primary wave fields. 1. Principle of phase determination from electron diffraction interference." *Acta Crystallogr.* **A 25**, 495–501 (1969).
4. J. M. Rodenburg and R. H. T. Bates. "The Theory of Super-Resolution Electron Microscopy Via Wigner-Distribution Deconvolution" *Philosophical Transactions of the Royal Society of London A: Mathematical, Physical and Engineering Sciences* 339, no. 1655 (1992): 521–553.
5. P. D. Nellist, B. C. McCallum, and J. M. Rodenburg. "Resolution beyond the 'information Limit' in Transmission Electron Microscopy" *Nature* 374, no. 6523 (1995): 630–632.
6. T.A. Caswell, P. Ercius, M.W. Tate, A. Ercan, S.M. Gruner, and D.A. Muller, "A High-Speed Area Detector for Novel Imaging Techniques in a Scanning Transmission Electron Microscope," *Ultramicroscopy* **109** (2009) 304–311.
7. M.W. Tate, P. Purohit, D. Chamberlain, K.X. Nguyen, R.M. Hovden, C.S. Chang, P. Deb, E. Turgut, J.T. Heron, D.G. Schlom, D.C. Ralph, G.D. Fuchs, K.S. Shanks, H.T. Philipp, D.A. Muller, and S.M. Gruner, "High Dynamic Range Pixel Array Detector for Scanning Transmission Electron Microscopy," *Microscopy and Microanalysis* **22** (2016) 237–249.
8. Y. Han, K. X. Nguyen, M. Cao, P. D. Cueva, S. Xie, M. W. Tate, P. Purohit, S. M. Gruner, J. Park, and D. A. Muller. "Strain Mapping of Two-Dimensional Heterostructures with Sub-Picometer Precision" *Nano Letters* **18**, (2018): 3746–3751.
9. H. T. Philipp, M. W. Tate, K. S. Shanks, L. Mele, M. Peemen, P. Dona, R. Hartong, G. Van Veen, Y. T. Shao, Z. Chen, J. Thom-Levy, D. A. Muller, and S. M. Gruner. "Very-High Dynamic Range, 10,000 Frames/Second Pixel Array Detector for Electron Microscopy" *Microscopy and Microanalysis* **28**, (2022): 425–440. doi:10.1017/S1431927622000174
10. M. J. Humphry, B. Kraus, A. C. Hurst, A. M. Maiden, and J. M. Rodenburg. "Ptychographic Electron Microscopy Using High-Angle Dark-Field Scattering for Sub-Nanometre Resolution Imaging" *Nat Commun* 3, (2012): 730.
11. Z. Chen, Y. Jiang, Y.-T. Shao, M. E. Holtz, M. Odstrčil, M. Guizar-Sicairos, I. Hanke, S. Ganschow, D. G. Schlom, and D. A. Muller. "Electron Ptychography Achieves Atomic-Resolution Limits Set by Lattice Vibrations" *Science* **372**, (2021): 826–831.
12. Z. Chen, E. Turgut, Y. Jiang, K.X. Nguyen, M.J. Stolt, S. Jin, D.C. Ralph, G.D. Fuchs, D.A. Muller (2022) Lorentz electron ptychography for imaging magnetic textures beyond the diffraction limit. *Nature Nanotechnology*, **17**(11):1165–1170.
13. K. X. Nguyen, P. Purohit, A. Yadav, M. W. Tate, C. S. Chang, R. Ramesh, S. M. Gruner, and D. A. Muller. "Reconstruction of Polarization Vortices by Diffraction Mapping of Ferroelectric PbTiO3 / SrTiO3 Superlattice Using a High Dynamic Range Pixelated Detector" *Microscopy and Microanalysis* 22, no. S3 (2016): 472–473.
14. A. Yadav et al, "Spatially Resolved Steady State Negative Capacitance", Nature, (in press)
15. S. Xie, L. Tu, Y. Han, L. Huang, K. Kang, K. U. Lao, P. Poddar, C. Park, D. A. Muller, R. A. DiStasio, and J. Park. "Coherent, Atomically Thin Transition-Metal Dichalcogenide Superlattices with Engineered Strain" *Science* 359, no. 6380 (2018): 1131–1136.
16. K. A. Spoth, K. X. Nguyen, D. A. Muller, and L. F. Kourkoutis. "Dose-Efficient Cryo-STEM Imaging of Whole Cells Using the Electron Microscope Pixel Array Detector" *Microscopy and Microanalysis* 23, no. S1 (2017): 804–805.

**Joachim Mayer, Knut Urban, Rafal Dunin-Borkowski and Carsten Sachse**

# The **Ernst Ruska-Centre** – celebrating its 20th anniversary

In January of 2004, Forschungszentrum Jülich and RWTH Aachen University signed a cooperation contract for the foundation of the Ernst Ruska-Centre for Microscopy and Spectroscopy with Electrons (ER-C). Since its establishment, the ER-C has been operated as a national user centre and has become one of the internationally leading centres in ultra-high-resolution transmission electron microscopy. The present infrastructure at the ER-C consists of twelve transmission electron microscopes (TEMs) and comprises seven aberration corrected state-of-the-art instruments as well as three cryo-TEMs. The centre, which is named after the Nobel laureate Ernst Ruska, has recently been expanded by adding groups active in life science and soft matter applications. The Ernst Ruska-Centre serves users in solid state physics and chemistry, materials science, soft matter and life science by providing them with access to the newest generation of instruments and by developing new methods and applications which are at the forefront of the international activities in the field.

The basis for its foundation was pioneering work on the correction of electron-optical lenses. After the transmission electron microscope was invented in the early 1930s by Knoll and Ruska, attempts to visualize atoms remained unsuccessful for decades as a result of lens imperfections, or aberrations, that could not be corrected. In an optical microscope, divergent lenses can be used to compensate for the aberrations of convergent lenses. However, divergent lenses cannot be built for electrons using rotationally symmetric magnetic fields. In the 1990s, Harald Rose from the Technische Universität Darmstadt, Max Haider from the European Molecular Biology Laboratory (EMBL) in Heidelberg, and Knut Urban from Forschungszentrum Jülich found a solution to this dilemma. They developed a corrector that could eliminate the effects of "spherical aberration" for electrons. Since none of the established funding sources promised support, it was the Volkswagen Foundation which finally committed to fund the development.

The world's first aberration corrected transmission electron microscope demonstrated its functionality and the achievable advancement in resolution in 1998. Thus we are also celebrating 25 years of aberration correction and the anniversary was also celebrated at the conference PICO 2023, which was supported by the EMS as an EMS extension. The prototype instrument is still on display at the Ernst Ruska-Centre (see **Figure 1**).

Since 2004, transmission electron microscopes that are equipped with spherical aberration correctors have been available commercially, with all leading electron optics manufacturers now offering this capability. In

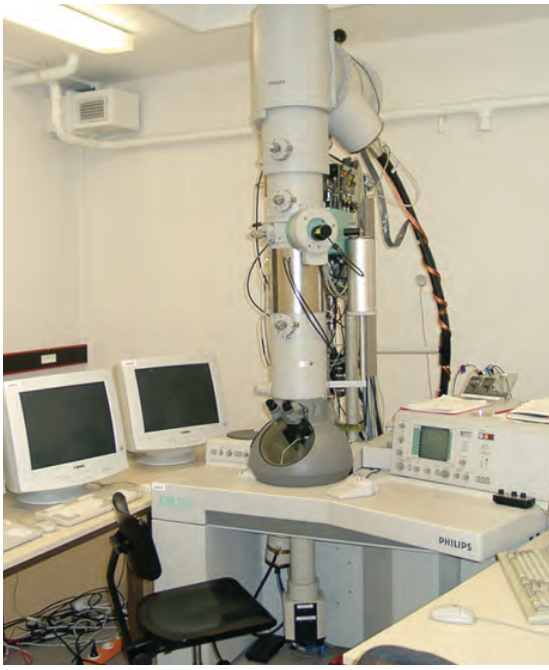


**Figure 1.** **The first aberration-corrected transmission electron microscope at the Research Center Jülich**

**Figure 2.** **Inauguration of the Ernst Ruska Centrum (ER-C) in 2006: (front row) Irmela Ruska, Ernst Ruska's widow, Knut Urban, the initiator and former ER-C director, and Joachim Mayer, director of the ER-C; (back row) Jürgen Ruska, Ernst Ruska's son, Burkhart Rauhut, Rector of RWTH Aachen University, Ulrich-Ernst Ruska, Ernst Ruska's son, and Joachim Treusch, Chairman of the Board of Directors, FZ Jülich**

2006, two TITAN 80-300™ microscopes from the Dutch-US company FEI were installed at the ER-C. They are able to visualize atomic structures with a resolution of 80 picometres. With the installation of these two Titan instruments, the inauguration ceremony of the ER-C took place and it was our pleasure to host three members of the Ruska family **(Figure 2)**.

As a next step in the development, in 2011 the ER-C took delivery of the PICO transmission electron microscope, which is one of only few high resolution electron microscopes in the world that can correct for an additional lens aberration – chromatic aberration **(Figure 3)**. Out of these, PICO is equipped with the most advanced Cc-corrector and apart from improving the resolution down to 50 picometres, the ability to correct for chromatic aberration also increases the precision with which atomic distances and displacements in materials can be measured, from 5 picometres to below 1 picometre.

With the PICO microscope, both scientists at the ER-C and external users can approach a performance level closer to the physical limit of electron optics for observations at the nanoscale. Picometre precision measurements are essential to be able to control and optimize components in nanoelectronics and nanotechnology. Scientists need insight into the world of atoms and the processes that take place on this scale to develop new materials for areas such as information technology and energy materials.

The next level of expansion was envisaged when, in the beginning of 2016, FZ Jülich together with its university partners RWTH Aachen University and Heinrich Heine University Düsseldorf have filed a major project proposal for consideration within the framework of the BMBF National Research Infrastructure Roadmap, which has been highly rated in the scientific review. In the proposal named ER-C 2.0, five innovative, next-generation devices of unprecedent capabilities

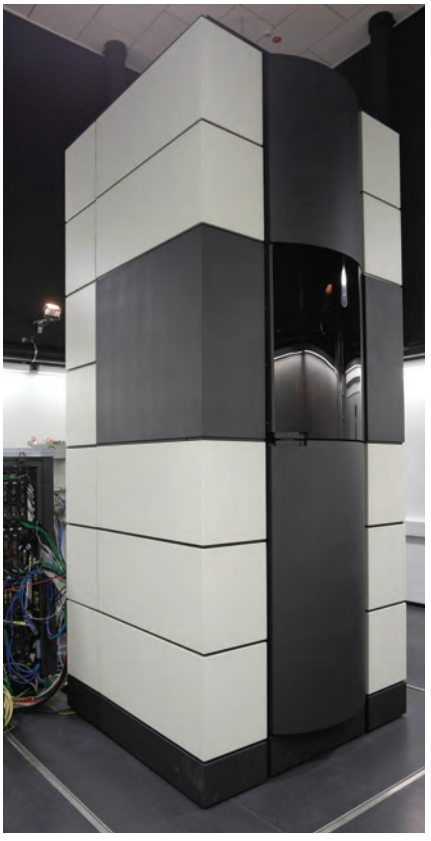

**Figure 3.** **The chromatic aberration corrected PICO instrument at the Ernst Ruska-Centre**

were outlined, which in a coordinated manner of operation will cover classical solids, nano-materials and soft matter right up to biomolecules and cell structures.

In support of this initiative, in 2017 the ER-C has been upgraded into the level of a separate institute at FZJ, including a new structural biology division from the life sciences, to further improve the performance of electron microscopy across the entire scientific spectrum in order to establish a top position worldwide.

After a long and painful waiting time, in fall of 2019 funding has been granted for Phase I of the expansion in which two of the unique instruments will be supported. In Phase II of the realisation of ER-C 2.0, three additional unique instruments will be installed, which will further extend the experimental portfolio of the Ernst Ruska-Center. With the ER-C 2.0 instruments, ultimate spatial, spectroscopic and temporal resolution will be achieved by combining novel electron optical components and detectors in an unprecedented manner. A new building with specifically designed microscope rooms will host the new instruments.

The new instruments will incorporate spherical and chromatic aberration correctors developed in Germany and will be equipped with novel capabilities, such as improved ultra-high-vacuum technology and helium cooling of the specimen chamber. Unique aspects of the microscopes will include capabilities for simultaneous atom probe tomography and electron microscopy, ultra-high-energy- resolution spectroscopy and the use of pulsed coherent electron sources for ultrafast experiments. The complementary nature of the new instrumentation will allow users from different research fields - reaching from physical sciences and materials science to life science - to access a broad spectrum of techniques and applications.

The ER-C will continue to be operated as a German user facility and all EMS members are cordially invited to submit a user proposal to the ER-C, details can be found at www.er-c.org. For academic users and users from public research centres the use of instruments is free of charge. ■

# The next 25 years of microscopy?

When you have read this booklet until this page, you could look back to the last 25 years of evolution in microscopy. Wouldn't you be interested to know, how microscopy will proceed over the next 25 years? Well, I am not the kind of visionary who could tell you – but these days we permanently hear of the power of artificial intelligence (AI). While in general AI can be used to mingle well-established knowledge to create successfully summaries, full texts and even images into something that looks convincingly new and original, one rarely finds attempts to ask AI about future developments. I did so, asking ChatGPT about the future of electron microscopy, specifically what an electron microscope would look like in 25 years from now. Since ChatGPT is a text-based AI software, I did not get an image, but a textual description, which I do not want to withhold from you...

**Figure 1a.** AI-generated images of "future" microscopes, resembling mostly standard light microscopes. AI also seems to adopt the (pre-feministic) habit of many manufacturers of having a young lady working on the machines in their sales brochures. All images generated by [Bing] - https://www.bing.com/images/create/

*"Title: "Quantum Vision: Electron Microscope 2049"*

*Description: In the year 2049, the electron microscope has undergone a remarkable transformation, merging cutting-edge advancements in nanotechnology, quantum computing, and artificial intelligence. The traditional bulky design has evolved into a sleek, minimalist structure that exudes sophistication and technological prowess.*

*At the core of this futuristic electron microscope is a quantum processor, capable of handling vast amounts of data with unprecedented speed and precision. The microscope's interface resembles a holographic display, allowing researchers to interact with virtual models of the microscopic world with intuitive gestures.*

*The electron source is now powered by miniature quantum emitters, producing electron beams of unparalleled coherence and intensity. This enhancement enables imaging at the atomic scale with astonishing clarity and detail, revealing intricate structures and phenomena previously hidden from view.*

*The sample chamber is enclosed within a transparent nanocomposite shell, providing a controlled environment for studying delicate specimens without interference from external factors. Advanced robotic systems handle sample manipulation with unparalleled accuracy, allowing for automated high-throughput imaging and analysis.*

*Artificial intelligence algorithms work in tandem with human operators, optimizing imaging parameters in real-time to adapt to the unique characteristics of each sample. The microscope's capabilities extend beyond imaging, enabling precise manipulation and control of individual atoms for nanoscale engineering and fabrication.*

*As researchers peer through the lens of this quantum-powered electron microscope, they unlock new frontiers in science and technology, unraveling the mysteries of the quantum realm and shaping the future of innovation."*

**Figure 1b.** AI-generated images of "future" microscopes, resembling mostly standard light microscopes. AI also seems to adopt the (pre-feministic) habit of many manufacturers of having a young lady working on the machines in their sales brochures. All images generated by [Bing] - https://www.bing.com/images/create/

I will leave it to the reader to judge on the content of this text and its relevance. To me, it sounds a bit like a politician's speech about something he wants to be realized, enhanced with fashionable buzzwords, but without knowing exactly how it could be achieved precisely. In the next step, I wanted to see what an electron microscope would look like in 25 years, and I asked the image generating AI of "Bing" (https://www.bing.com/images/create/) to produce an image of an "artists view of a future electron microscope" in various styles.

I received a large number of pictures; many of them, however, came up with a defamiliarized image of a regular light microscope with some added

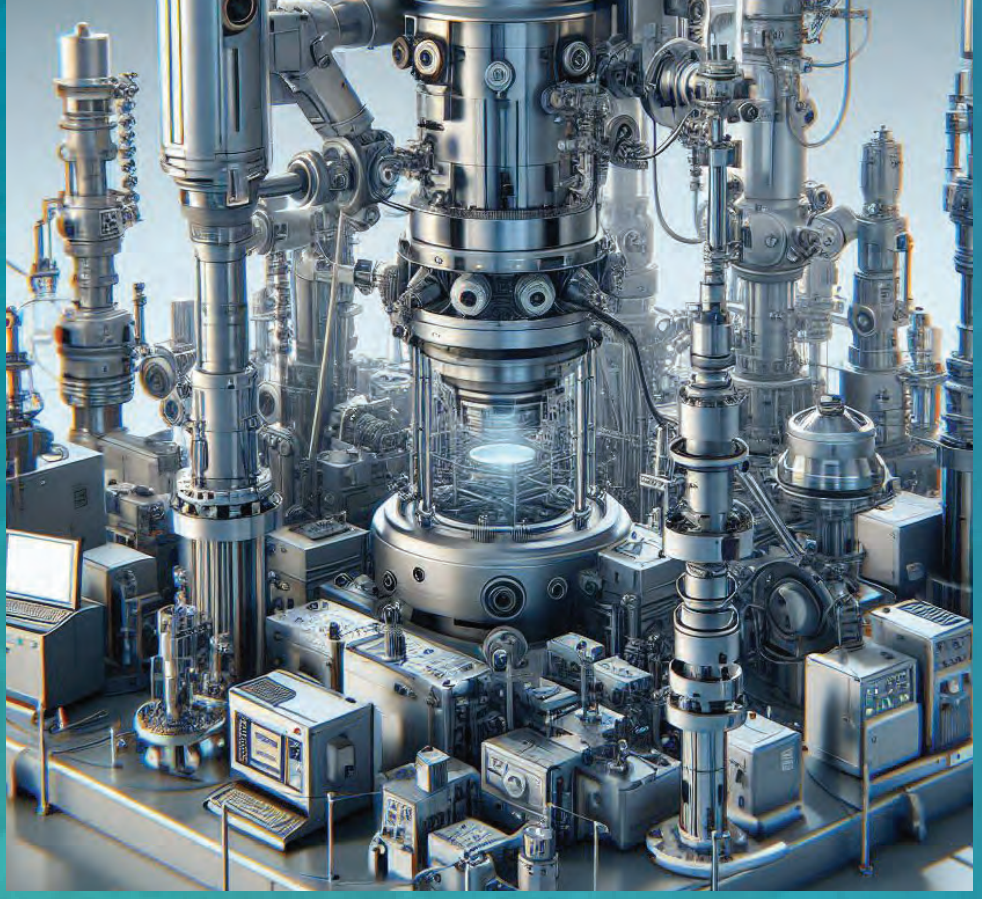

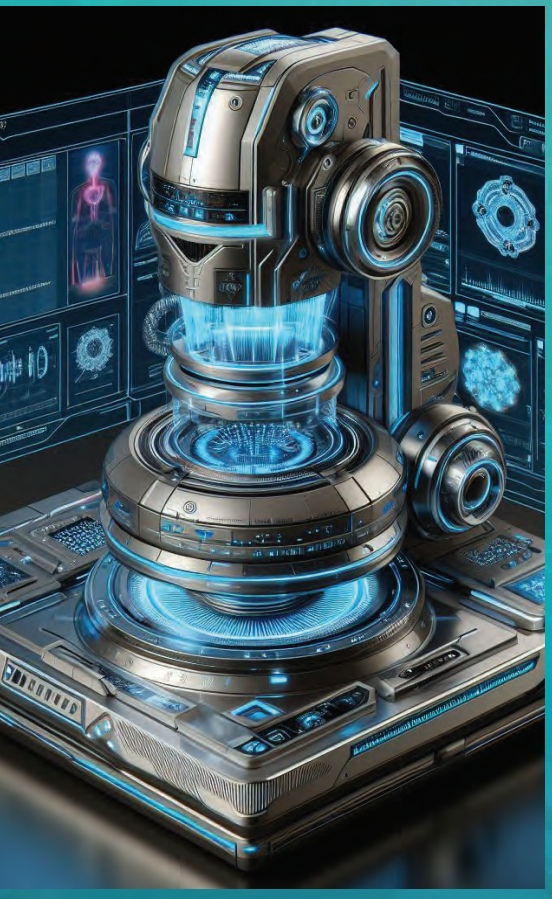

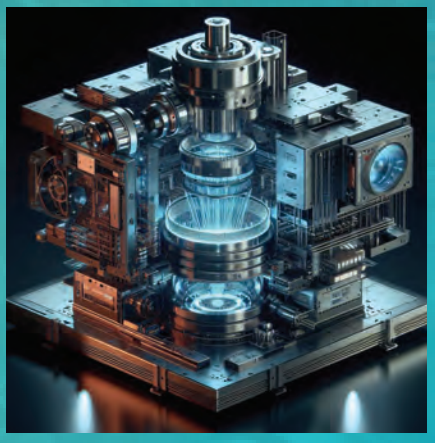

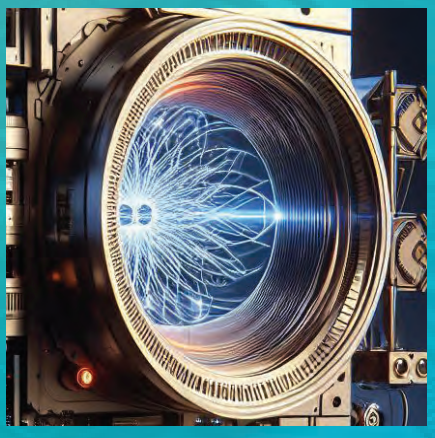

**Figure 2a.** AI-generated images of "future" microscopes with very technical appearance. Some seem extremely condensed, while others appear gigantic. All images generated by https://www.bing.com/images/create/

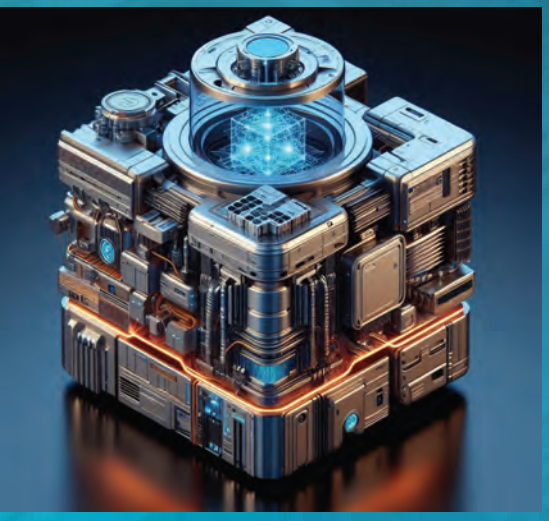

periphery – I will show some of them in ***Figures 1 a)*** and ***b)***, as I found them quite entertaining.

Further images can be coarsely sorted into three categories, a pronounced technically-looking design ***(Figures 2a*** and ***b)***, designs which are purely abstract ***(Figure 3)*** or even comic-strip-like ***(Figure 4)*** and designs, where the underlying art style can be easily recognized ***(Figure 5)***.

**Figure 2b.** AI-generated images of "future" microscopes with very technical appearance. Some seem extremely condensed, while others appear gigantic. All images generated by https://www.bing.com/images/create/

For the last category, it is interesting to note that the underlying style, dictated by my request to create the image in the painting technique of a certain epoch or even artist, often leads to a mixture of environments (including the persons) that belong to the style demanded by me, but the microscopes themselves – although also painted in the "historic" style – seem much more futuristic in their appearance. They all have in common that the mere dimensions of the microscopes seem to have grown to easily fill huge halls – quite in contrast to the "sleek, minimalist structure" predicted by ChatGPT.

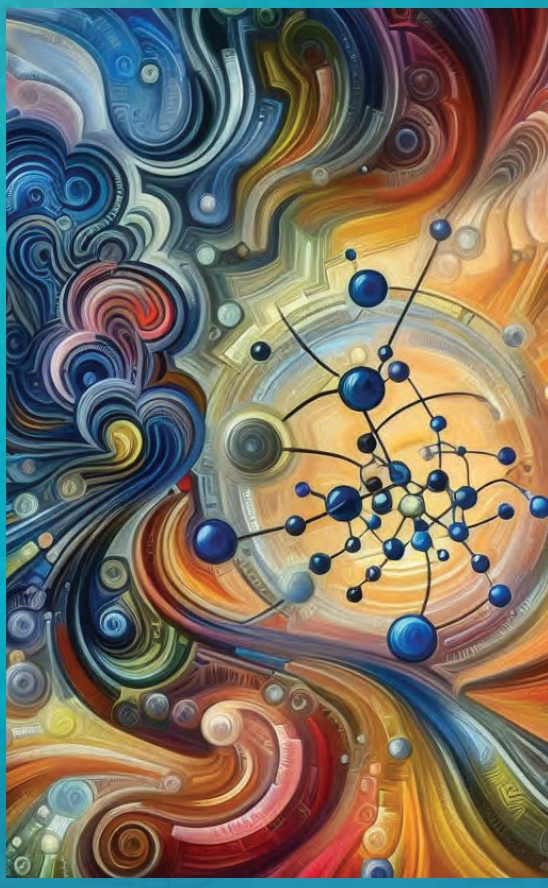

**Figure 3.** **Examples of abstract "future microscopes".**

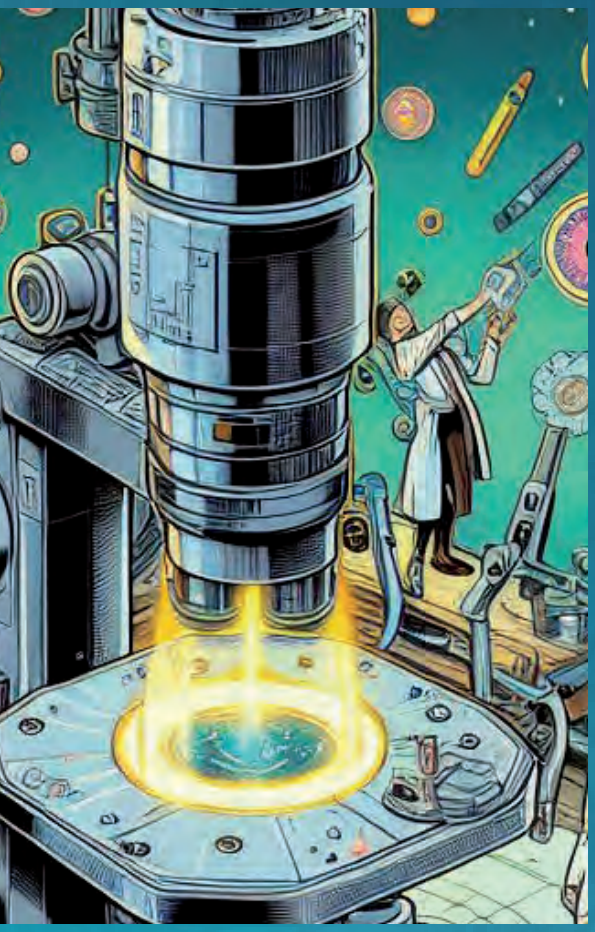

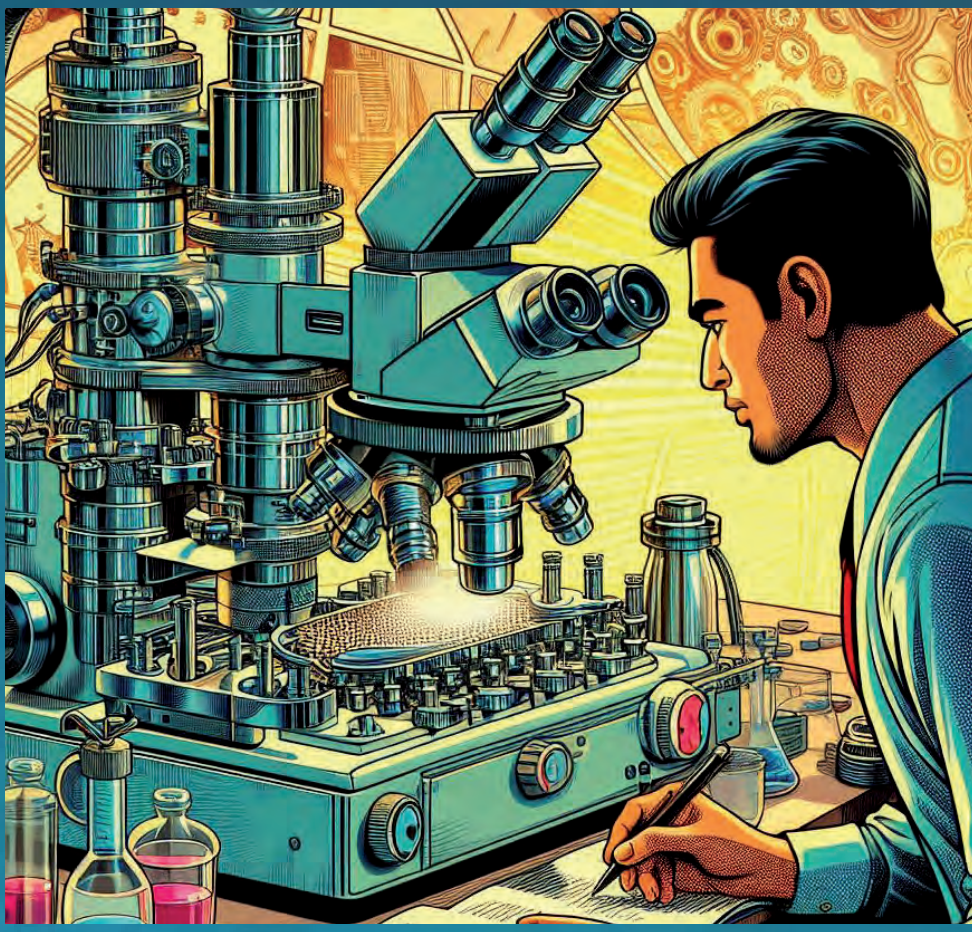

**Figure 4.** **Examples of comic-strip-like "future microscopes".**

All these AI-generated images may simply serve as oddities, they can also be considered to be some visualized "science fiction" which may (or not) stimulate your imagination as to what possible aspects of the given "predictions" might show up in reality and if one would like this reality to come true or not. Will the future of microscopy be heavy mechanical work, as shown in ***Figure 6***? Or will the future be extremely leisurely – thanks to AI ***(Figure 7)***? Will we operate our machines by gestures, using a pointed stick instead of a mouse ***(Figure 8)***? And finally: will we gain complete insight into complex organisms or self-assembled structures like nobody ever saw before ***(Figure 9)*** ?

While I hope that you may find these images entertaining, and also as quite interesting pieces of "work" by AI, I am sure that the real microscope of the future will be designed by real microscopists and engineers who understand what scientists need. I fully appreciate the benefits that come from AI when it comes to the fast scanning of huge datasets in search for certain features. I even recognize the possibility of what may be considered as "creativity" when AI "raises a flag" upon the appearance of features which cannot be assigned to known categories und as such have a probability to be something entirely new, detected for the first time by an AI search.

**Figure 5.** AI-generated images of "future" microscopes in various artistic styles. Most of the microscopes have a clear tendency to be quite huge machines, embedded in environments belonging to the artist's epoch. All images generated by https://www.bing.com/images/create/

**Figures 6 & 7.** This future microscope model seems to imply hard work to operate... while the model below suggests very leisurely working conditions.

**Figures 8 & 9.** Will the operation of microscopes be done using a stick instead of a mouse? Will we gain insight into the true interaction inside an organism?

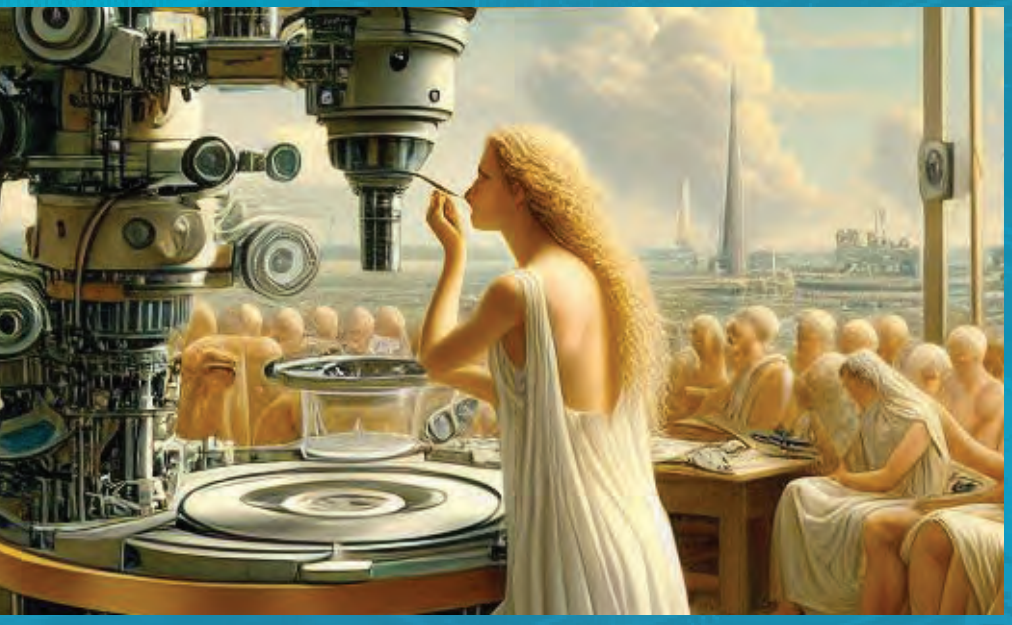

At this moment, however, I still have my doubts that any entity other than a well-educated scientific spirit will have the ability to – after a long lasting effort – understand what any newly found feature does exactly, why it is necessary in the environment found and how it interacts with other already known structures. Further, I believe it will be the task of the beforementioned scientists to speculate about its possible usefulness for our society, and how or if it should be exploited – I may be wrong though, but future will show!

**Josef Zweck (University of Regensburg, Germany)**

**References**:

[1] OpenAI. (2024, March 22). ChatGPT conversation. Online chat. Retrieved from https://chat.openai.com/. Example context: Asking what an electron microscope would look like in 25 years from now.

[2] [Bing] https://www.bing.com/images/create/

emsis

# TEM Cameras and Applications

## The right ones...

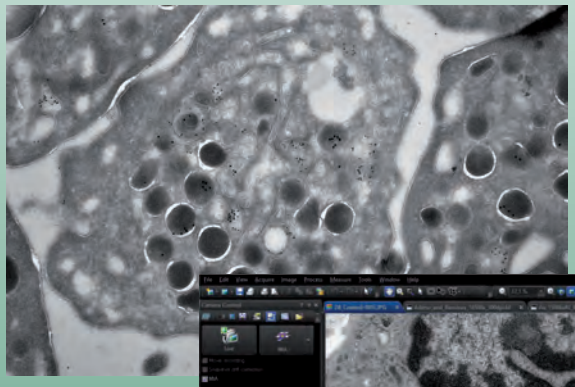


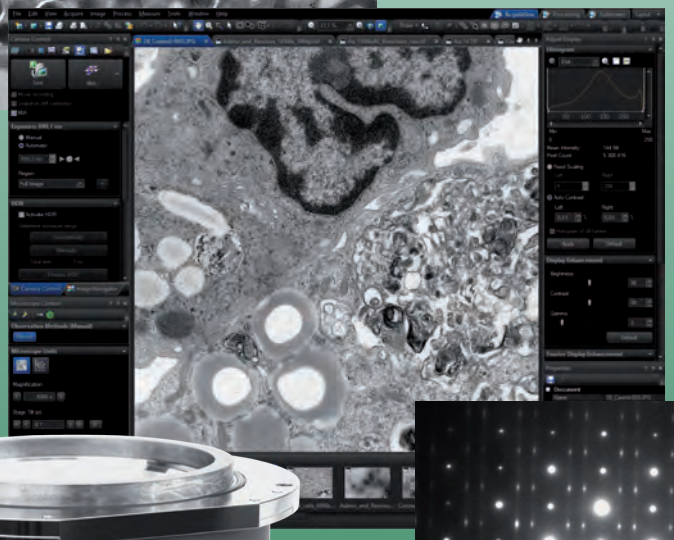


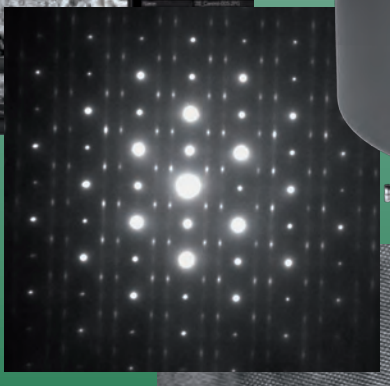


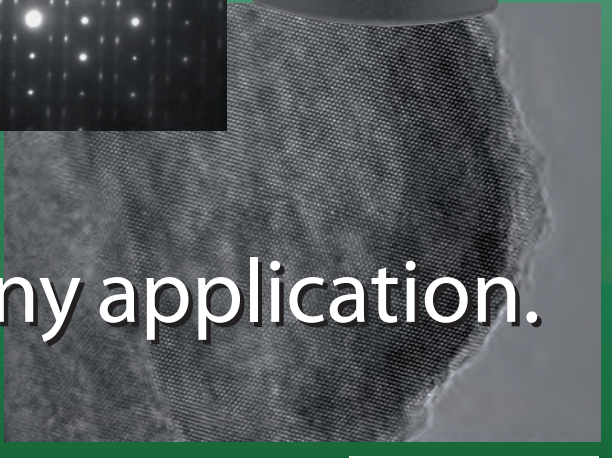

## ...for any application.

EMSIS GmbH

Mendelstraße 17
48149 Münster, Germany
Phone: +49 (0)251 297962-0
Fax: +49 (0)251 297962-90
E-mail: info@emsis.eu
www.emsis.eu

# ADVANCING SCIENCE BY ENGAGING INGENUITY

## Introducing Biolyst

Find out more about **Biolyst**

**Focused on serving the scientific community**

In a world of supply chain disruptions, rising costs, reduced funding, pressure to accelerate scientific advancements, and the ever-growing need for effective research and clinical outcome — the needs of scientists and clinicians are constantly growing.

**Products and services that help you deliver authentic data**

Our integrated company delivers a broad portfolio of over 30,000 lab products across microscopy, histology, and other diagnostic areas — positioning us to help clinicians and researchers advance discovery in the Life Sciences.


biolyst SCIENTIFIC

*Big Enough To Deliver, Small Enough To Care.™*

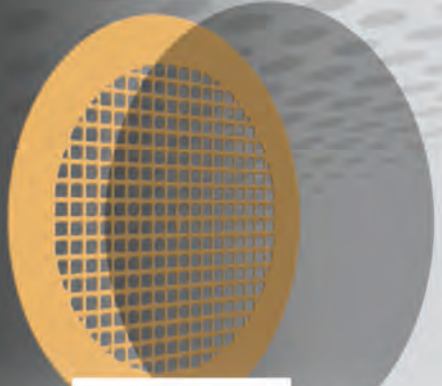

# C-flat™

The premier holey carbon grid for cryo-TEM

C-flat is an ultra-flat, holey carbon-coated TEM support grid. Unlike competing holey carbon films, C-flat is manufactured without plastics, so it is clean upon arrival and the user has no residue to contend with.

**Not sure if C-flat™ is right for your application?**

Now you can try it out with a trial size of 10 per pack in our most popular sizes and types!

Find out more about **C-flat™**

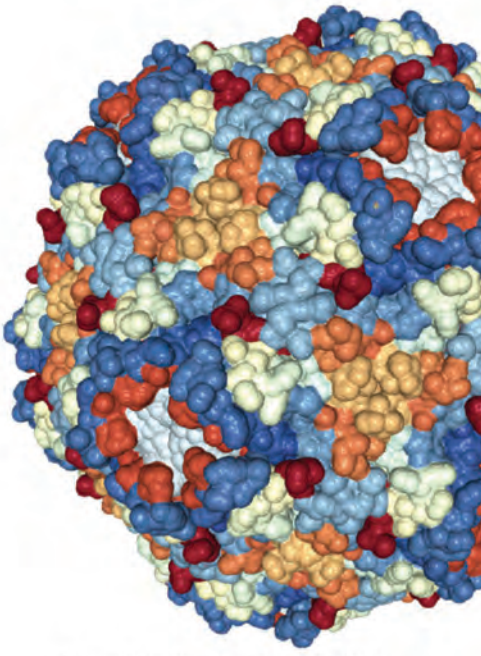

**Above:** 2.9 Angstrom Resolution Cryo-EM 3-D Reconstruction of Close-packed PCV2 Virus-like Particles: PDB ID: 3JCI Liu, Z., Guo, F., Wang, F., Li, T.C., Jiang, W. (2016) Structure 24: 319-328

**Electron Microscopy Sciences**

POWERED BY biolyst SCIENTIFIC

1560 Industry Rd. • Hatfield, PA 19440 • info@emsdiasum.com • **www.emsdiasum.com**